DTIC FILE COPY

A MODEL OF TEMPERATURE EFFECTS IN
PULSED AND CONTINUOUS WAVE CO_2 LASERS
AND OPTIMIZATION USING
RESPONSE SURFACE METHODOLOGY

THESIS

Thomas B. Melancon, B.S.
Captain, USAF

AFIT/GSO/ENP/ENS/89D-5

DEPARTMENT OF THE AIR FORCE

AIR UNIVERSITY

AIR FORCE INSTITUTE OF TECHNOLOGY

Wright-Patterson Air Force Base, Ohio

89 12 26 159

AFIT/GSO/ENP/ENS/89D-5

A MODEL OF TEMPERATURE EFFECTS IN PULSED AND

CONTINUOUS WAVE CO_2 LASERS AND

OPTIMIZATION USING RESPONSE SURFACE METHODOLOGY

THESIS

Presented to the Faculty of the School of Engineering

of the Air Force Institute of Technology

Air University

In Partial Fulfillment of the

Requirements for the Degree of

Master of Science in Space Operations

Thomas B. Melancon, B.S.

Captain, USAF

December 1989

Approved for public release; distribution unlimited

Preface

The first purpose of this study is to improve the pulsed CO_2 laser model built by Major Stone, AFIT/ENP, by including the effects of temperature change throughout the laser pulse. The second purpose is to build a continuous wave (CW) CO_2 laser model. The two models will complement each other for the study of trends in the lasers, for the simulation of laser systems, and as instructional aids. The last purpose of this study is to explore optimization using response surface methodology (RSM).

Throughout the model building process Major Stone, my advisor, gave me invaluable help, guidance, and the wisdom of experience. I am also indebted Major Kelso, my co-advisor, for help and feedback during the writing process, and to Major Bauer for guidance with RSM.

My greatest thanks, however, is due my wife, Angela, who expected nothing but the best from my efforts, was my greatest encourager, and endured my emotional absence for many weeks. She gave me peace and freedom to work by expertly managing the household, raising the children, taking them to the doctor, teaching them diligently and expertly, and introducing them to the Lord.

<div align="right">Thomas B. Melancon</div>

Table of Contents

vi

List of Figures

List of Tables

AFIT/GSO/ENP/ENS/89D-5

Abstract

The purpose of this study is to develop models of pulsed
and continuous wave (CW) CO_2 lasers on a personal computer,
and to explore optimization of the computed output power
using response surface methodology (RSM).

The first program is based on a four-level point model
of a pulsed CO_2 laser that predicts the temperature rise and
the effects of temperature on the power, energy, and gain of
the pulsed laser. The second program, derived from the
first, is based on a four-level point model of a continuous
wave CO_2 laser and calculates the power, gain, small-signal
gain, and saturation flux of the CW laser. Both models were
verified and extensively validated against published data
with good results.

Finally, this study explored the optimization of the CW
laser model using RSM and found an operating point for
maximum power at 10 torr and 4% CO_2.

Several recommendations are included for upgrading the
CO_2 laser models and continuing the optimization.

A MODEL OF TEMPERATURE EFFECTS IN PULSED AND

CONTINUOUS WAVE CO_2 LASERS AND

OPTIMIZATION USING RESPONSE SURFACE METHODOLOGY

I.   INTRODUCTION

Background

Since the invention of the carbon dioxide (CO_2) laser in
1964, CO_2 lasers have proven superior in many applications
because of their high efficiency and output. They are
currently being considered for a space-borne LADAR (laser
radar) system as an integral part of the Strategic Defense
Initiative. Both continuous wave (CW) and pulsed CO_2 lasers
would be part of such a system.

Many researchers have worked to optimize both the CW and
pulsed CO_2 laser, and several have built computer models.
Major Stone, AFIT/EN, built a model of a pulsed CO_2 laser on
a personal computer to investigate its trends, model a CO_2
LADAR system, and optimize the computed output.

Statement of the Problem

While Major Stone's current pulsed laser computer model is good, it has limitations. It cannot simulate a CW laser, is difficult to optimize, and accounts for only two of six possible temperature dependent parameters. In his current model, temperature is accounted for only by the change in density of the active medium and the change in the line width. Temperature needs to be accounted for by the change in the rotational levels of the CO_2 molecules, by the change in their relaxation rates, by the change in the thermal population of the vibrational levels, and by the change in the heat capacity of CO_2. Integrating these additions into the Runge-Kutta integration algorithm which calculates the laser output would allow a more accurate simulation of the pulsed CO_2 laser.

In addition, the computer model could be expanded to simulate a CO_2 CW laser. A CW model would complement the pulsed model, could simulate a more complete LADAR system, and might be more easily optimized.

Objectives of the Research

This thesis will expand the current computer model of the CO_2 laser through three objectives.

The first objective of the research is to write an algorithm to be incorporated into the current computer model

of a pulsed CO_2 laser to model the temperature change of the active medium and to iteratively calculate the temperature dependent parameters.

The second objective is to build a simple, user-friendly, fast-executing computer model of a CW CO_2 laser.

The third objective is to explore using response surface methodology (RSM) to optimize the computed output power of the CW laser model and to evaluate its use for optimizing the pulsed laser model.

Scope and Limitations. This thesis effort will only consider temperature effects on the gas kinetics and photon interaction in the active medium of the pulsed CO_2 laser. The temperature effect on laser structure, like the mirrors, will not be considered. In addition, the temperature effect on the optical quality or frequency of the laser beam will not be considered.

The CW model will also only consider the reaction kinetics of the active medium that produce the laser beam. This study will not include fluid dynamics (flowing systems), heat transfer, resonator modes, or the physics of electron beam pumping.

Assumptions. Both the pulsed and CW models in this study rest on the assumption that Gilbert's four-level point model is adequate. Gilbert assumes that the vibrational and rotational modes reach equilibrium much faster than other

3

processes and the excited states of CO_2 and N_2 are sparsely populated. The following processes are assumed by Gilbert to be slow or have little effect and are ignored: the dissociation of CO_2, the relaxation of the CO_2 001 vibrational level directly to the ground state, and the radiative relaxation of the excited states. Thus, all relaxation rates are collisional. Finally, the rate of energy exchange between excited N_2 and CO_2 is assumed to be much faster than the relaxation of either N_2 or CO_2 (11:2524-26). Gilbert's assumptions are further enumerated in the literature review.

This study also adopted some of Stone's assumptions. He assumes that only one fourth of the CO_2 molecules that relax from the upper vibrational level (001) add to the population of the lower vibrational level (100). Stone also assumes that the laser operates in only one resonator mode and lases on the center of the P(20) line shape.

This study added the assumption that only one fourth of the CO_2 molecules that leave the upper laser level by stimulated emission also add to the population of the lower vibrational level.

This study made three additional assumptions while building on Gilbert's and Stone's models. The model of the temperature effects in the pulsed laser assumes constant gas density throughout the laser pulse forming process. To

4

calculate gas heating, any energy added by the electron beam pump that does not appear as molecular vibrational energy or laser energy is assumed to be thermal energy of the gas. In addition, only the heat capacity of CO_2 is assumed to change significantly with temperature over the operating range of tne laser.

The CW laser model included all the above assumptions and is modeled as a four-level point model at steady state. The excited populations, photon density, and temperature are assumed to be constant throughout the laser cavity. No specific accounting of the heat removal system is included; it is assumed that the cooling system is able to maintain a specified bulk temperature in the laser. In addition, the quasi-Voigt line shape is assumed to be adequate.

Finally, for the RSM study, this study assumes that a third-order polynomial is adequate to fit the computed power from the CW laser model over the region of interest.

II. LITERATURE REVIEW

Overview

This literature review describes the lasing process, a pulsed CO_2 laser, and analytical models of the pulsed CO_2 laser. A review of the effects of temperature on the laser follows, and then equations for the temperature dependent parameters are described. Last, the energy balance equations required to calculate the temperature rise of a laser during operation are presented.

The Lasing Process

The foundation of the CO_2 laser is the vibrational and rotational energy levels of the CO_2 molecule and their interaction with the laser light. The following simplified illustration (Figure 1) of how the energy levels of the CO_2 molecule produce laser light will provide the background for understanding the effects of temperature on the lasing process. The 000 level is the ground vibrational mode, the 100 energy level is the first symmetric stretch vibrational mode, the 010 and 020 energy levels are the bending vibrational modes, and the 001 energy level is the asymmetric stretch vibrational mode.
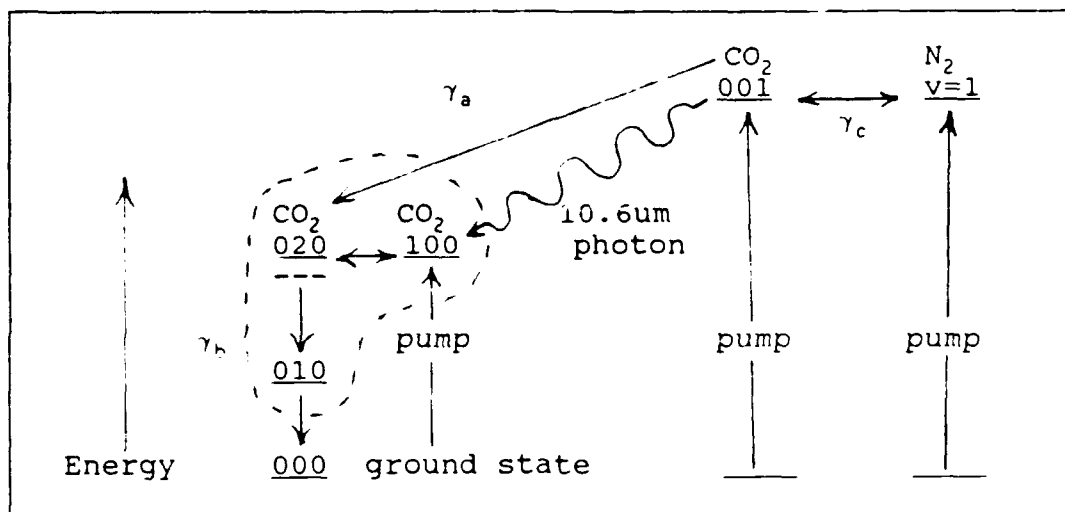
Figure 1. CO_2 Laser Vibrational Energy Levels (γi = collisional relaxation rates.)

At room temperature, nearly all of the CO_2 molecules are in the ground vibrational state (000). An electron beam, normally produced by a cathode and anode at high voltage, is used to excite the molecules to the different vibrational energy levels. This process is called pumping. Nitrogen is almost always mixed with the CO_2 in the active medium (the gas mixture in the laser) because N_2 is excited more efficiently than CO_2 and very readily transfers its vibrational energy to the CO_2, pumping it up to the 001 level.

The 001 level, called the upper vibrational level, will emit a photon with a wavelength of 10.6 microns (in the far infrared spectrum) and leave the molecule in the 100 level, called the lower vibrational level. If this photon interacts with another CO_2 molecule in the 001 level, it can

stimulate the second molecule to emit a photon in the same direction and in phase with the first. This is called stimulated emission. However, in a process called stimulated absorption, if the photon encounters a CO_2 molecule in the 100 level, the molecule can absorb the photon and be raised to the 001 level.

A complete description of the CO_2 molecule's energy state must include the rotational energy levels, which also participate in the lasing process. Rotational energy levels, described by a "j" number, are spaced much more closely than vibrational levels, and each vibrational level contains many rotational levels. For the purposes of this study, a single CO_2 molecule can have only one vibrational and one rotational level. Thus, the complete description of the upper laser level is 001, j = 19, and the lower laser level is 100, j = 20. This is called the P(20) transition, and is the normal lasing transition for the CO_2 laser. The CO_2 laser normally operates on the P(20) line shape (produced by the P(20) transition) because j=19 is the most populated rotational level at room temperature.

If the active medium of the laser is to produce a net positive output of photons for the laser beam, there must be more molecules in the upper laser level (001, j=19) than in the lower laser level (100, j=20). This unnatural state of

affairs is called a population inversion and is absolutely necessary for lasing.

After a molecule is excited, it can either lase or relax collisionally by transferring its vibrational energy to another molecule or to the walls of the laser cavity. It can also relax radiatively by emitting a photon that carries away the vibrational and rotational energy the molecule loses.

The quantum efficiency of the CO_2 laser can also be deduced from the energy level diagram. It is the ratio of the energy carried away by the emitted photon to the energy stored in the CO_2 molecule at the 001 level. This is approximately 38% and is the limiting efficiency for the laser.

In summary, the electron beam pumps some of the CO_2 up to the 001 level (either directly or through the N_2) to produce a population inversion. The excited CO_2 molecule lases on the P(20) transition, producing a 10.6 micron photon and leaving the CO_2 molecule in the 100, j = 20 state. This molecule then relaxes through the 020 and 010 levels to the ground state, giving up the excess vibrational energy as heat. At the ground state, it can be pumped up to lase again. This process occurs in both CW and pulsed lasers.

9

Pumping the Laser. As mentioned previously, the laser is pumped by applying a high voltage across the anode and cathode in the laser cavity. The product of the voltage and the resulting current is equal to pump power, $Pin = E \ I_c$, where Pin is the pump power, E is the voltage, and I_c is the current. The current is proportional to the electron number density in the active medium, N_e, and is often held fairly constant. The voltage, however, is often varied with the total molecular number density, N_o, so as to keep E/N_o constant at approximately 2.0×10^{-16} V-cm2 (24:159). This produces an average electron energy of about 2 eV, which is the most efficient for pumping N_2 (24:67). According to Witteman, electrons with less than 0.3 eV of energy heat the gas instead of exciting the upper vibrational states of CO_2 and N_2. Electrons with more than 3 eV excite electronic states of the molecules, resulting in lower efficiency (24:67).

Since the best pump efficiency is obtained by keeping E/N_o, and thus the average electron energy, constant, then the pump power is proportional to the total number density and electron density:

$$Pin = (E/N_o) \ N_o \ I_c \ \propto \ (E/N_o) \ N_o \ N_e \qquad (1)$$

If the electron number density is not constant but is also proportional to the molecular number density (to keep the ratio of electrons to molecules equal), then the pump power varies as the square of the molecular number density.

Description of a Pulsed TEA CO_2 Laser

A Transversely Excited Atmospheric (TEA) pulsed CO_2 laser is one of the possible CO_2 laser systems that capitalize on the lasing process described above. It can operate at high pressure (up to several atmospheres) and is capable of very high energy output. In one possible configuration of a TEA laser, the laser cavity consists of a long cavity (which contains the active medium), a fully reflective mirror at one end, and an output mirror at the other end. The cathode and anode are positioned parallel to the cavity so that the electrons flow through the active medium transversely to the axis of the cavity.

During operation, the active medium is pumped with a pulse of electrons (the pump pulse) which flow from the cathode to the anode. This pulse of electrons excites a number of CO_2 molecules, which begin to lase. The number of photons in the cavity continues to build exponentially until the gain decreases below the threshold gain, and the laser pulse stops building. This short pulse of laser radiation

11

begins to exit the laser through the output mirror while it is forming and is completely gone in a few microseconds.

Gilbert's Model of a CO_2 Pulsed Laser

Stone's current computer model of a pulsed TEA laser is based on the work of Gilbert, et al. (11:2523-35), and understanding Gilbert's model is basic to understanding Stone's model. Gilbert's work was particularly suited to adaptation to a personal computer by Stone because Gilbert used a four-level point model and several simplifying assumptions that reduced the computational complexity.

Description of a Four-Level Point Model. Gilbert's four-level point model assumes that both a four-level model and a point model are adequate. A point model assumes the population inversion and the radiation intensity are equal at every point throughout the laser cavity. This assumption limits the rate at which the photons can leave the cavity, and it also limits the round trip gain - length product of the laser to less than one. Both limits mean a point model applies only to a short laser or low gain lasers.

A four-level point model keeps track of the populations in four energy levels. Gilbert chose the four levels to be:

1. CO_2 (001), the upper vibrational level;

2. CO_2 (100 + 020 + 010), the lower vibrational level plus levels it is in equilibrium with;

12

3. N_2 (v=1), the first excited state of N_2;

4. and the ground states of CO_2 and N_2.

The foundational assumption for a four-level model is that the relaxation rate between the 100 and 020 vibrational levels of CO_2 is much faster than the other relaxation rates, and so the 100 and 020 levels are always roughly in equilibrium. Using Witteman's rate equations, the rate for exchange between the 100 and 020 levels is 1.2×10^9 per sec, γ_b is 2.05×10^6, and γ_a is 8.6×10^4 per sec at $300°K$ and 1 atm (24:164).

Other authors, however, have used five-level models that separate CO_2 (100) from CO_2 (020 + 010). For a comparison of my four-level model (derived from Gilbert's model) and Witteman's five-level model, see page 70.

Gilbert's Assumptions. In addition to the assumption that a four-level point model is adequate, Gilbert made three other major simplifying assumptions. The first assumption is that the vibrational and rotational modes reach equilibrium much faster than the other processes in the laser. The second assumption is that the excited states of CO_2 are sparsely populated. The third assumption is that all reaction rates except those specifically accounted for are negligible. These assumptions were confirmed by Gilbert in the literature or through his experimentation with an actual laser (11:2523-27).

13

Fast Vibrational and Rotational Equilibrium. Gilbert's first simplifying assumption is that the vibrational and rotational modes reach equilibrium faster than other laser processes. The vibrational and rotational modes reach equilibrium very quickly because the CO_2 molecule can exchange vibrational or rotational energy every few collisions, and the time between collisions is very small compared to other processes in the laser. This was confirmed by Witteman, who reported the lifetime of the CO_2 001 level to be 10^{-3} seconds, while the time between collisions is only 10^{-8} seconds at 10 torr (24:63). At higher pressures, the collision time can be 10^{-10} seconds, while the pulse forming process takes approximately 10^{-8} seconds. Each vibrational and rotational distribution is thus maintained in equilibrium by frequent collisions throughout the pulse forming process, which allows the complex rotational distribution to be ignored for a four-level model (11:2523-27).

Sparsely Populated Excited States. Gilbert's second simplifying assumption is that the excited states are sparsely populated. Assuming the excited states of CO_2 are sparsely populated led Gilbert to assert that the relaxation rates are independent of the concentration of the excited states, the ground state population stays essentially constant, and the pumping efficiency of CO_2 does not vary

with the concentration of N_2 (11:2523-27). See page 74 for an analysis of this assumption.

This assumption of sparsely populated excited states also means that the lowest excited levels above ground state contain almost all the excited molecules. This model assumes that all the CO_2 excited by the electron beam is pumped into the 100, 010, 020, and 001 levels, and all the N_2 excited can be found in the first N_2 vibrational level (v=1).

Negligible Reaction Rates. Gilbert's third simplifying assumption is that all the reaction rates except those specifically accounted for are negligible. The following processes are assumed by Gilbert to be slow or have little effect and are ignored: the dissociation of CO_2, the relaxation of the 001 level directly to the ground state, and the radiative relaxation of the excited states. In addition, the rate of energy exchange between excited N_2 and CO_2 is assumed to be much faster than the relaxation of either N_2 or CO_2.

All of the above assumptions and simplifications allowed Gilbert to model the very complex CO_2 laser as a four-level system, described by four coupled rate equations (11:2523-27).

Gilbert's Rate Equations. The heart of the Gilbert's model consists of four differential rate equations which

describe the rate of change of the upper vibrational level, the lower vibrational level, the excited N_2, and the photons in the cavity as follows:

$$dn_a/dt = I \sigma c(n_{b'} - n_a) - \gamma_a n_a + \gamma_c(n_c - n_a) + w_a \qquad (2)$$

$$dn_{b'}/dt = I \sigma c(n_a - n_{b'}) + \gamma_a n_a - \gamma_b n_{b'} + w_b \qquad (3)$$

$$dn_c/dt = \gamma_c(n_a - n_c) - \gamma_{co} n_c + w_c \qquad (4)$$

$$dI/dt = -\gamma_o I + I \sigma c(n_a - n_{b'}) + n_a w_s \qquad (5)$$

where n_i is the number density of the ith excited level, I is the photon flux, γ_i is the relaxation rate from the ith level, and w_i is the pump rate into the ith level. The subscripts are defined, in general, as follows: a refers to CO2 (001), b' refers to CO_2 (100 + 010 + 020), and c refers to N_2 (v=1) (11:2525). All the terms are specifically defined in appendix A.

Stone's Model of a Pulsed CO_2 Laser

Stone took Gilbert's model, modified it, and wrote the model into Quick BASIC computer code to fit on a personal computer. This fast executing code was designed to demonstrate the trends of a pulsed CO_2 laser.

Stone's Modifications. Stone's modifications to Gilbert's model included adding one change and two major

16

assumptions, changing the rate equations, and using Witteman's line width and relaxation rate equations.

The first change is that the lower vibrational level consists of only CO_2 (100), the lower excited state that actually interacts with the laser photon, as opposed to Gilbert's lower vibrational level, which consists of three excited levels, CO_2 (100 + 020 + 010). The first assumption is that the 020 and 010 levels are always in equilibrium with the CO_2 (100) level and equal to it.

Stone changed Gilbert's rate equations by incorporating the above assumptions, adding the degeneracy ratio, and separating the rates between CO_2 (001) and N_2 (v=1). Thus Stone's model is still a simple four-level model, but the rate equations are changed as follows:

$$dn_a /dt = I \sigma c(gu/gl \; n_b - n_a) - \gamma_a \; n_a + \gamma_{co2} \; n_c$$
$$-\gamma_{cn2} \; n_a + W_a \qquad (6)$$

$$dn_b /dt = I \sigma c(n_a - gu/gl \; n_b) + \gamma_a \; n_a/4 - \gamma_b \; n_b + W_b \qquad (7)$$

$$dn_c /dt = \gamma_{cn2} \; n_a - \gamma_{co2} \; n_c + W_c \qquad (8)$$

$$dI/dt = I \sigma c(n_a - gu/gl \; n_b) - I/\tau_{cav} + n_a \; W_s \qquad (9)$$

where n_b is the population of CO_2 (100) level, gu/gl is the degeneracy ratio, γ_{co2} is the energy transfer rate from N_2 to CO2, γ_{cn2} is the rate from CO_2 to N2, and τ_{cav} is the photon lifetime in the cavity. The divisor of 4 in the equation

17

for n_b accounts for the assumption that only one fourth of the CO_2 (001) molecules that relax to the lower vibrational level enter the 100 level: the other three fourths enter the double 020 levels and the 010 level, which are roughly in equilibrium with the 100 level. The term for direct relaxation of N_2, $\gamma_{co} n_c$, was dropped from Equation 4 because Stone assumed that all the N_2 relaxes through the CO_2 vibrational levels.

The second assumption added by Stone is that the laser always operates in one laser cavity mode and on the center of the P(20) line shape. Thus, only the rotational levels j=19 and j=20 participate in lasing. Although Gilbert mentioned that the point model does not limit the number of cavity modes that can exist inside the cavity (11:2523-27), Stone assumes one longitudinal cavity mode only.

Calculation of the Laser Output. The coupled differential rate equations presented by Gilbert and modified by Stone (Equations 6 to 9) are integrated in Stone's computer model with a fourth-order Runge-Kutta integration algorithm to calculate the laser output over time.

Stone's Accounting of Temperature. In solving the coupled rate equations, temperature is used in Stone's model to calculate two parameters: the line width -- used to calculate the gain -- and the density of the gas mixture in

18

the laser. The line width, $\Delta\nu$, is related to temperature by $\Delta\nu = \Delta\nu o*(300/T)^{\frac{1}{2}}$, where $\Delta\nu$ is the line width at temperature T, $\Delta\nu o$ is the line width at 300°K, and T is the temperature in °K, assuming constant pressure.

The density of the gas is calculated using the ideal gas law at constant volume, $N_o = P/kT$. The density and mix of the gas determines the number of CO_2 molecules available to lase.

Temperature Effects in the Laser

Although Stone's computer model accounted for two temperature dependent parameters, it did not account for all the effects of temperature. The temperature of the gaseous medium greatly affects the power output of a CW laser and the total energy and shape of the pulse from a TEA laser. The greatest effects are reducing the gain, limiting the potential power, and reducing the optical quality of the laser output. The following paragraphs discuss the effects of temperature on a CO_2 laser.

Reduced Gain. The first effect of increased temperature is reduced gain. Temperature reduces the gain through three mechanisms: reducing the population inversion, decreasing the radiative cross section, and reducing the number density of the gas. The gain equation

19

$$G = (n_a \sigma_U - n_b \sigma_L \, gu/gl) \approx \sigma (n_a - n_b) \tag{10}$$

illustrates each of these effects. Increasing temperature will reduce the population inversion, $(n_a - n_b)$, by increasing the population of the lower vibrational level, n_b, and increasing the relaxation rate of the upper vibrational level, n_a, (24:3, 71). Both effects reduce the population inversion and thus reduce the gain of the laser.

Increasing temperature will also increase the line width and decrease the population of rotational level $j = 19$, both of which decrease the radiative cross section, and thus reduce the gain. The last effect of temperature on gain is to reduce the number density in the gas (at constant pressure), and thus reduce the number of CO_2 molecules available to be excited and lase.

Fowler found that the small-signal gain drops off to nearly zero at temperatures of 500 to 700°K. His conclusion is, "Low gas temperature is seen to be one of the most important properties that a CO_2 laser plasma can have" (10:3484-86).

One exception to the rule, however, was highlighted by Deutsch. He found that "the more effective rotational cross relaxation at higher temperatures can result in an increase of the saturation parameter and can partially compensate for the decrease of gain with temperature" (6:947). In spite of

this partial compensation, the CW laser Deutsch studied decreased in power from 43 watts to only 28 watts as the temperature of the cooling jacket was raised from -60°C to +90°C (6:974).

Power Limitation. The second effect of increased temperature is limited power. Witteman found, like Deutsch, that the power decreases with increasing temperature. According to Witteman, since the quantum efficiency is 38%, at least 62% of the power introduced by the pump is eventually converted to heat. This heat reduces the gain, which limits the power output. At about 150°C (423°K), the power begins to decrease. Without active cooling to carry away the generated heat, the maximum pump energy is 300 joules/liter (J/l) and the maximum output is 40 J/l (24:3).

To overcome this limitation, Witteman discussed two types of active cooling that have been designed into many lasers. In the first type, the gaseous medium is cooled by conduction through the walls of the laser cavity to a water (or other coolant) jacket. The second cooling technique is to replace the hot gas with new, cool gas by flowing the gas through the laser cavity (24:3). Taking this technique one step further, Mitsuhiro studied a fast flowing CW CO_2 laser operated below room temperature and found a 50% increase in power at 200°K. He also found the pump efficiency increased from 15% to 20% (13:680). Drobyazko found a similar 50%

increase in energy for a cooled, pulsed CO_2 laser operated at 200°K. He found the heat created during the pulse formation at room temperature increased the lower vibrational level population to the point of terminating the pulse before the upper vibrational level was depleted (8:974).

Reduced Optical Quality. The last effect of high temperature in the laser medium is to reduce the optical quality of the laser. Poor optical quality of the laser beam is the result of inhomogeneities in the laser medium. These inhomogeneities arise when a temperature change causes the density and refractive index of the gas to change. Both CW and pulsed TEA lasers are vulnerable to temperature variations. Witteman calculated the temperature profile in the medium of a CW laser and found the temperature varied from 290°K at the cavity wall to over 800°K at the center for an input energy of 500 watts/meter (24:91). The resulting density gradient acts like a diverging lens to spread the beam and distort its intensity profile.

The heat introduced to the medium of a pulsed laser also changes its density and optical properties. Milonni calculated a temperature rise from 300 to 550°K in 25 microseconds during the pulse forming process of a high-power laser (15:3595). Fedorov calculated approximately the same temperature rise in 15 microseconds for an input energy

22

of 250 J/l. This rapid rise in temperature creates a local pressure wave with non-uniform density which travels through the laser cavity at the local speed of sound. The transit time of the pressure wave, however, is longer than laser pulse time, so the effect on optical quality is not severe (9:629-30). This model does not calculate the effect of temperature on optical quality.

Temperature Dependent Parameters

Of the three major effects of temperature, two -- reduced gain and power limitation -- are mathematically described by six temperature dependent parameters. The six parameters are the thermal populations of the vibrational levels, the thermal population of the rotational energy levels (j levels) of the CO_2 molecule, the relaxation rates of the vibrational energy levels of the molecules, the line width, the gas density, and the heat capacity of CO_2.

Thermal Populations of the Upper and Lower Vibrational Levels.
The first temperature dependent parameter is the thermal population of the vibrational levels (CO_2 001 and 100). The thermal population of a vibrational level is described by the Boltzmann equation:

$$N_i = N_o \exp(-E_i/k\ T) \qquad (11)$$

where N_i is the number of molecules in the ith vibrational level, N_o is the number of molecules in the ground level, and E_i is the energy difference between the ground and the ith vibrational level.

The thermal population of the vibrational levels is distributed exponentially. At low temperatures the exponential term is very small and the population of the lower vibrational level is small. At higher temperatures the population can be substantial -- 2.0% at $500°K$ and 6.2% at $700°K$ for CO_2 (100).

Thermal Population of the Rotational Levels. The second temperature dependent parameter is the thermal population of the rotational levels. The fraction of molecules in a rotational level is also given by the Boltzmann equation, presented by Witteman as:

$$f_{vi} = n_{vj} / n_v = C \ (2j+1) \ exp(-F(j) \ h/k \ T) \qquad (12)$$

where

$$C \quad = \quad 2 \ h \ B_v \ /k \ T, \text{ a normalization factor}$$

$$F(j) = \quad B_v \ j(j+1) + D_v \ j^2(j+1)^2 \ (Hz)$$

$$B_v, D_v = \quad \text{rotational constants, different for each}$$
$$\text{vibrational level (Hz) (24:16)}$$

24

and where f_{vj} is the fraction of molecules in vibrational

level v that are in rotational level j, n_{vj} is the number of

molecules in rotational level j and vibrational level v, and

n_v = number of molecules in vibration level v.

This equation describes the population of the rotational

level in the upper laser level, j=19 (f_U), and the lower

laser level, j=20 (f_L), for the P(20) transition at

temperature T, and is used in the calculation of the

radiative cross sections, σ_U and σ_L. Figure 2 shows the

distribution of the rotational levels are not exponential as
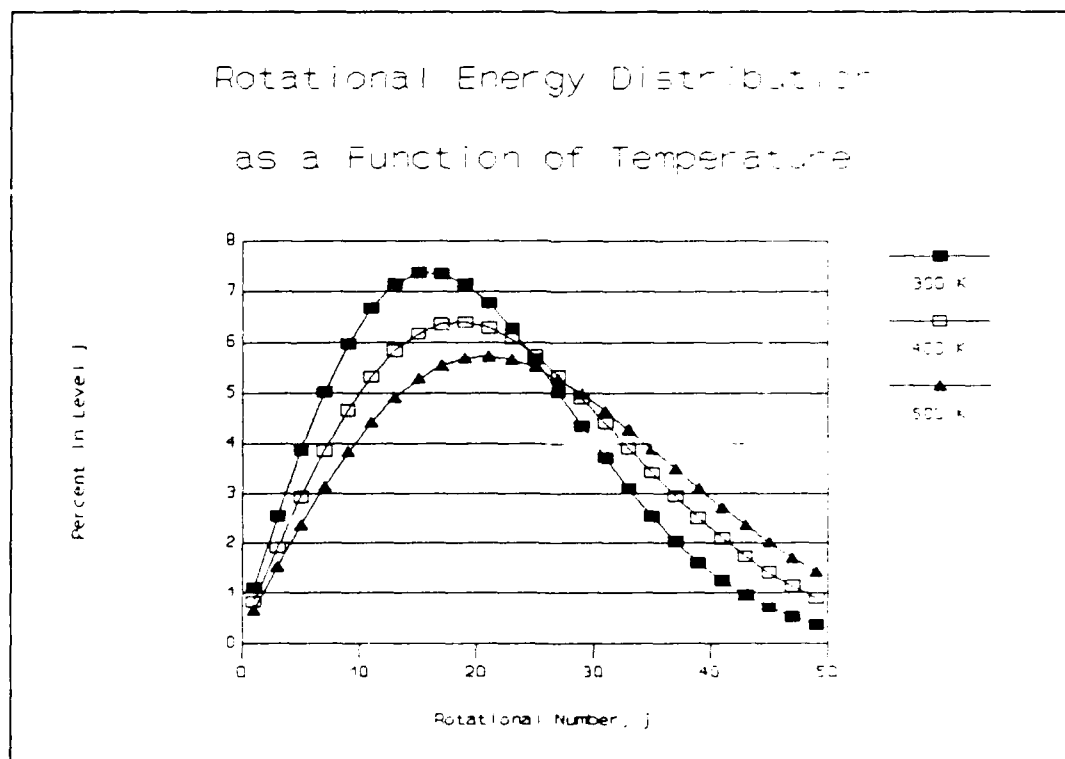
Figure 2. Rotational Distribution as a Function of Temperature. Calculated from Equation 12.

25

expected, but peak at different values of j depending on the temperature.

Relaxation Rates. The third set of temperature dependent parameters are the relaxation rates (γ). According to Witteman, the time constant τ ($1/\gamma$) is a function of pressure, the number density and type of collision partners, and the temperature. For example, the time constant for the relaxation to ground state from the upper vibrational level (001) is approximated by:

$$\tau_3 = \tau_{3_0} \left(\frac{T_0}{T}\right)^{\frac{1}{2}} \exp\left[h(\nu_3 - \nu_2 - \nu_1)\left(\frac{1}{k\,T} - \frac{1}{k\,T_0}\right)\right] \qquad (13)$$

where $\tau_{3_0} = (P(\Sigma \; \psi_i \; K_i))^{-1}$, the time constant at the baseline temperature for the particular pressure and gas mix involved, and K_i is the rate constant for gas component i. Finally, ν_i is the frequency of emission for the CO_2 100, 010, and 001 levels, respectively.

Other authors, however, have proposed different models for the temperature dependence of the time constants. Douglas-Hamilton used the relation $\tau = 1/(\Sigma(\psi_i \; k_j))$, where ψ_i is the fraction of a component and k_j is the rate for that component. The rate constant, k_j is then a function of inverse of the cube root of the temperature, $k_j = (T)^{-1/3}$, and is displayed in graphical form (7:7-10). Wutzke, on the other hand, used a fitted curve of the form:

26

$$\gamma = \text{sum } (K_i \ N_i) \tag{14}$$

$$K_i = A'x^2 \exp(-B'x + C'x^2 + D'x^3) \tag{15}$$

where γ is the relaxation rate, K_i are fitted rate constants for the gas components, N_i is the number density of gas component i, $x = T^{-1/3}$, and $A'-D'$ are fitted constants (25:100-115).

Figure 3 shows a comparison between the relaxation rates calculated by Witteman, Equation 13, and Wutzke, Equations 14 and 15.
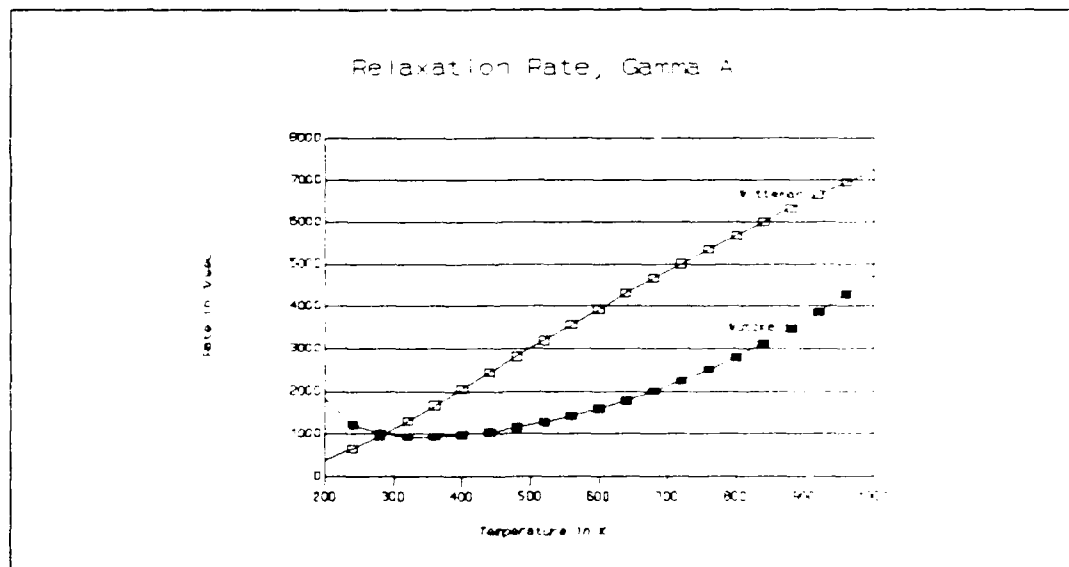
Figure 3.   Comparison of γ_a Calculated by Witteman and Wutzke, as a Function of Temperature. Pressure = 10 torr; Mix = 10% CO_2, 10% N_2, 80% He.

Line Width.   The line width is the fourth temperature dependent parameter.   Line width is described by two

different equations, depending upon the pressure. At relatively high pressure (greater than 50 torr), the line shape is Lorentzian (pressure-broadened), but at less than 10 torr the line width is Doppler-broadened.

Lorentzian Line Width. The pressure-broadened Lorentzian line width has been measured by several researchers. Brimacombe measured the half width at half maximum line widths (cm^{-1}) at the P(16) and P(32) lines and found the following relations for pressure broadening:

At constant number density:

$$\Delta \nu = P/760[\Sigma(\psi_i\ a_i)](T/300)^n \tag{16}$$

At constant pressure:

$$\Delta \nu = P/760[\Sigma(\psi_i\ a_i)](300/T)^{1-n} \tag{17}$$

where a_i are linear functions of the rotational number and the exponential term, n, equals 0.42 ± 0.06 .

The value of n compares favorably with the value measured by Pack and quoted by Brimacombe as 0.38 for helium broadening (4:1671-72). In addition, Gross measured the self-broadened line width of CO_2 (CO_2 colliding with CO_2) and found n to be 0.7 (12:2253).

Witteman gave the pressure-broadened line width (Hz) as (24:61):

$$\Delta \nu_p = 3.925 \times 10^6 (\psi CO_2 + 0.73 \psi N_2 + 0.64 \psi He) P (300/T)^{\frac{1}{2}} \qquad (18)$$

Doppler-Broadened Line Width. The second form of line broadening is Doppler broadening. For the CW laser at low pressure, where pressure broadening is not a factor, Witteman gives the Doppler line width (Hz) as (24:60):

$$\Delta \nu_d = \nu [(\ln 2) \ 2 \ k \ T/M \ c^2]^{\frac{1}{2}} \qquad (19)$$

where ν is the laser frequency at line center and M is the molecular weight of the lasing molecule (CO_2).

The line widths are used to calculate the radiative cross sections, σ_u and σ_l, where σ is inversely proportional to the line width.

Gas Density. The fifth temperature dependent parameter is gas density. The number density of the gas is calculated by the ideal gas law, $N_o = P/k \ T$. Brimacombe stated that a pulsed laser operates at constant volume, so the density of the gas does not change during the laser pulse (4:1671).

Heat Capacity. The sixth and last temperature dependent parameter is the heat capacity of CO_2. The heat capacity of poly-atomic molecules increases with temperature because

29

molecular vibrational levels can become populated, absorbing energy that would otherwise increase the temperature of the gas. Of all the gases used in the CO_2 laser, only the CO_2 (010) vibrational level is significantly populated at the laser's operational temperatures (300 - 700°K). Therefore, only the heat capacity of CO_2 varies significantly with temperature and is described by Vincenti as

$$Cv = R \left\{ 5/2 + \left[\left(\frac{h\,\nu_1}{2\,k\,T} \right) \Big/ \sinh\left(\frac{h\,\nu_1}{2\,k\,T} \right) \right]^2 \right\}$$ (20)

where Cv is the constant volume heat capacity of CO_2 (23:136). The next paragraphs will discuss the calculation of the temperature rise in the laser medium during operation.

Temperature Rise During Lasing

Since the temperature of the lasing medium has such a large effect on the laser output, "it is therefore imperative to determine the kinetic gas temperature" (25:116). The gas temperature may be determined by accounting for all the energy that is introduced into the gaseous medium by the electron beam pump. The electron beam energy is divided into exciting the CO_2, the N_2, and directly heating the gas. Some of the excited CO_2 and N_2 molecules contribute their energy to the laser output, but

30

the rest relax to the ground state, giving their energy up to heat. Anywhere from 5% to 20% of the electron beam energy directly heats the gas (7:28), and no more than 38% (quantum efficiency) of the rest can be converted into laser output. Milonni calculated the temperature rise to be approximately constant over the time span of 25 microseconds (15:3595). A well-designed CO_2 laser can have an overall energy efficiency of 10% - 20%.

Energy Balance Equations. An energy balance equation can be used to calculate the amount of energy that is introduced as heat and raises the temperature of the gas. An equation that accounts for nearly all the energy introduced by the electron beam was presented by Milonni:

$$q = (W - R_e) - R_{st} + R_{vt} + R_{vv} \qquad (21)$$

where

q = rate thermal energy is added to the gas

W = rate total energy is added to the medium by pump

R_e = pump rate into all vibrational levels

R_{st} = rate energy is lost to stimulated radiation

R_{vt} = rate energy is converted to heat from vibrational relaxation to the ground state

R_{vv} = rate energy is converted to heat from vibrational energy exchanges between molecules

31

The first term on the right, $(W - R_e)$, accounts for energy from the pump that is converted directly into heat (15:3596).

Each of the terms presented above has been calculated explicitly by Wutzke (25:49-50, 116-119) for each of the major vt and vv reactions. Wutzke estimated the 80% of all the heat added to the gas comes from the vt reactions. In addition, he expands q to be $q = (dT/dt)[\Sigma(\psi_i\ C_i)]$ where dT/dt is the change in gas temperature with time, ψ_i is the fraction of the various gas components, and C_i is the heat capacity of each gas component (25:50).

The only energy not accounted for in the energy balance equations is the thermal energy lost to the laser cavity walls. In a CW laser at steady-state operation, the thermal energy transported through the cavity walls must equal the thermal energy created, and a steady-state temperature is reached. For a pulsed laser, however, the laser pulse is formed and gone so quickly that none of the heat is conducted away during the pulse; it all stays in the gas to raise its temperature.

III. PULSED CO_2 LASER MODEL, METHODOLOGY and ANALYSIS

Overview

In this chapter, the development of the temperature dependent pulsed CO_2 laser model, henceforth referred to as "the author's model" or "this model", is discussed in detail. In addition, the verification (internal tests) and the validation (external tests) of the model are presented and analyzed. Finally, the limits of the model, both theoretical and practical, are discussed.

Developing the Model

This model incorporates four major changes to Stone's pulsed CO_2 model: thermal populations of the excited vibrational states, thermal populations of the upper and lower rotational levels, another divisor of four in the rate equation for the population of the lower laser level (n_b), an energy balance to calculate the new temperature, and a recalculation of the temperature dependent parameters.

Rate Equations. The rate equations incorporate the first three major changes. The thermal populations of the upper and lower vibrational levels, n_{ae} and n_{be}, are included in the rate equations for n_a and n_b. The fraction of CO_2

33

molecules in the upper and lower rotational levels are incorporated into the radiative cross sections σ_U and σ_L. These temperature dependent parameters are calculated by Equations 11 and 12. The extra divisor of four in the rate equation for n_b is discussed below.

$$d(n_a)/dt = I\ c(gu/gl\ \sigma_L\ n_b - \sigma_U\ n_a) + \gamma_a(n_{ae} - n_a)$$
$$- \gamma_{cn2}\ n_a + \gamma_{co2}\ n_c + w_a \tag{22}$$

$$d(n_b)/dt = I\ c(\sigma_U\ n_a - gu/gl\ \sigma_L\ n_b)/4$$
$$+ \gamma_a(n_a - n_{ae})/4 + \gamma_b(n_{be} - n_b) + w_b \tag{23}$$

$$d(n_c)/dt = \gamma_{cn2}\ n_a - \gamma_{co2}\ n_c + w_c \tag{24}$$

$$d(I)/dt = I\ c(\sigma_U\ n_a - gu/gl\ \sigma_L\ n_b) - I/\tau_{cav} + n_a\ w_s \tag{25}$$

where n_{ie} are thermal equilibrium number densities of CO_2 001 and 100 levels, and σ_U and σ_L are the effective radiative cross sections of the upper and lower laser levels.

The thermal population of N_2 was not included because no direct relaxation term (similar to γ_a) was found.

Rate Equation for n_b. The extra divisor of four in the rate for the population of the lower vibrational level, n_b, is based on the assumption that only one fourth of the CO_2 molecules that leave the upper vibrational level by stimulated emission enter the 100 level to increase n_b.

Stone assumed that only one fourth of the CO_2 molecules that relax from the upper vibrational level (001) enter the

34

100 level. These molecules enter one of the two 020 levels, and then very quickly thermalize to the other three vibrational levels in equilibrium with it (100, the other 020, and 010).

Stone continued to assume, however, that all of the CO_2 molecules that leave the upper vibrational level by stimulated emission enter the 100 level. This caused a problem in the energy balance, so this study assumes that only one fourth of the CO_2 molecules that leave the upper vibrational level by stimulated emission enter the 100 level to increase n_b. These CO_2 molecules from stimulated emission, like those from relaxation, are thermalized very quickly to equally fill all four levels (the 100, two 020, and 010 levels). The new rate equation for n_b is Equation 23 above.

Energy Balance to Calculate the New Temperature. The third major change to Stone's model is the set of energy balance equations to calculate the energy that goes into heating the gas, and the corresponding temperature rise. As explained in the literature review (pages 19), high temperature is detrimental to the laser, and lasing causes the temperature of the active medium to increase due to the transfer of vibrational energy to translational energy (heat) as the lower vibrational level (100) relaxes to ground state. The energy balance equations required to

calculate the increasing temperature are derived using the conservation of energy principle. The principle of conservation of energy maintains that the total energy input to the laser (pump energy) is equal to the sum of the energy accumulated in the laser (vibrational and translational energy) and the energy leaving the laser (photon energy). This study accounted for energy in six different "bins" and balances them to keep the total input equal to total accumulated plus total out. The six "bins" are pump energy; vibrational energies of n_a, n_b, n_c; photon energy; and translational (heat) energy.

Pump Energy. The first energy bin is pump energy. In the pulsed CO_2 laser model the pump is defined by the number of molecules pumped into excited vibrational states. In addition, a variable fraction of the pump energy also directly heats the gas and is accounted for. The pump energy is modeled by the following equations:

$$W = ((Wc + Wa)h\,\nu_3 + 4\,Wb\,h\,\nu_1) / (1 - f_h) \qquad (26)$$

$$TotPumpE(j) = TotPumpE(j-1) + W\,\Delta t \qquad (27)$$

where W is the rate energy is pumped into the laser medium, f_h is the fraction of pump energy that directly heats the gas, $TotPumpE(j)$ is the cumulative pump energy at step time step j, and Δt is the time step size in units of laser

36

cavity lifetime. The pump energy input to the laser is incremented at each time step until the pump is turned off.

Vibrational Energies. The next three energy bins are the vibrational energies. At each time step the total vibrational energy of the excited populations over and above the thermally excited populations of CO_2 and N_2 were also calculated as follows:

$$NaEng = (n_a - n_{ae})\ h\ \nu_3, \qquad for\ CO_2\ (001) \qquad (28)$$

$$NbEng = 4(n_b - n_{be})\ h\ \nu_1, \qquad for\ CO_2\ (100) \qquad (29)$$

$$N2Eng = (n_c - n_{ce})\ h\ \nu_3, \qquad for\ N_2\ (v=1) \qquad (30)$$

where NiEng is the energy density of the corresponding vibrational level added by the pump.

The factor of 4 in NbEng accounts for CO_2 vibrational levels 100, 010, and the two levels of 020. Assuming that the 100, two 020, and 010 levels are in equilibrium and equally populated, then the sum of the vibrational energy stored in each is equal to four times the energy stored in the 100 level.

Photon Energy. The fifth energy bin is photon energy. The total cumulative photon energy is calculate by

$$Energy(j) = Energy(j-1) + Power(j)\ \Delta t \qquad (31)$$

37

where Energy(j) is the cumulative photon energy (J/m^3) at
the jth time step, Power(j) is the current laser light power
(W/m^3), and Δt is the time step. This is a rectangular
approximation to integration using Simpson's rule (17:108).

Thermal energy. The sixth and last energy bin is
thermal (translational) energy. The pump energy that does
not appear as photons or vibrational energy appears as heat
in the laser medium and is calculated as follows:

$$TotHeatE(j) = TotPumpE(j) - (N2Eng(j) + NaEng(j)$$
$$+ NbEng(j) + Energy(j)) \qquad (32)$$

The new temperature is calculated from the thermal
energy using an equation derived from Wutzke:

$$T = T_{init} + TotHeatE(j) \, / \, (N_o \, k \, \Sigma(\psi_i \, Cv_i)) \qquad (33)$$

where T is the new temperature of the laser medium, T_{init} is
the initial temperature at time 0, TotHeatE(j) is the
cumulative thermal energy added to medium since time 0, and
Cv_i is the constant volume heat capacity of constituent i
(25:49).

Recalculation of the Temperature Dependent Parameters.
The fourth major change to Stone's model is the
recalculation of the temperature dependent parameters. Once

38

a new temperature is calculated, the temperature dependent
parameters (described in Chapter II) can be recalculated.
These temperature dependent equations were placed inside the
integration loop of the computer code to be recalculated
each time step. A review of the five sets of temperature
dependent equations used in the computer code follows.

Thermal Population of Excited Vibrational Levels.
The first set of temperature dependent equations is the
thermal population of the excited vibrational states. The
thermal equilibrium population of an excited vibrational
level at temperature T is described by Equation 11.

Thermal Populations of Rotational Levels. The
second set of temperature dependent equations that are
recalculated are the populations of rotational levels j = 19
and j = 20. Equation 12 is used to calculate f_u, the
fraction of CO_2 molecules in rotational level 19 for the
upper vibrational level (001), and f_l, the fraction in
rotational level 20 for the lower vibrational level (100).
Because the model assumed lasing in one cavity mode and on
line center only, these two fractions are the only sets of
CO_2 molecules that actually participate in lasing.

Relaxation Rates. The third set of temperature
dependent equations are the vibrational relaxation rates.
The temperature dependent relaxation rates were calculated

using the reciprocal of the time constants found in
Witteman's work:

$$\gamma_a = \gamma_{a'} \left(\frac{T}{300}\right)^{\frac{1}{2}} \exp\left[-h(\nu_3 - \nu_2 - \nu_1)\left(\frac{1}{k\,T} - \frac{1}{k\,300}\right)\right] \qquad (34)$$

$$\gamma_b = \gamma_{b'} \ (T/300)^{\frac{1}{2}} \exp\left[-h\ \nu_2\left(\frac{1}{k\,T} - \frac{1}{k\,300}\right)\right] \qquad (35)$$

$$\gamma_{cn2} = \gamma_{cn2'} \ (T/300)^{3/2} \qquad (36)$$

$$\gamma_{co2} = \gamma_{co2'} \ (T/300)^{3/2} \qquad (37)$$

where γ_i is the temperature dependent relaxation rate of
vibrational level i and $\gamma_{i'}$ is the relaxation rate at $300°K$
(24:165-6).

As mentioned in the literature review (page 14), the
rotational relaxation rates are assumed to be infinite.

Line Width. The fourth temperature dependent
parameter is the line width. Witteman's equation for line
width (Equation 18) was modified to change it to a constant
number density line width as opposed to Witteman's constant
pressure line width equation. The modification was derived
using the ideal gas law, $P = N_o kT$. Since the number
density is assumed to remain constant, the pressure is
proportional to temperature. Substituting for P in Equation
18 changed the $(300/T)^{\frac{1}{2}}$ term to $(T/300)^{\frac{1}{2}}$ as follows:

$$v = 7.85(\psi CO_2 + 0.73 \ \psi N_2 + 0.64 \ \psi He)P(T/300)^{\frac{1}{2}} \qquad (38)$$

40

where P is now the initial pressure. The form of this equation matches Brimacombe's constant number density line width (4:1672). This study choose Witteman's line width over Brimacombe's because Witteman was published four years later, and there is very little difference between the two equations.

Heat Capacity. The fifth and last temperature dependent parameter is the constant volume heat capacity of CO_2, calculated using Equation 20.

Summary of Model Development. In summary, the major changes to Stone's model operate in the following way. Beginning with the initial conditions, the model calculates the total energy supplied by the pump for one time step. It then calculates which bins that energy has been transferred to, and by subtraction, calculates the fraction of pump energy that heats the gas. Using the constant volume heat capacities of the gaseous components, the model then calculates the new temperature of the laser medium. At the beginning of the next time step, the model recalculates the temperature dependent parameters using the new temperature, and then begins the energy balance calculations again to find the next new temperature for the next time step.

Verification and Analysis

Verification is a set of internal tests to confirm the model is functioning as expected. Since Gilbert's and Stone's models were previously verified, this study verified only the three major changes to Stone's model and that those changes interacted correctly with the overall model. Thus verification occurred in the following five steps:

1. First, this study verified that the temperature did rise monotonically throughout the laser pulse.

2. Next, the adverse effects of the temperature rise on gain, power, and total energy in the pulse were verified.

3. Third, this study verified the effect of the thermal equilibrium populations.

4. Fourth, this study verified that changing the rate equation for n_b did change the pulse shape and the excited populations.

5. Last, this study verified that the overall computer code functioned correctly with the new changes.

In the following paragraphs, each verification step is presented and then analyzed.

Verifying the Temperature rise. The study first verified that the temperature did rise during the pump pulse and the laser pulse. The energy balance equations

calculated a temperature rise (Figure 10, page 56) that is proportional the pump energy, as expected.

Verifying the Effect of Temperature on Peak Gain. Next, the study verified the effect of temperature on peak gain (Figure 4). As expected, the peak gain decreased an order of magnitude as the initial temperature increased from 200 to 700°K. Although the temperature increases above the initial temperature throughout the laser pulse, the increase does not play a significant role because most of the

Peak Gain vs Init Temp
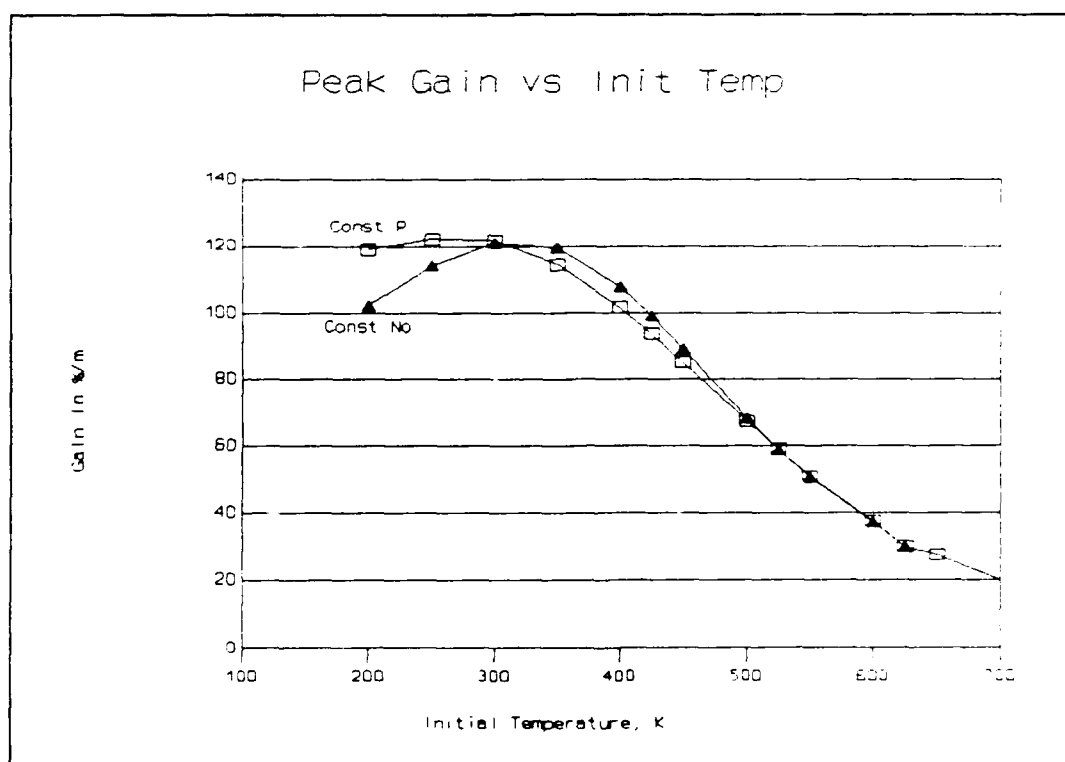
Figure 4. Peak Gain vs Initial Temperature. Const P = 1 atm; Const No = 2.44×10^{24}; Mix = 10% CO_2, 10% N_2, 80% He; Pump Eff = 0.2; Length = 1 m; Refl = 71.6%; Pump Pulse = 200 nsec, square; Losses = 0.

temperature rise occurs after the gain and power peak.
Figure 4 shows the gain does not decrease monotonically, but
peaks at about 300°K.

This local maxima in the gain curves may be due to three
competing factors that influence the gain: the populations
n_a and n_b; their relative relaxation rates, γ_a and γ_b; and
the radiation cross section, σ. Two of these parameters,
the populations and the radiative cross section, decrease
the gain with increasing temperature, but the effect of the
relaxation rates tends to help the gain at higher
temperatures.

These competing effects may be seen in the gain
equation, Equation 10, where the gain is directly
proportional to the population difference and σ, the
radiative cross section. As the temperature increases above
200°K, the relaxation rates of both n_a and n_b increase, but
γ_b increases faster than γ_a, possibly increasing the
population difference and thus the gain and power. However,
as the temperature increases above 300°K, both populations
n_a and n_b decrease through relaxation, decreasing the
potential population difference. In addition, the radiative
cross section decreases, further decreasing the gain. The
following table illustrates the change in ratio of
relaxation rates, σ, and gain with temperature at 1 atm
pressure and a gas mix of 10% CO_2, 10% N_2, 80% He.

Table I.   Gain vs Temperature

Temperature	γ_b / γ_a	σ_u (m^2)	Gain (%/m)
200°K	12	11.5 x10^{-24}	119
250°K	18	10.2 x10^{-24}	122
300°K	24	8.9 x10^{-24}	122
500°K	42	5.5 x10^{-24}	67.5
700°K	54	3.7 x10^{-24}	20.0

The difference between the peak gain at constant pressure and constant number density at low temperatures (shown in Figure 4) is probably a function of the total number density.   At high temperatures the effects of relaxation rates and radiative cross section overpower the effect of total number density.

Verifying the Effect of Temperature on Peak Power and Pulse Shape.   The study then verified the effect of temperature on peak power and pulse shape.   Figure 5 shows the peak power, at constant pressure and constant number density, which also reach a maximum at an intermediate temperature (about 350°K).   This behavior was not expected at first, and could not be confirmed in the literature. Since power is a function of gain, however, and observing the behavior of the gain, it is reasonable to expect the peak power to occur at an intermediate temperature.   With

45
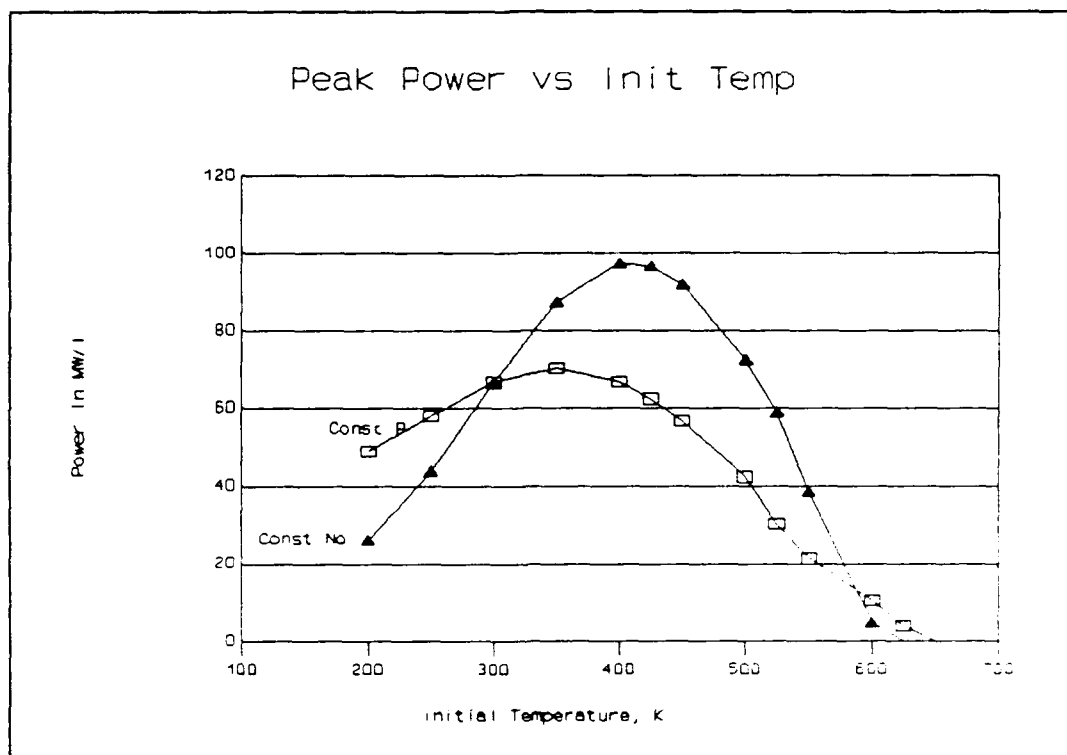
Figure 5. Peak Power as a Function of Initial Temperature. Same conditions as Figure 4.

the effect of number density removed (constant number density curve, Figure 5), the temperature has a much greater effect on the peak power. At temperatures below 300°K, the number density of CC_2 is higher for the constant pressure case, and the power is higher. At temperatures above 300°K, the pressure for the constant number density case is higher than 1 atm, so the relaxation rates and the number density are higher. These higher relaxation rates may enhance the peak power up to the point where the temperature kills the gain.

Figures 6 and 7 show the effect of initial temperature on the shape and timing of the laser pulse over the temperature range of 200 to 600°K for both constant pressure and constant number density.

Pulse Shape vs Temperature
Constant Pressure
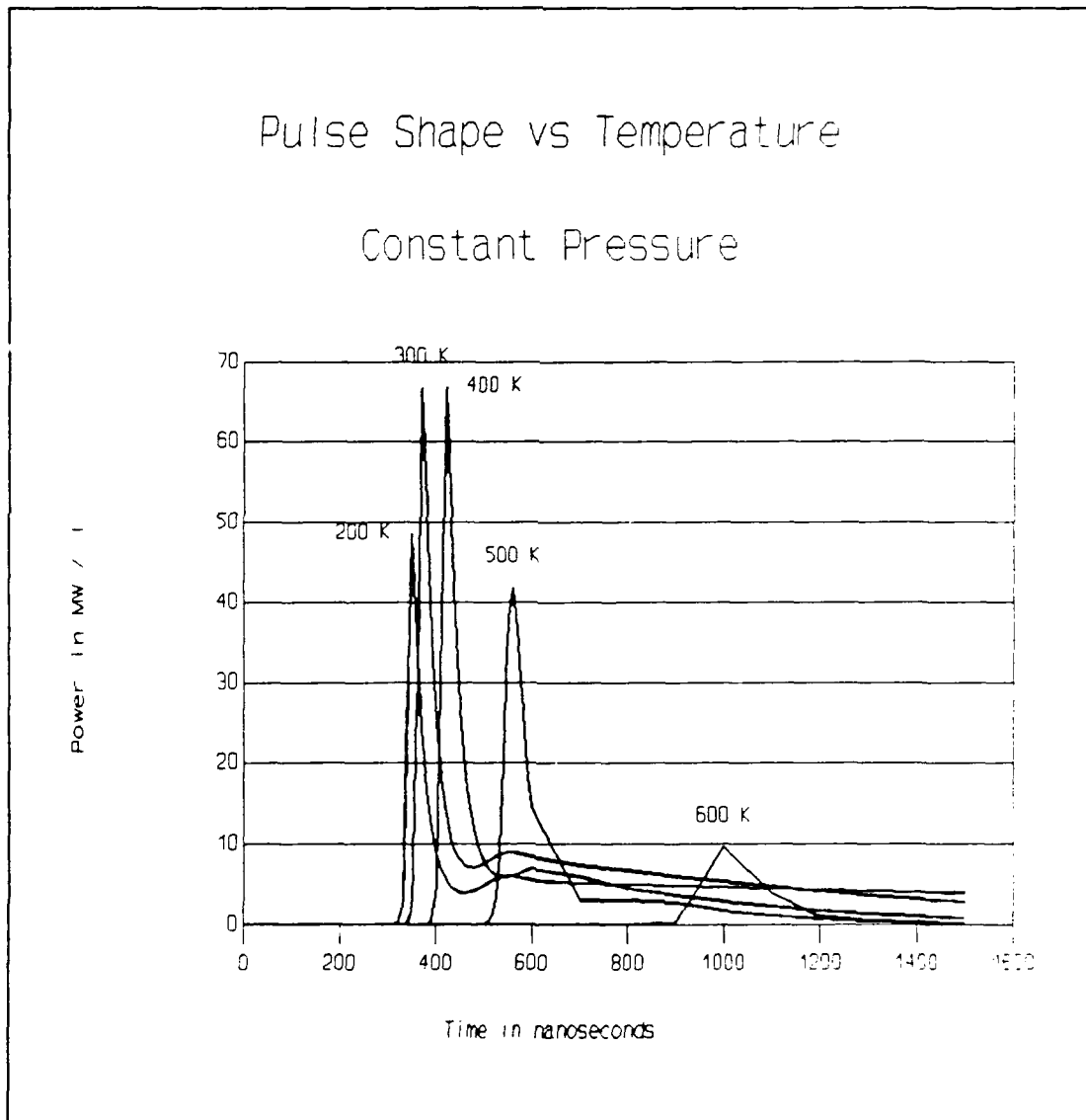
Figure 6. Laser Pulse Shape vs Initial Temperature at Constant Pressure of 1 atm. Mix = 10% CO_2, 10% N_2, 80% He; Pump Eff = 0.2; Length = 1.0 m; Refl = 71.6%; Pump Pulse = 200 nsec, square; Losses = 0%.

47
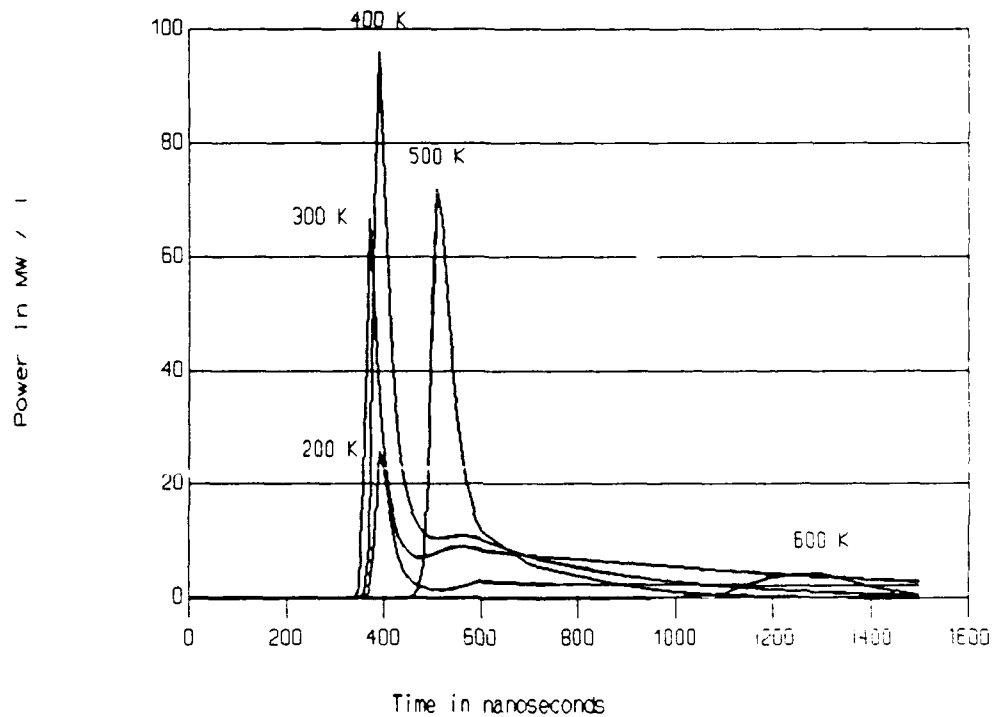
Figure 7. Laser Pulse Shape vs Initial Temperature at Constant Number Density. No = $2.44 \times 10^{25}/m^3$, Pressure = 1atm*(Temp/300). Other conditions same as Figure 6.

Again, the effect of temperature is much more pronounced for the constant number density case.

Figures 8 and 9 show the effect of initial temperature on the shape and timing of the laser pulse at both low and high pressures.
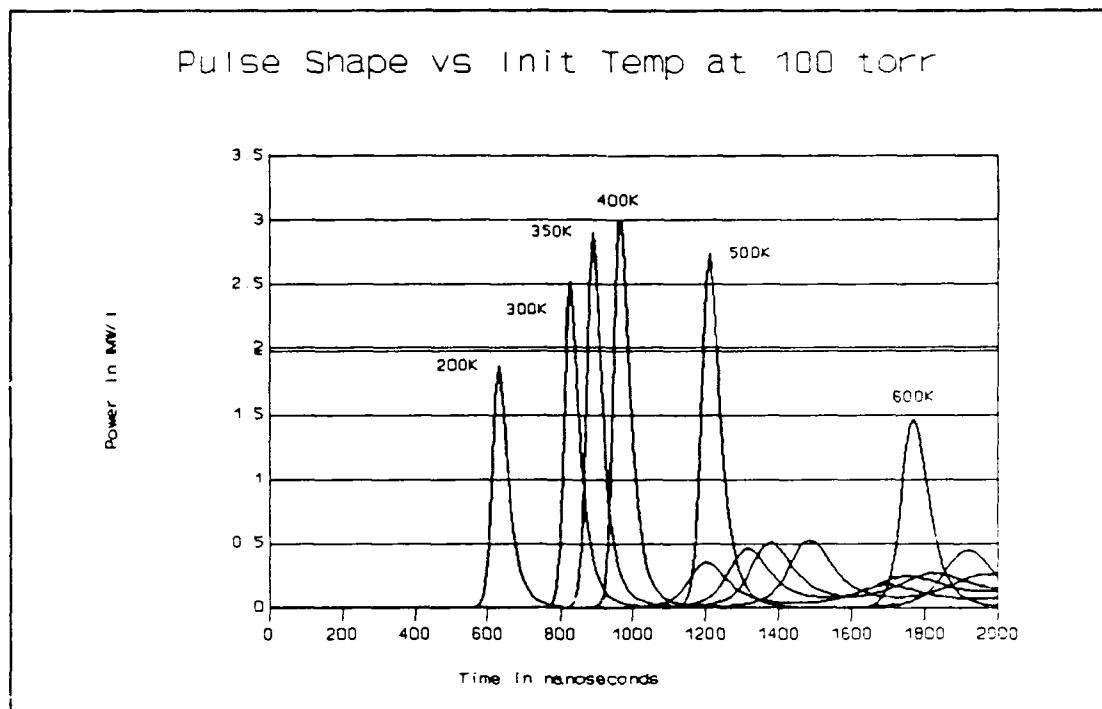
Figure 8. Laser Pulse Shape vs Initial Temperature at Low Pressure (100 torr). Other conditions same as Figure 6.
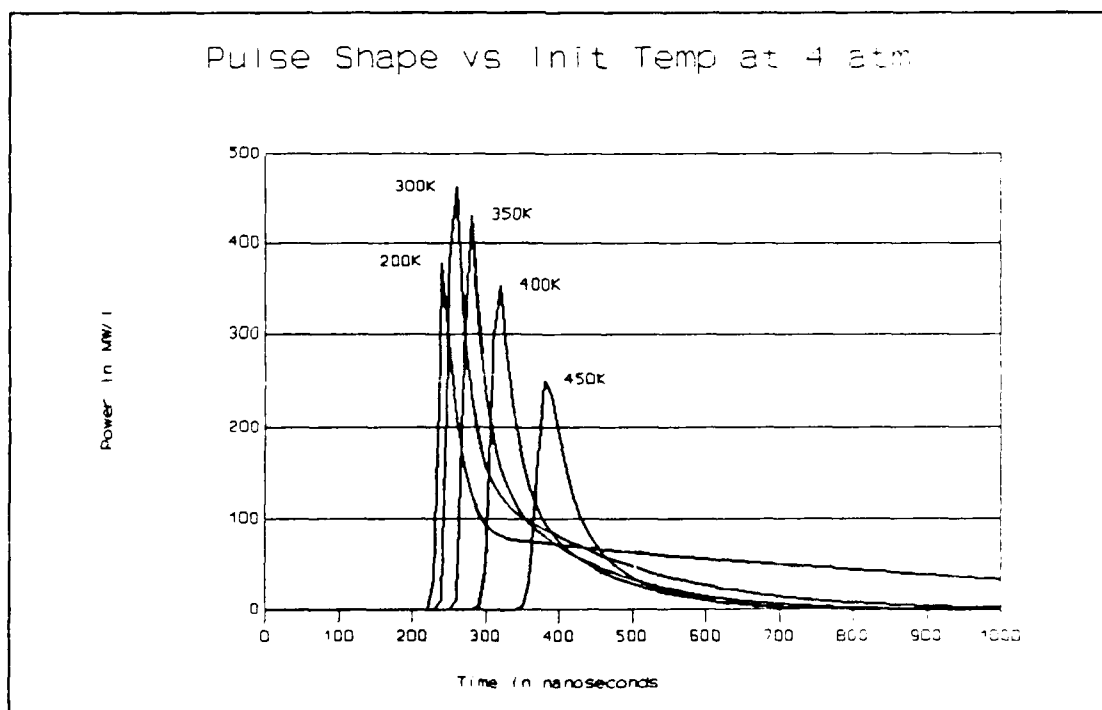
Figure 9. Laser Pulse Shape vs Initial Temperature at High Pressure (4 atm). Other conditions same as Figure 6.

49

Another effect of temperature on the power is that the rising temperature during the laser pulse decreases the energy in the tail portion of the pulse and causes the pulse to terminate sooner. Figure 10 shows the calculated temperature rise during a high energy laser pulse. Figure 11 compares a constant temperature laser pulse against the rising temperature pulse.
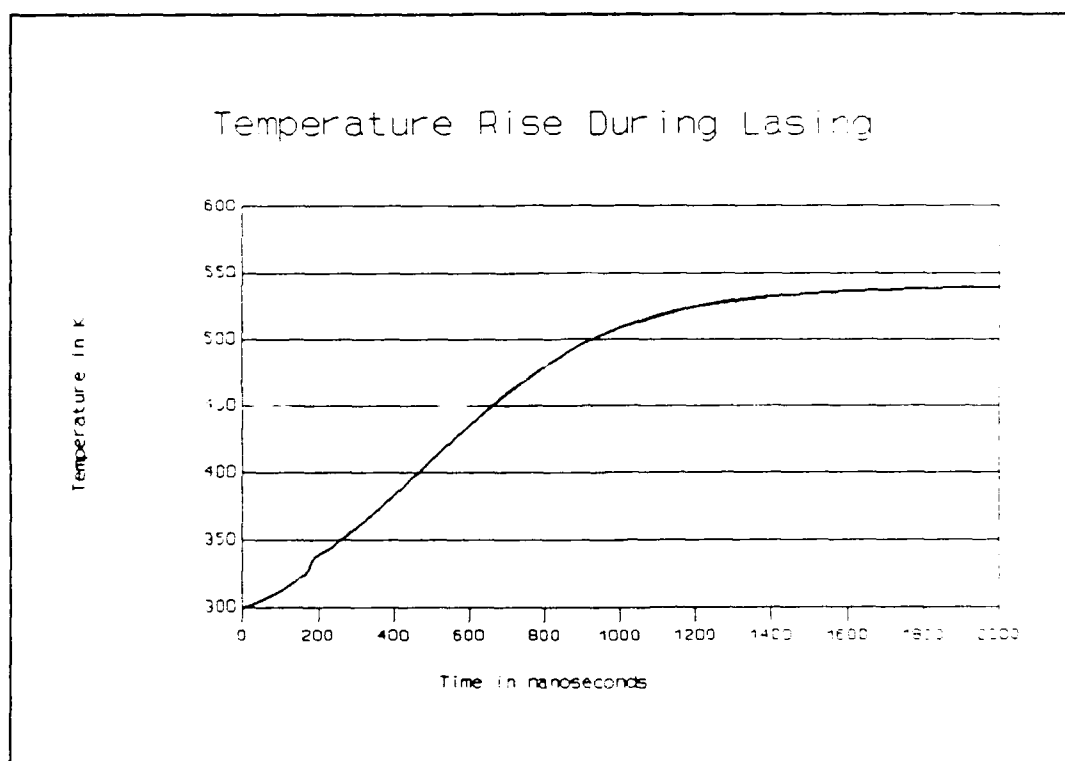
Figure 10. Calculated Temperature Rise During the Laser Pulse for the Rising Temperature Pulse (Pulse 1) in Figure 11.
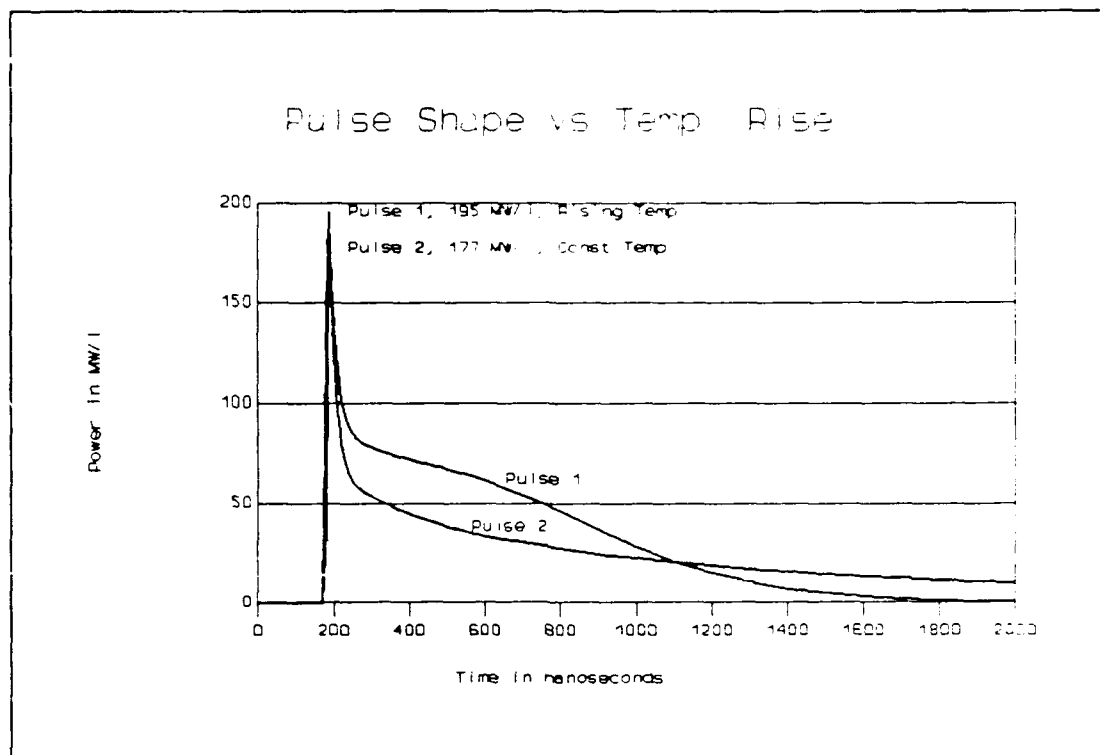
Figure 11. Comparison of Laser Pulse Shapes, Rising Temp (Pulse 1), Const Temp (Pulse 2). P = 1 atm; T = 300°K; Mix = 17% CO_2, 33% N_2, 50% He; Pump Eff = 0.4; Length = 1.0 m; Refl = 71.6%; Pump Pulse = 200 nsec, square; Losses = 0%.

The rising temperature in pulse 1 increases the relaxation rates, which drains the energy out of the upper vibrational level, n_a, and reduces the height and length of the tail portion of the laser pulse.   Figure 12 shows the effect of the temperature rise on the excited CO_2 populations, n_a and n_b.

51
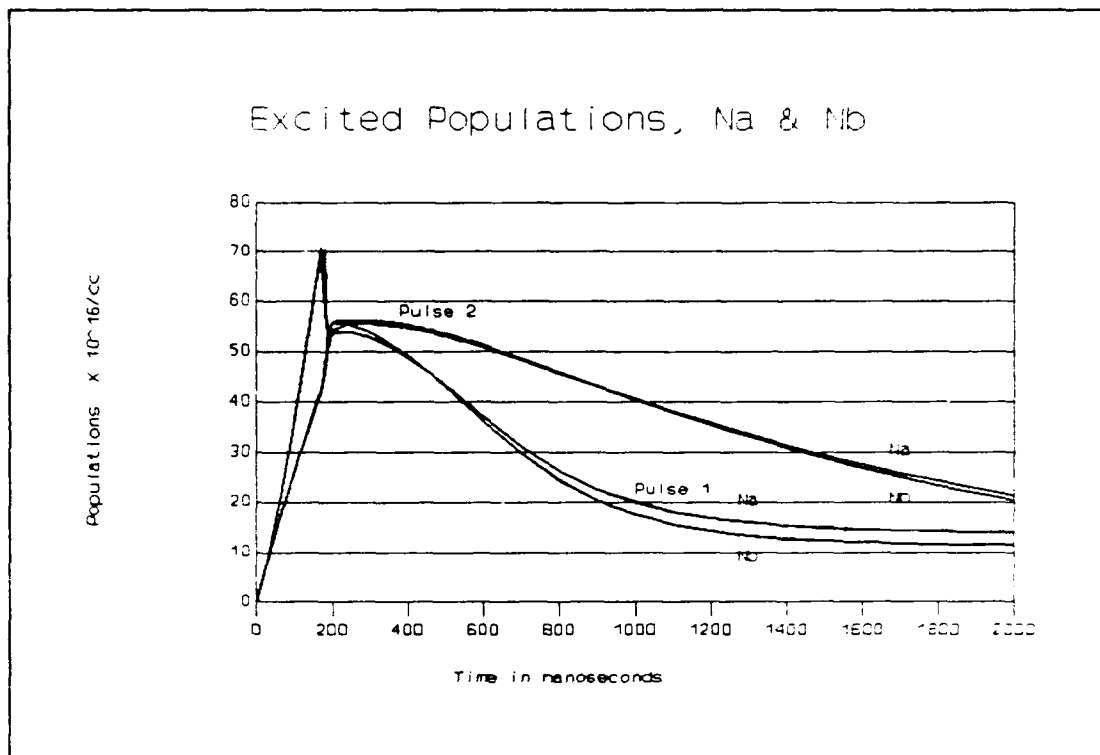
Figure 12. Populations of the Upper Vibrational Level, n_a, and the Lower Vibrational Level, n_b, for the Rising Temp (Pulse 1) and the Const Temp Pulses (Pulse 2) in Figure 11.

Although the absolute populations of the upper and lower vibrational levels, n_a and n_b, are affected immediately after the laser spike, the gain is not. The gain in both the constant temperature and the rising temperature pulses are nearly identical out to about 2000 nanoseconds, where the increasing temperature begins to shut down the gain of the rising temperature pulse. The increased temperature shuts down the gain by rapidly draining n_a and increasing the thermal population of n_b.

<u>Verifying the Effect of Temperature on Energy</u>. The last laser parameter to be affected by temperature is the energy of the laser pulse. Unlike the power and gain, the total energy in the laser pulse does not peak at an intermediate temperature, but decreases steadily with temperature as shown in Figure 13. This was expected, and occurs because
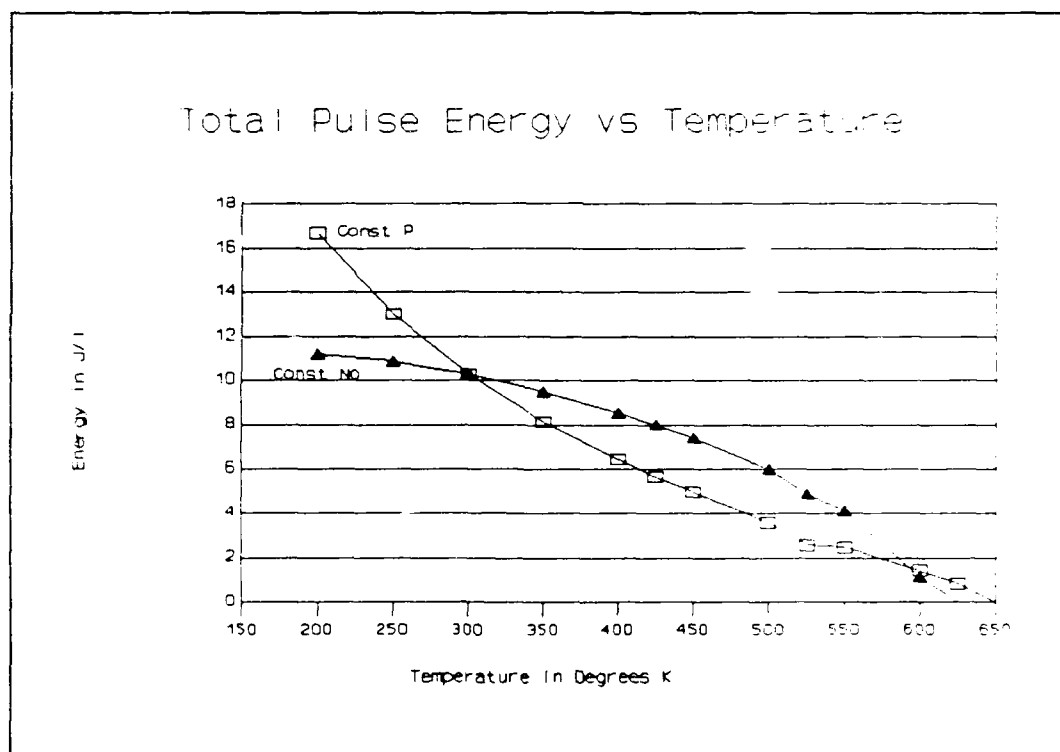
Figure 13. Total Energy in the Laser Pulse vs Initial Temperature. Const P = 1 atm, Const Nc = $2.44 \times 10^{25}/m^3$; Mix = 10% CO_2, 10% N_2, 80% He; Pump Eff= 0.2; Length = 1.0 m; Refl = 71.6%; Pump Pulse = 200 nsec, square; Losses = 0%.

the number of CO_2 molecules available to lase decreases with temperature at constant pressure. Even when the number density of CO_2 is held constant, the total laser energy still decreases with increasing initial temperature as shown

53

in Figure 13. The energy available in the upper vibrational
level drains out faster through relaxation at higher
temperatures and is unavailable for lasing.

Verifying the Effect of the Thermal Equilibrium
Populations of the Excited States. The third major change
that this study verified is the effect of the thermal
equilibrium populations, n_{ae} and n_{be}, on the excited
populations during lasing. This effect is best seen at high
temperature. Figure 14 shows n_a and n_b for a pulse at
600°K.
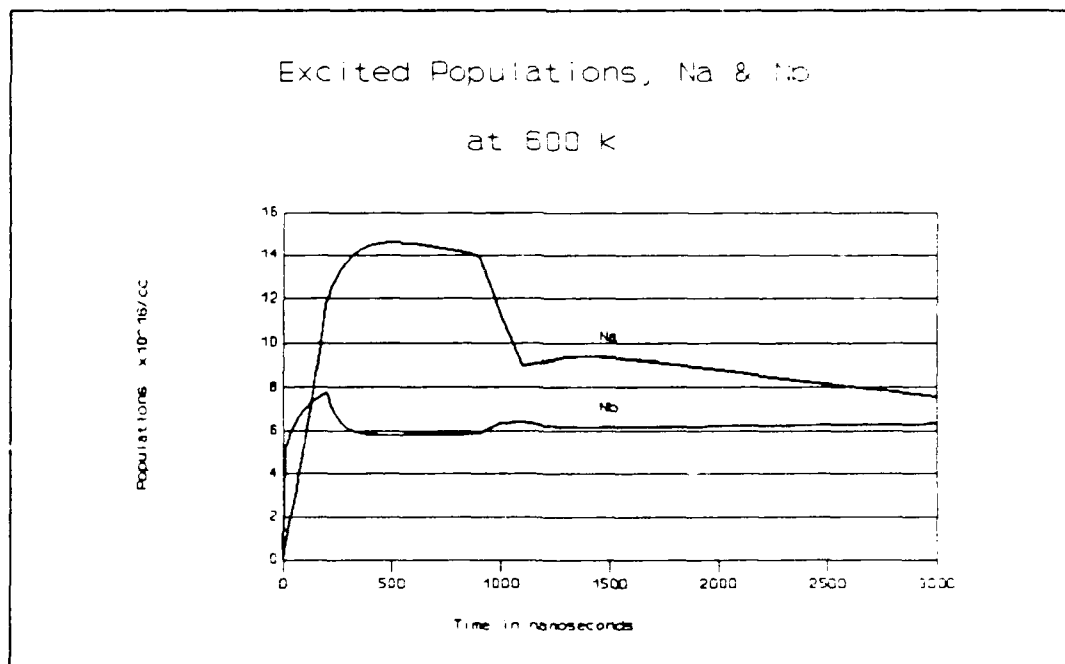
Figure 14. Upper and Lower Vibrational Populations, n_a
and n_b, at 600°K. P = 1 atm; Mix = 10% CO_2, 10% N_2, 80% He;
Pump Eff = 0.2; Length = 1.0 m; Refl = 71.6%; Pump Pulse
= 200 nsec, square; Losses = 0%.

At time 0, n_b starts at its thermal population for 600°K (5×10^{16}/cc), and is pumped up from there. After the pump pulse, it quickly drains back down to its thermal population (6×10^{16}/cc) for the current temperature in the laser (about 630°K). The laser spike barely effects n_b and it remains at its thermal population (6×10^{16}/cc) for the current temperature for the rest of the pulse. n_a, on the other hand, is pumped far above its thermal population and lases. It eventually relaxes down to its thermal population of about 0.7×10^{16}/cc at the end of the run.

Verifying the Effect of the New Equation for n_b. The fourth major change to Stone's model that this study verified is adding the divisor of four to the photon flux term in the differential equation for n_b. This equation will be referred to as the new rate equation for n_b (Equation 23). As expected, the additional divisor of four in the rate equation for n_b had a significant effect on the peak power and the populations of n_a and n_b after the power peaks. It was not expected, however, that there would be no effect on the gain. Figure 15 shows the populations n_a and n_b throughout the laser pulse for both the old and new equation for n_b.

The populations n_a and n_b are much lower after the pulse spike using the new equation. This occurs because only one fourth of the CO_2 molecules that transition from 001 due to
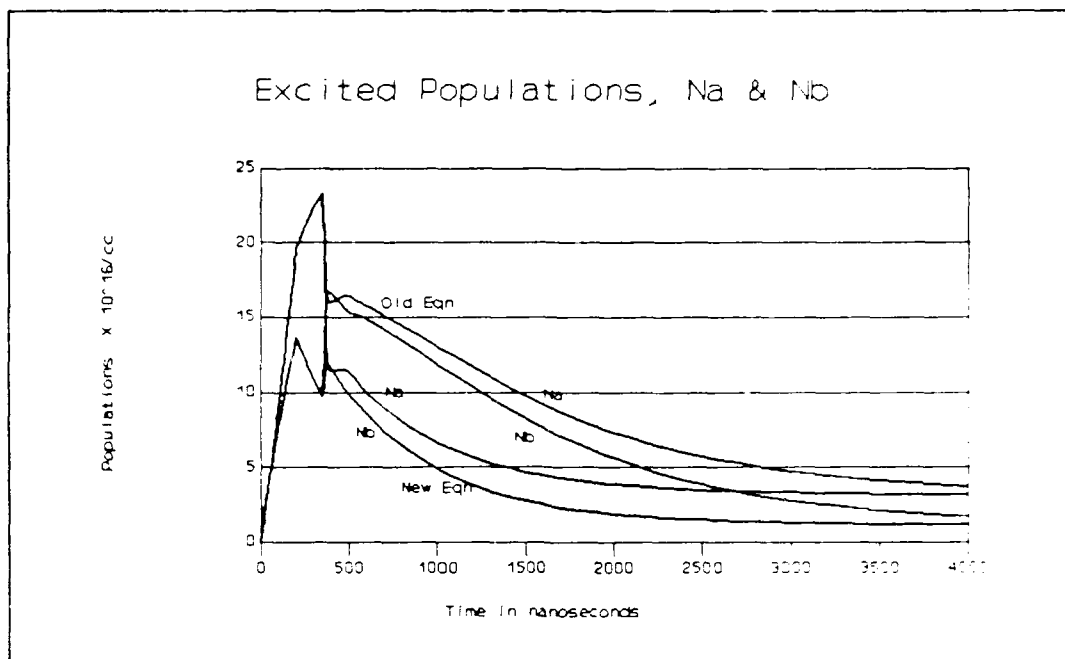
Figure 15. Upper and Lower Vib Pops, n_a and n_b, Calc by Old Eqn for n_b, and New Eqn for n_b. $P = 1$ atm; $T = 300°K$; Mix = 10% CO_2, 10% N_2, 80% He; Pump Eff = 0.2; $L = 1.0$ m; Refl = 71.6%; P.P. = 200 nsec, sqr; No Loss.

stimulated emission enter 100. Thus, n_b grows to only one fourth it's original value during the laser pulse spike, but n_a is driven down to meet n_b. The extra molecules in 001 that respond to stimulated emission add to the laser spike and increase the peak power 77%.

The gain, however, is nearly identical in each case. The gains for the old and new equation are nearly identical because the gain is proportional to the population difference, which stays approximately the same (Figure 15).

Verifying the Overall Computer Code. Finally, this study verified that the overall computer code functioned correctly with the new changes. This was done by varying

56

all ten input parameters and observing the resulting laser pulse, temperature change, and the upper and lower laser populations, n_a and n_b. In each case, the results were consistent with the input parameters.

Validation and Analysis

Validation involves a set of external tests to compare the calculated output with actual laser output and with other CO_2 laser models. This study validated three areas of the model: power and energy vs temperature, the temperature rise, and the pulse shape.

Validating the Power and Energy vs Temperature. This study first validated the relationship of power and energy vs temperature (Figure 16). Witteman stated that the pulsed laser's output begins to decrease above about $450°K$ (24:3). In studying the CW laser, Fowler found that the power drops off sharply at higher temperatures ($500 - 700°K$). Since the pulsed laser depends on the same mechanisms to produce laser power, its power and total energy should also drop off sharply at higher temperatures. Figure 16 shows both the power and total energy of this pulsed model decrease sharply toward zero at $600+°K$.

The power and energy of the pulse decrease with temperature because the number density decreases, the
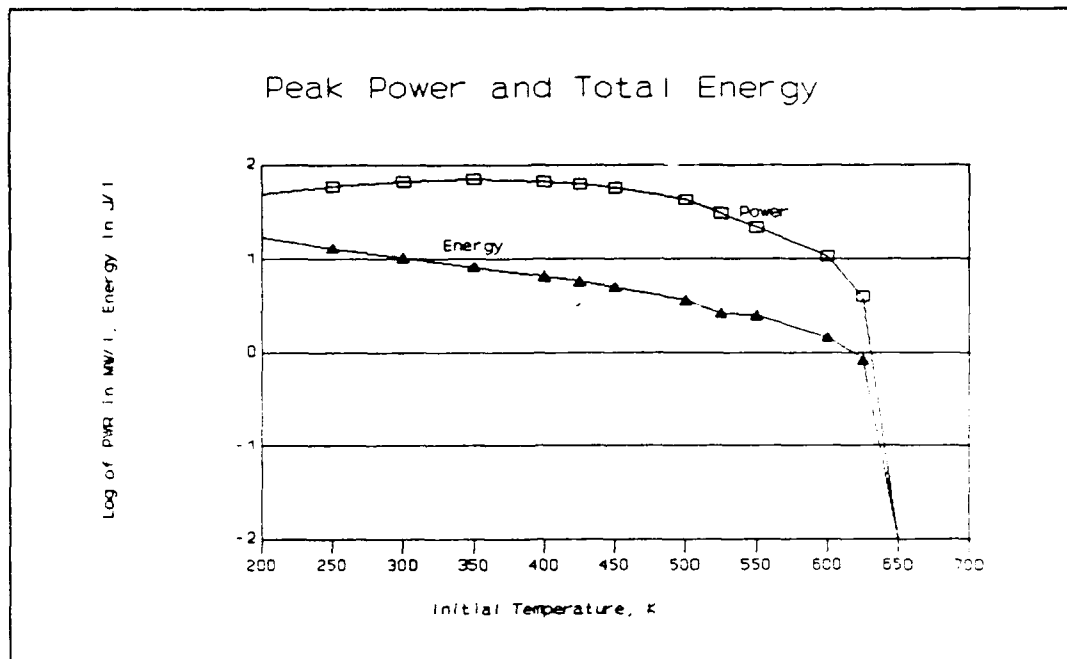
Figure 16. Peak Power and Total Pulse Energy vs Initial Temperature. P = 1 atm; Mix = 10% CO_2, 10% N_2, 80% He; Pump Eff = 0.2; Length = 1.0 m; Refl = 71.6%; Pump Pulse = 200 nsec, square; Losses = 0%.

relaxation rates increase, and the gain substantially decreases. When the gain drops below the threshold gain, the laser shuts down.

At low temperatures (200°K), the power should increase 20 - 50% according to Mitsuhiro for the CW laser (13:68). Drobyazko showed that at 200°K, the total pulse energy increased 50% for a pulsed laser (8:29). Figure 13 on page 53 shows my model calculated a 62% increase in total pulse energy at 200°K at constant pressure, and a 9% increase at constant number density. The increase in number density at constant pressure and low temperature accounts for most of the increase in the total pulse energy. At constant numbe⁻

58

density, the reduced relaxation rates at low temperature
probably account for the small increased total energy.

Validating the Temperature Rise. This study next
validated the temperature rise. Milonni's pulsed CO_2 laser
model included an energy balance and he calculated a 'inear
temperature rise from $300°K$ to $500°K$ in 25 microseconds
during the pump pulse (15:3695). Fedorov also calculated
the same linear temperature rise during the pump pulse
(9:630). This study duplicated Fedorov's conditions (a 30
μsec pump pulse of 250 J/l and mix of 3:2:1 $He:N_2:CO_2$) and
obtained a linear temperature rise from 300 to $550°K$ during
the pump pulse.

Validating the Pulse Shape. Last, this study validated
the pulse shape against data supplied by Manes. Manes used
a five-level model of a TEA pulsed CO_2 laser to calculate
pulse shape for different initial conditions. He made three
sets of three runs each. In the first set he set the cavity
length to 0.48 meter, and varied the pump energy. In the
second set, he set the cavity length to 2.5 meters and
varied the pump energy. For the last set of runs, he kept
the pump energy and cavity length constant and varied the
gas mix. He compared his model with the output from an
experimental pulsed CO_2 laser and found "good agreement"
(14:5077). He did not include the rise in temperature in
the laser medium because he found the rise to be only about

59

$50°K$ and to have little effect (14:5075). In duplicating his conditions, this study found the largest temperature rise to be $125°K$, and the average to be $70°K$.

Throughout the nine test runs duplicating Manes' initial conditions, the change in peak power and delay time always agreed with the trend in Manes' calculated output. In addition, the relative size and structure of the tail portion of the pulse agreed with Manes' calculations (Figures 17 to 22).

In each of the Figures showing the calculated pulse shapes for comparison against Manes' pulse shapes, P.E. is the pump energy for that pulse, in J/l.
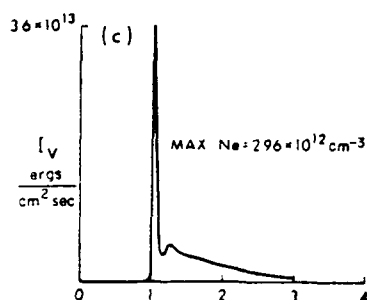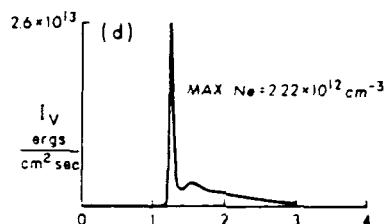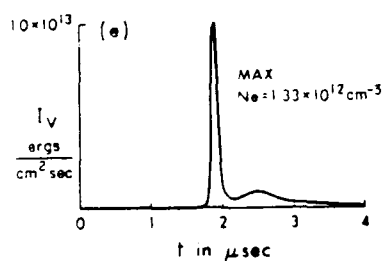
Figure 17. Pulse Shape vs Pump Energy from Manes' Study. Length = 0.48 m; Pressure = 1 atm; Temperature = 300°K; Mix = 10% CO_2, 10% N_2, 80% He; Refl = 74%; Pump Pulse = 1 μsec, sin shape; Losses = 0%.   Reprinted from (14:5074)

61

Calculated Pulse Shape

Resonator Length = 0.48 m
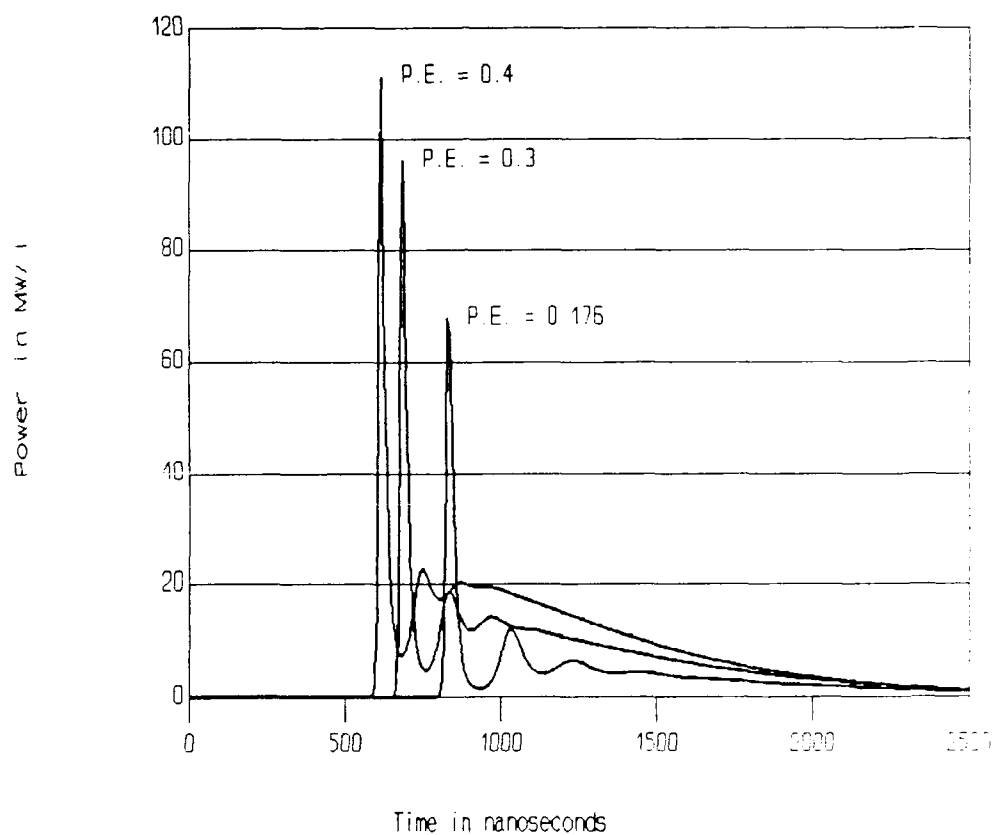
Figure 18. Calculated Pulse Shape as a Function of Pump Energy. Resonator Length = 0.48 m. Same conditions as Figure 17.

Peak Power =
22 MW/l

4.0×10^{13}

I_V
$\frac{ergs}{cm^2 sec}$

MAX. Ne $= 1.63 \times 10^{12} cm^{-3}$

(a)

0   1   2   3   4

500 nsec/div.

Peak Power =
11 MW/l

2.0×10^{13}

I_V
$\frac{ergs}{cm^2 sec}$

MAX. Ne $= 0.74 \times 10^{12} cm^{-3}$

(b)

0   1   2   3   4

500 nsec/div.

Peak Power =
5 MW/l

0.9×10^{13}

I_V
$\frac{ergs}{cm^2 sec}$

MAX. Ne $= 0.44 \times 10^{12} cm^{-3}$

(c)

0   1   2   3   4

200 nsec/div

t in μsec
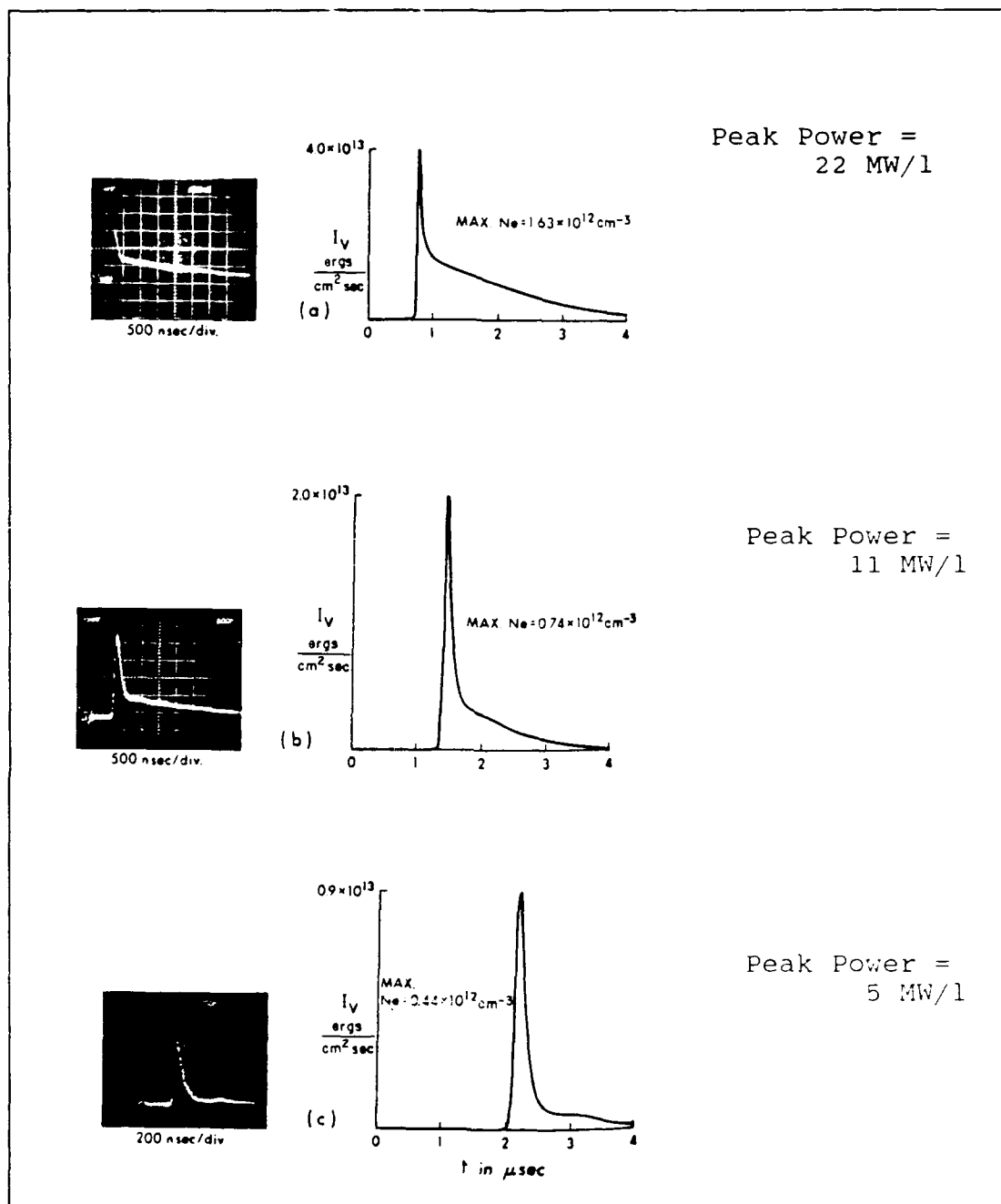
Figure 19. Pulse Shape vs Pump Energy from Manes' Study. Length = 2.5 m; Pressure = 1 atm; Temperature = $300^\circ K$; Mix = 10% CO_2, 10% N_2, 80% He; Refl = 70%; Pump Pulse = 1 μsec, sin shape; Losses = 0%.   Reprinted from (14:5074)

63

Figure 20. Calculated Pulse Shape as a Function of Pump Energy. Resonator Length = 2.5 m. Same conditions as Figure 19.
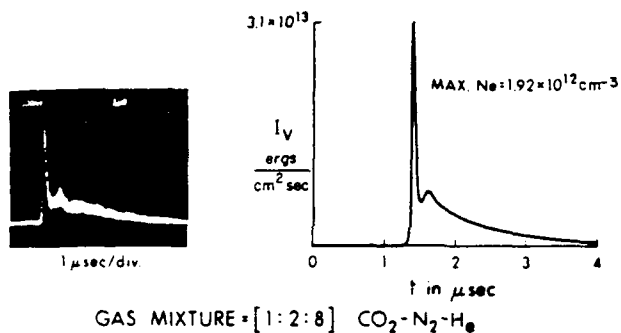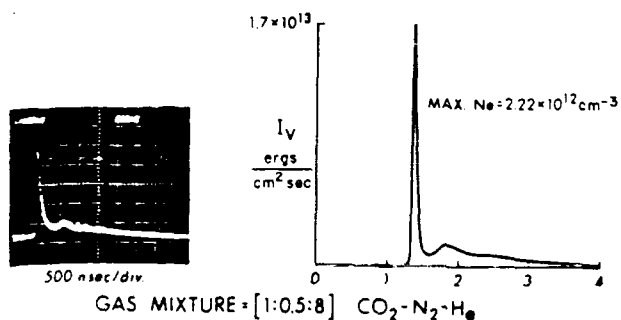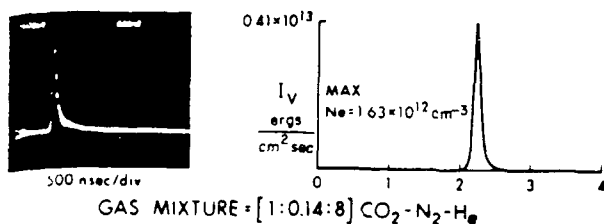
Figure 21. Pulse Shape vs Gas Mix from Manes' Study. Length = 0.48 m; P = 1 atm; T = 300°K; Refl = 74%; Pump Pulse = 1 μsec, sin shape; Losses = 0%. Reprinted from (14:5075)
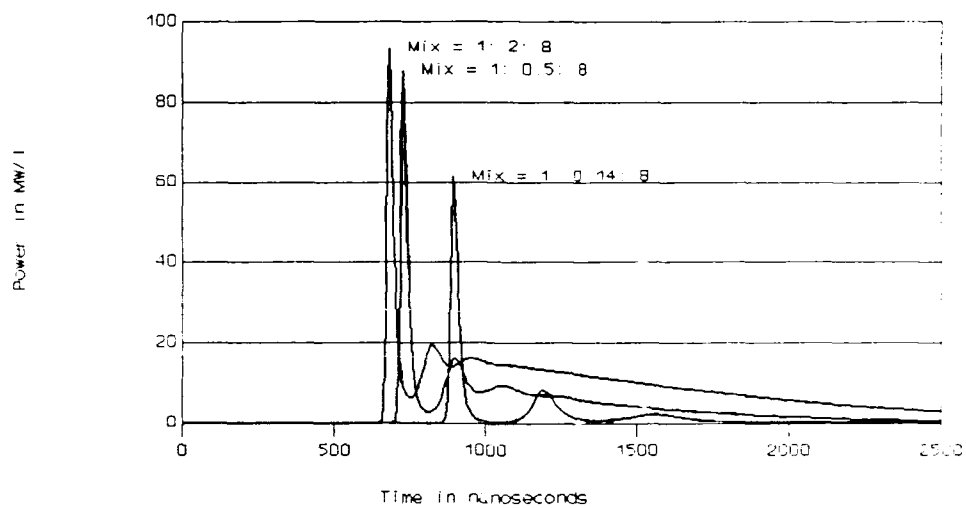
Figure 22. Calculated Pulse Shape as a Function of Gas Mix. Resonator Length = 0.48 m. Same conditions as Figure 21.

Thus, under Manes' initial conditions, the author's

model is able to meet its goal of correctly showing trends

in the shape and delay of the laser pulse. The largest

difference in power between Manes' calculations and this

model's is about 69%, and occurs during the set of runs

where the gas mix is varied. The largest difference in

delay time (60%) also occurs while varying the gas mix.

This study also validated the pulse shape against

Witteman's experimental and model data, both of which

include a temperature rise. The actual output of Witteman's

small pulsed CO_2 laser is shown in Figure 23.
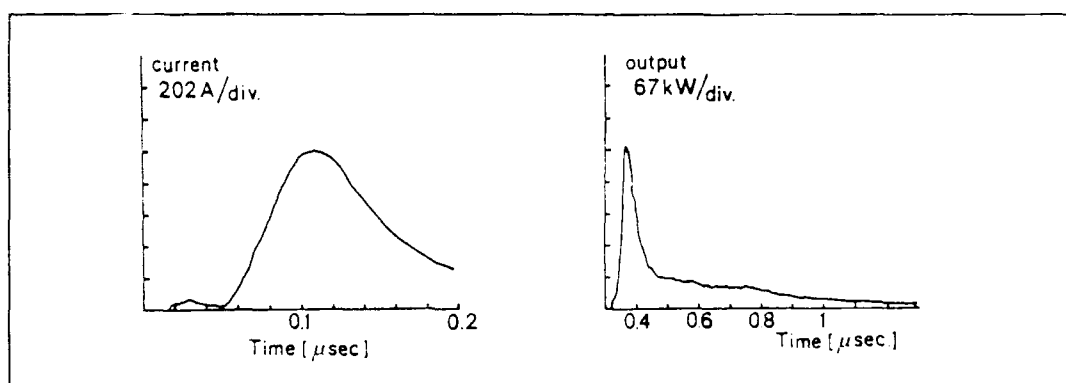
Figure 23.   Experimental Pump Pulse and Laser Pulse. P =
1 atm; T = 300°K; E/N = 5.2×10^{-16} V-cm2; Active L = 13 cm;
Elctrd Gap = 0.56 cm; Optical L = 24 cm; Mix = 20% CO_2, 20%
N_2, 60% He; Refi = 78%.   Reprinted from (24:167)

The calculations of output power and gain from

Witteman's five-level model are shown in Figure 24.

This study duplicated Witteman's conditions, then varied

pump efficiency to match the peak power and delay time of

67
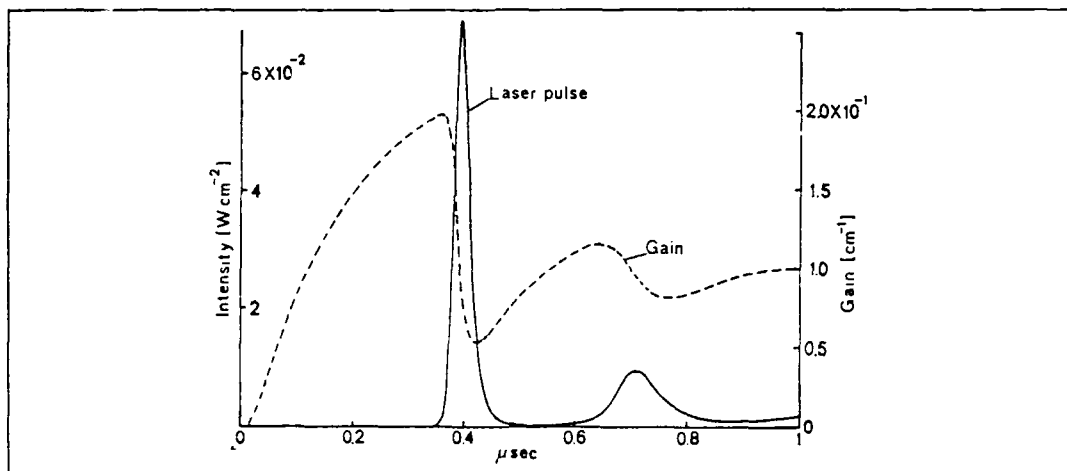
Figure 24. Calculated Laser Pulse and Gain from Witteman's Five-Level Model, same conditions as the Experimental Laser in Figure 23. Reprinted from (24:168)

Calculated Power and Gain
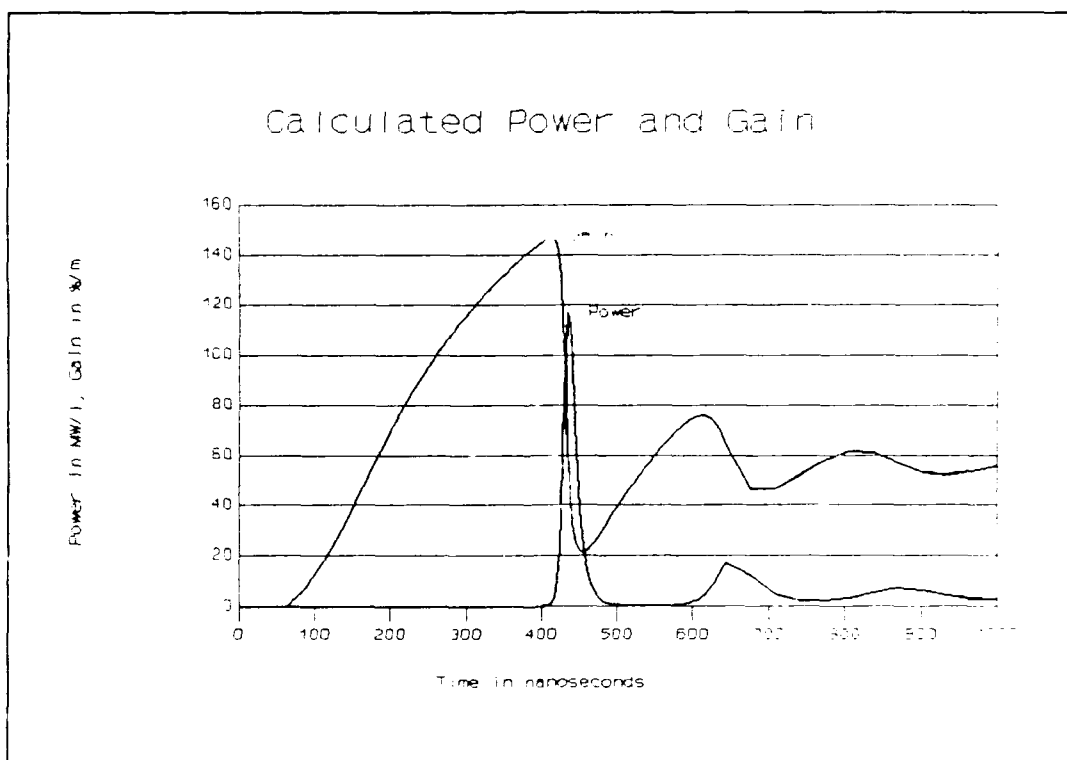
Figure 25. Calculated Laser Pulse and Gain using Four-Level Model, Duplicating the Conditions of Figure 23. Pump pulse = 200 nsec, sin shape; Pump Eff = 0.1; Losses = 2%.

the experimental laser in Figure 23. Figure 25 shows this

68

model's calculated power and gain.

The shape and timing of this model's calculated power and gain curves are very close to Witteman's calculations. However, the absolute value of Witteman's peak power and gain do not match either the experimental laser or this model's calculations. It is possible that there is an error in the label on Witteman's axis. This four-level model, however, approximated the shape produced by Witteman's five-level model very closely under the conditions listed in Figure 23.

Summary of Validation. In each validation, the trends calculated by the model were correct. The model correctly calculated a linear temperature rise during the pump pulse, and correctly predicted the change in power and energy of the laser pulse as the temperature changed. Last, the model correctly calculated the change in pulse shape, both peak power and delay time, over a wide input parameter space.

Limits of the Model

This pulsed CO_2 laser model is intended to show trends, and Gilbert's original assumptions introduce an error factor of about two compared to actual laser output. The changes incorporated in the author's model may have improved that somewhat. The first limitation to the author's model then, is that imposed by the assumptions used in building the

model. Gilbert's assumptions that limit the author's model are those inherent in the four-level model, the point model, fast vibrational and rotational equilibrium, and sparsely excited molecular states.

Four-level Model. The first limit to this thesis model is the use of the four-level model. The foundational assumption for a four-level model is that the relaxation rate between the 100 and 020 vibrational levels of CO_2 is very fast, and that the 100, two 020, and 010 levels are roughly in equilibrium and equally populated.

Witteman, however, stated that the 100 and 020 levels are not equally populated throughout the laser pulse and that a five-level model is necessary to model a pulsed CO_2 laser (24:68). Witteman built a five-level model and modeled a pulsed laser, calculating the vibrational temperature of each level throughout the pulse (Figure 26).

In Figure 26, T_1 (100) and T_2 (020) are nearly identical except at the peak of the laser pulse, where $T_1 = 550°K$ and $T_2 = 425°K$. Those vibrational temperatures translate to populations of 2.9% and 1.0%, respectively. Therefore, the populations of 100 and 020 are indeed not equal during the peak of the laser pulse.

However, these unequal populations had little effect on the shape of the laser pulse, as demonstrated during the validation against Witteman's model (Figures 24 and 25).
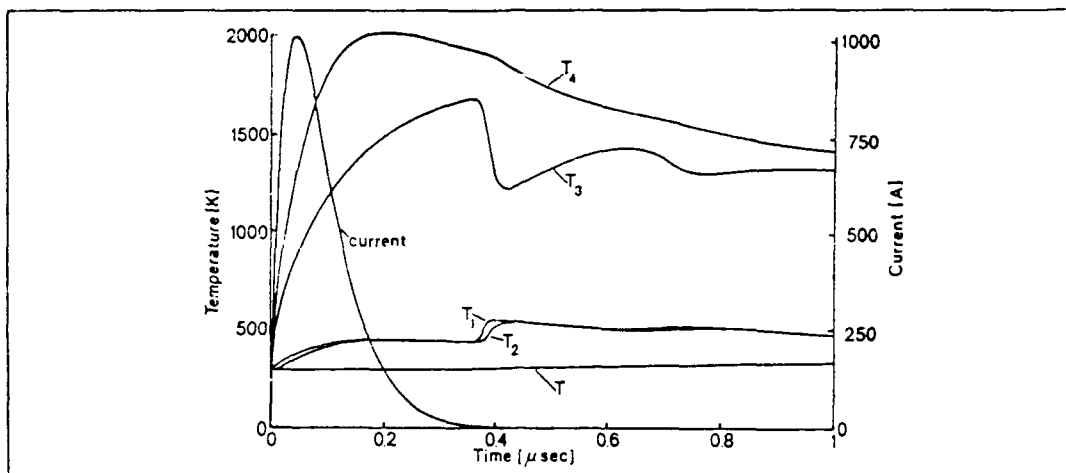
Figure 26. Calculated Vibrational Temperature from Witteman's Five-Level Model. T_1 = Vib Temp of CO_2 100, T_2 = Vib Temp of CO_2 020, conditions are same as Figure 23. Reprinted from (24:168)

The shape and timing of the pulse produced by this four-level model is very close to the pulse produced by Witteman's five-level model, under the conditions of Figure 25.

The four-level model was also compared against Manes' five-level model. In discussing his five-level CO_2 model, Manes found that his output was very sensitive to the relaxation rate between the 100 and 020 levels (14:5077). Although Manes found this sensitivity to the 100 to 020 rate, this four-level model correctly calculated every trend in pulse shape and delay time for each of the nine runs. The author's model agreed quantitatively with his to ± 60% in both peak power and pulse delay.

Point Model. The second limit to this thesis model is the use of the point model. Since the point model assumes

71

homogeneous flux throughout the cavity, gain should be
limited to about 100%/m, the laser cavity length to less
than 1 meter, and the output mirror reflectivity to greater
than 50%. However, during validation of the pulse shape
against Manes' calculations, the author's model accurately
calculated the pulse shape for a 2.5 m laser with a peak
gain of 91%/m. In addition, the model very accurately
calculated the pulse shape for a 0.24 m cavity with a peak
gain of 150%/m while validating against Witteman's data
(page 67). In both cases the output mirror reflectivity was
greater than 50%. Perhaps, then, a better limit on the gain
and length of the cavity is that the product of the gain (in
%/m) and length (in m) be limited to about 200%.

Fast Vibrational and Rotational Relaxation. The third
limit to this thesis model is the assumption of fast
vibrational and rotational relaxation. As long as the pulse
forming process occurs in tens of nanoseconds the assumption
of fast vibrational relaxation will not be violated because
the vibrational relaxation takes tenths of nanoseconds.

For rotational relaxation (exchange), Drobyazko
calculated the effect on the pulse shape for both infinite
(fast) and finite rotational exchange. He found at 114 torr
that the pulse peaked about 50% lower for a finite
rotational exchange rate vs a "fast" rate, and the finite

rate pulse matched the experimental pulse extremely well (8:28).

The reason there is a difference in peak power between the two exchange rates is that the calculated population of CO_2 molecules in the $j = 19$ rotational state in the upper laser level is a function of the rotational exchange rate. If the rate is assumed to be infinite, then the population of $j = 19$ is instantly replenished by collisions as lasing depletes the $j = 19$ population, and the $j = 19$ population remains at its thermal equilibrium value (f_U).

If the rotational exchange rate is finite, however, the replenishment by collisions is not instant, and the population of $j = 19$ is a function of the competing rates of replenishment by collisions and depletion by lasing. Replenishment requires that a CO_2 molecule in the upper vibrational level collide and have its rotational energy altered to $j = 19$. This process takes some time and is one of the determining rates for the actual (reduced) population of $j = 19$ during lasing. Rotational exchange becomes faster at higher pressures and higher temperatures because collisions occur more frequently, and the assumption of fast rotational exchange '   ,es better.

The consequence of assuming fast rotational exchange is that the author's model may overestimate the peak power by up to 50% at low (100 torr) pressures (8:28).

Sparsely Populated Excited States. The fourth limit to this thesis model is the assumption of sparsely populated excited states. The assumption of sparsely populated excited states allows simplification of the relaxation and pump rates (page 14). This assumption can be violated under certain initial conditions of high pump energy and/or small concentrations of CO_2 which cause the upper vibrational level to become heavily populated.

Smith studied the vibrational temperature (a measure of population) of the upper vibrational level (CO_2 001) as a function of pump energy and found that the 001 level can become saturated at high pump energy (Figure 27). When the 001 level becomes heavily populated, the rate of depopulation through super-elastic collisions becomes equal to the pump rate, and the population stops increasing (18:1038).

This study duplicated the conditions of Figure 27 and calculated the resulting vibrational temperature of n_a (001 level) at peak gain, shown in Figure 28.

While n_a is sparsely populated (low end of the curve), both curves have the same slope and show a linear dependence on the pump energy. When excited CO_2 (shown on the upper curve of Figure 28) exceeds 20% of the total CO_2, however, the curves diverge. Since the author's model contains no provisions for super-elastic collisions, nor does it account
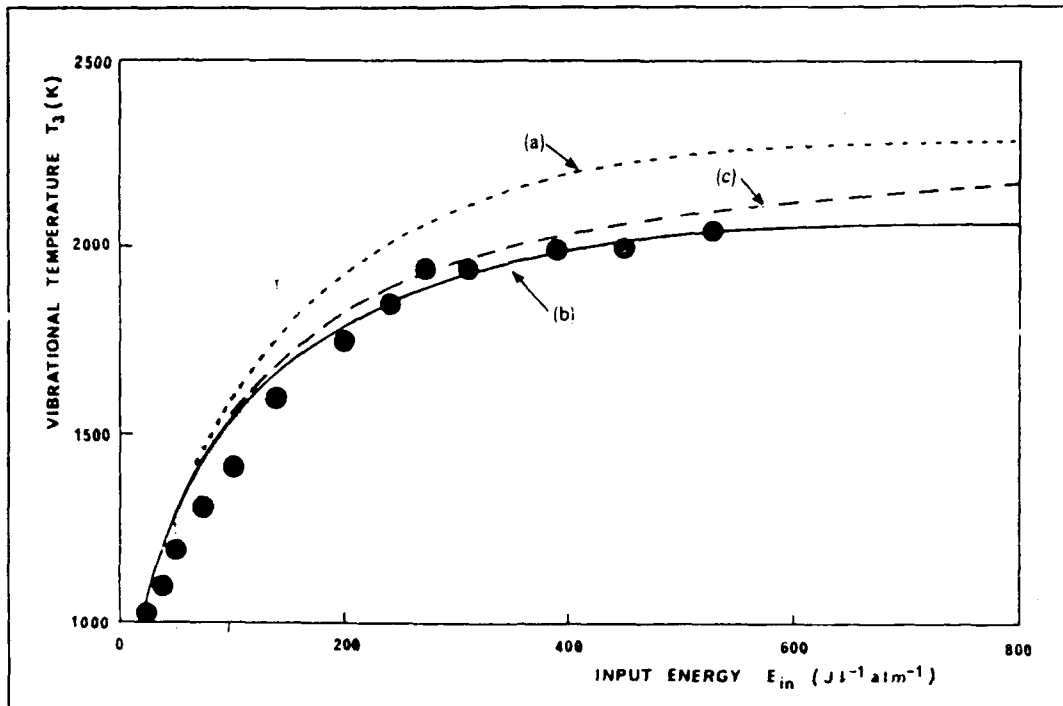
Figure 27. Calculated and Experimental Vibrational Temperatures of the Upper Vibrational Level (CO_2 001) as a Function of Pump Energy. Mix = 13% CO_2, 9% N_2, 78% He. (c) 760 torr, 100 nsec pump. Reprinted from (18:1038)
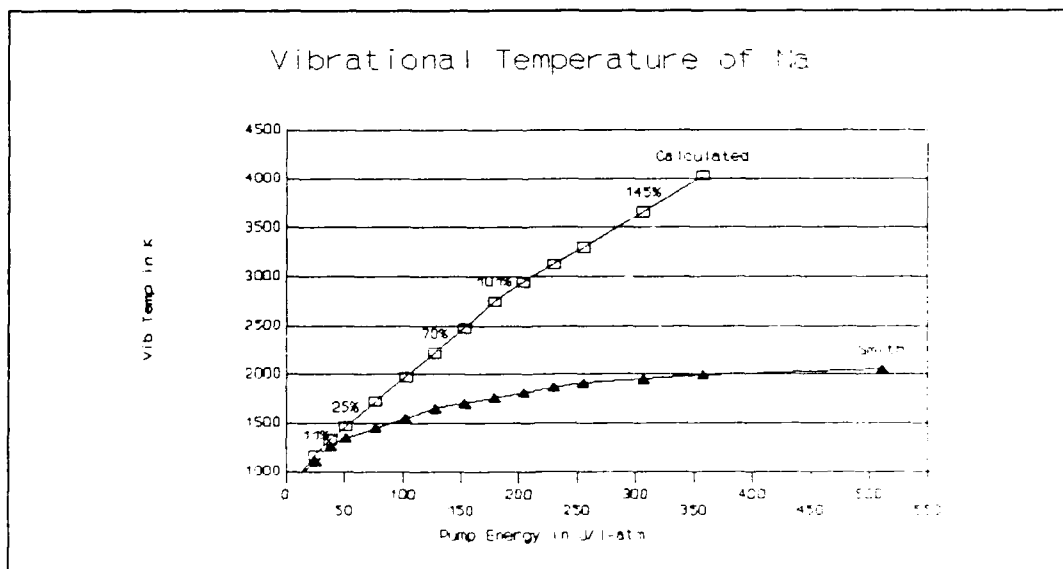
Figure 28. Calculated Vibrational Temperatures of CO_2 001 vs Pump Energy. P = 760 torr; T = $300°K$; Mix = 10% CO_2, 10% N_2, 80% He; L = 1.0 m; Refl = 71.6%; Pmp = 200 nsec, sqr; No Loss. Lower Curve Extracted from (18:1038)

75

for ground state population, it cannot model saturation. Therefore, the vibrational temperature of 001 continues in a linear dependence on pump energy, even out to where excited CO_2 is greater than 100% of the total CO_2.

Under the conditions of Figure 28 (P = 1 atm, mix = 10% CO_2, 10% N_2, 80% He), then, the pump efficiency (fraction of N_2 pumped into v=1) is limited to 0.2 to keep the excited populations to 20% or less.

Practical Limits Found During Validation. In addition to limits imposed by assumptions of the model, there may be practical limits found during validation. The one practical limit found during validation was the limit to pump efficiency (fraction of N_2 pumped into v=1) imposed by the assumption of sparsely populated excited states. The pump efficiency is limited to 0.2 at 1 atm and 10% CO_2 to keep the population of the excited states to 20% or less. Otherwise, the model performed better than the theoretical limits imposed by the above assumptions.

Limits Imposed by Equations and Data. The last set of limits to the model are imposed by the range of validity of the equations used. The pressure and temperature are limited by the valid range of the line width equation and the relaxation rate equations.

The pressure is limited to the range of 0.1 atm to 10 atm by the line width equation. Below about 0.1 atm, the

76

line width ceases to be purely pressure-broadened and becomes more Doppler-broadened. Above 10 atm, the assumption that the gases in the laser medium are ideal breaks down, and the equation for pressure-broadened line width is no longer valid.

The temperature is limited to approximately 200 to 700°K by range of relaxation data found in the literature. Both the line width and relaxation rates were extracted from Witteman, but he did not include a temperature range over which his equations are valid. Other authors, however used relaxation rate data that was good from 200 to over 1000°K (25:105)(21:30)

Summary of Model Limitations. In summary, the model is limited by the assumptions and by the valid range of the equations used. The point model assumption limits the product of the gain and the length to less than 200% and the output mirror reflectivity to greater than 50%, while the assumption of fast relaxation rates limits the laser pulse length to about 10 nanoseconds or greater. The assumption of sparsely populated excited states limits the pump efficiency to 0.2 or less when the mix contains 10% CO_2 and 10% N_2. The assumption that a four-level model is adequate, however, does not appear to place any limitations on the model. The last set of limits are imposed by the valid range of the line width equation and relaxation rate

equations, and they limit the pressure to 0.1 to 10 atm, and the temperature to 200 to 700°K.

IV. CONTINUOUS WAVE CO_2 MODEL, METHODOLOGY AND ANALYSIS

Overview

This chapter describes continuous wave (CW) CO_2 lasers, several models of such, and the development of the author's model, also refereed to as "this model". Then the verification of the code and its validation against experimental CO_2 lasers and other CO_2 laser models is described. Finally, the limits of the model are presented.

Description of a CW Laser

CW CO_2 lasers are used in many applications in industry and science, and come in many sizes and types. The cavity can be sealed (closed off) or open with the active medium flowing through it. In a flowing system, the gases can flow transverse to the laser axis or longitudinally (along the laser axis). Excitation of a flowing system is usually via an electron beam, whereas a sealed system can also be excited by radio frequency energy. Power can range from a few watts to many kilowatts, and the pressure of the active medium can range from a few torr to about 300 torr.

Steady-State Conditions. Regardless of the configuration of the CW laser, all CW lasers are steady-state devices. Neglecting starting and shutdown conditions, the pump energy, photon flux, populations, and temperature in the laser do not change significantly.

Although the steady-state values of photon flux, pump energy, or excited populations don't vary in time, they can vary with position in the cavity. For example, most stable resonators produce a Gaussian laser beam which has the greatest intensity in the center of the beam and very small intensity on the outer edge of the beam. In the laser cavity, therefore, the beam is most intense in the center and less intense at the radial edge. The pump energy and excited populations can also vary with radial and axial position, depending on the type of CW laser.

Survey of Previous Models of CO_2 CW Lasers

Since the conditions in a CW laser depend on its type and configuration, a model is usually based on a certain configuration of CW laser. These previous models show the complexity of most CW CO_2 models compared to the author's model. Reviewing these other models also provides a basis for determining the reasons for differences in calculated output between more complex models and the simple model

reported here. A short description of seven other CO_2 CW

models, some of which are used in validation, follows:

1. Witteman modeled a small, sealed CO_2 laser and

calculated the temperature as a function of radial position.

He modeled the electron beam pump and the photon flux as

functions of radial position, and determined the resulting

excited population. Solving iteratively, he found the

temperature as a function of pump energy and radial

position. The temperature in the center of a sealed laser

can be up to 500°K higher than the wall temperature (24:78-

91).

2. Wutzke modeled a fast transverse flow CO_2 laser

with a six-temperature model and found very good agreement

with experiment (25:i,ii).

3. Beverly adapted Wutzke's model to a fast flow axial

laser and also found very good agreement. His model

calculated the steady-state excited populations as a

function of axial position and included the effect of gas

heating (1:26,27).

4. Parazzoli successfully modeled a small, sealed CO_2

laser excited by radio frequency energy. He modeled the

excited populations as a function of x, y, and z position in

the rectangular cavity. He included the radio frequency

wave guide effects, the optical mode in the rectangular

cavity, and the effects of the walls on the relaxation of

the excited species. Because the system is non-flowing, he set the rate equations to zero and iteratively solved the resulting non-linear equations. Parazzoli obtained a temperature profile similar to Witteman (16:479-488).

5. Mitsuhiro built and modeled a cryogenically cooled laser of the fast-flow transverse type. His study included eight different vibrational levels of CO_2 and nine vibrational levels of N_2. He studied the effects of temperature, pressure, and gas flow rate on power output (13:677-680).

6. Deutsch experimentally studied a small, sealed, low power industrial laser and recorded its output as a function of pump power, output coupling, jacket temperature, and operating life (6:972-975).

7. Finally, Fowler constructed a four temperature traveling wave model of a CW CO_2 laser. He modeled the effects of temperature, pressure, and gas mix on the small-signal gain and saturation flux. He constructed the model using energy levels instead of excited populations (10:3480-3487).

Developing the CW Laser Model

The assumptions used in developing this CW model are nearly identical to those used in the pulsed CO_2 model, except steady-state conditions are assumed to exist in the

laser. Although the assumptions are similar, many of the
calculations are different, including: the solution of the
simultaneous state equations using Newton's method, the
quasi-Voigt line shape, and new output parameters of small-
signal gain and saturation flux.

Assumptions. The assumptions for the CW model are
almost identical to the assumptions used for the pulsed
model because the same model framework was used. The
notable exception is the assumption of steady-state
conditions. A review of the important assumptions follows:

Steady-State Conditions. As previously stated, the
CW laser is a steady-state device, so the conditions in the
laser are assumed to be constant during operation. Assuming
steady-state conditions in the laser means that the
differential equations describing the populations and photon
flux (Equations 22 to 25) can be set equal to zero, yielding
four non-linear, algebraic equations of state. All the rest
of the assumptions discussed are similar to those in the
pulsed model.

Four-Level Model. The second major assumption of
the CW model is that a four-level model is sufficient to
show trends. The four-level system assumes very fast
exchange rates among the rotational levels and between the
100 and 020 vibrational levels of CO_2. Witteman asserted
that a four-level model is adequate for a CW laser because

under steady-state conditions, the 100 level is in equilibrium with the 020 level (24:69).

Point Model. The third major assumption is that a point model of the CW laser is sufficient. A point model assumes that:

1. The pump energy and photon flux completely and uniformly fill the laser cavity.

2. The excited populations are not a function of time (steady-state) or of position in the cavity.

3. The temperature is uniform and constant throughout the cavity. No radial temperature profile exists as in Witteman's or Parazzoli's models. This is different than the pulsed model where the temperature changed with time.

4. Finally, there are no wall effects.

Sparsely Populated Excited States. The fourth major assumption is that the excited populations are much smaller than the ground state populations for CO_2 and N_2.

Lasing on Line Center. The last major assumption is the laser operates on line center of the P(20) transition.

Calculations. Although the assumptions are similar, many of the required calculations are different from the pulsed model. The six differences are: solution of the set of state equations, the line shape, the threshold gain and

cavity lifetime, the small-signal gain, the saturation flux, and finally, the Rigrod equation. In addition, steady-state conditions mean the temperature does not change, so the energy balance calculations are not used.

Solving the Equations of State. Instead of using a Runge-Kutta routine to integrate the differential rate equations, solution of the CW model requires solving four simultaneous non-linear equations of state derived from those rate equations (Equations 22 to 25). Under the steady-state conditions of the CW laser, the differential rate equations can be set equal to zero, yielding:

$$d(n_a)/dt = 0 = I\ c(gu/gl\ \sigma_L\ n_b - \sigma_U\ n_a) + \gamma_a(n_{ae} - n_a)$$
$$- \gamma_{cn2}\ n_a + \gamma_{co2}\ n_c + w_a \qquad (39)$$

$$d(n_b)/dt = 0 = I\ c(\sigma_U\ n_a - gu/gl\ \sigma_L\ n_b)/4 + \gamma_a(n_a - n_{ac})/4$$
$$- \gamma_b(n_{be} - n_b) + w_b \qquad (40)$$

$$d(n_c)/dt = 0 = \gamma_{cn2}\ n_a - \gamma_{co2}\ n_c + w_c \qquad (41)$$

$$d(I)/dt = 0 = I\ c(\sigma_U\ n_a - gu/gl\ \sigma_L\ n_b) - I/\tau_{cav} \qquad (42)$$

The spontaneous term $(n_a\ w_s)$ was dropped from the equation for flux (Equation 25) because it is negligible compared to the steady-state flux. After a simple iterative

85

technique failed to solve the above four simultaneous equations, Newton's method was used. As described by Burden, Newton's method consists of iteratively solving the following matrix equations:

$$Y = inv(J(X)) \; F(X) \tag{43}$$

$$X = X + Y \tag{44}$$

where

$X \quad = (n_a, \; n_b, \; n_c, \; I)$

$F(X) = (d(n_a)/dt, \; d(n_b)/dt, \; d(n_c)/dt, \; dI/dt)$, calculated using Equations 39 to 42 above

$J(X) = $ The Jacobian matrix of $F(X)$ (5:499)

The computer model solved the matrix equation for Y, Equation 43, using the lower-upper decomposition method written in FORTRAN by Press (17:35-37) and translated into Quick BASIC for this model. The matrix Equations 43 and 44 are considered solved and the iterations are complete when the solution to the equations converge to the tolerance set by the modeler.

Quasi-Voigt Line Shape. The second major change from the pulsed to the CW model is the use of the quasi-Voigt line shape instead of a pressure-broadened line shape. This study chose the quasi-Voigt line shape because it can

be solved analytically and is accurate over a broader pressure domain than either the Doppler or pressure line shapes. The Doppler line shape is most prominent at pressures below 10 torr, and the pressure line shape takes over above 50 torr (24:59-61). Many CO_2 CW lasers operate between these pressures where the line shape is neither a Doppler or pressure line shape.

The true line shape in this intermediate pressure region is a result of both Doppler and pressure effects and the Voigt line shape models this very well. The true Voigt line shape, however, is described by a transcendental equation that cannot be solved analytically; therefore the quasi-Voigt line shape is used. The quasi-Voigt line shape at line center is described in Beverly's article by the following equation:

$$Sv = ((\ln2/\pi)^{\frac{1}{2}} \Delta\nu_d + \Delta\nu_p/\pi) \; / \; (\Delta\nu_d^2 + \Delta\nu_p^2) \tag{45}$$

where

Sv = quasi-Voigt line shape at line center (sec)

$\Delta\nu_d$ = Doppler line width, half width at half max (Hz)

$\Delta\nu_p$ = Pressure line width, half width at half max (Hz)

87

The effective radiative cross section for the upper laser level (and lower laser level) is then calculated by modifying Beverly's equation as follows:

$$\sigma_U = f_U \ A \ Sv \ c2 \ / \ 8 \ \pi \ \nu2 \qquad\qquad (46)$$

where fU is the fraction of CO2 001 molecules in the j=19 rotational level, A is the Einstein coefficient, and ν is the laser frequency in Hz (1:33). Figure 29 shows a comparison between radiative cross sections calculated using Doppler, pressure, and quasi-Voigt line shapes.
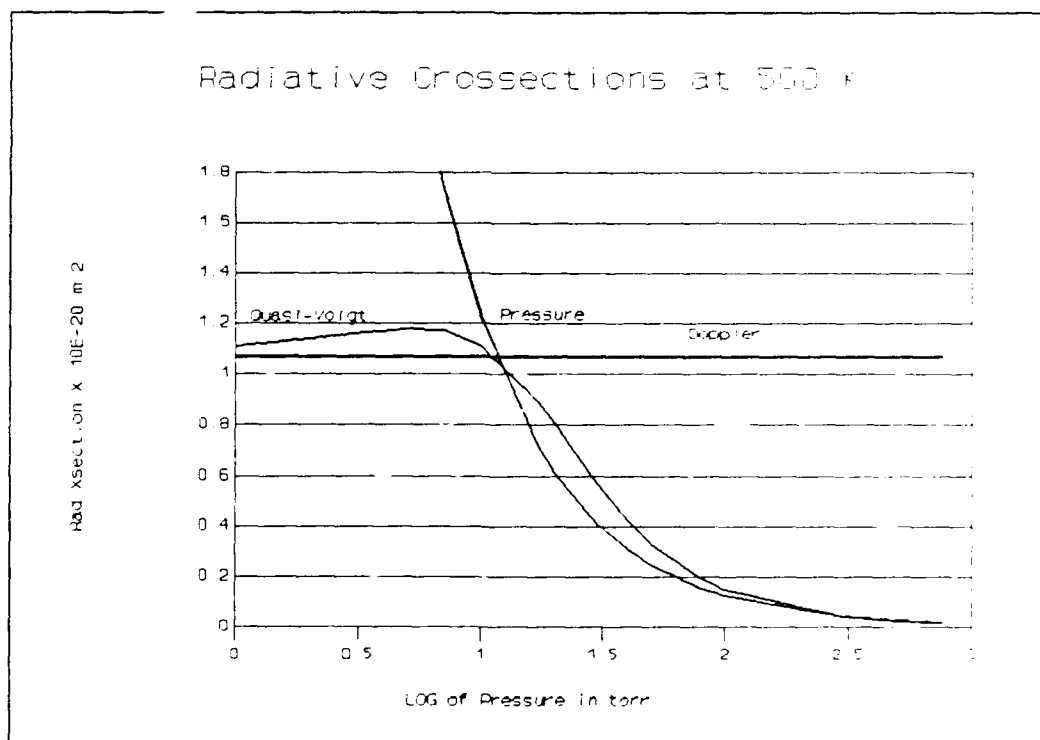
Figure 29. Comparison of σ_U at 500°K vs Pressure. Calculated using Doppler, Pressure, and Quasi-Voigt Line Shapes. Gas Mix = 10% CO_2, 10% N_2, 80% He.

88

Threshold Gain and Cavity Life Time. The next
major change is the calculation of the threshold gain and
the cavity lifetime. Whereas the pulsed model incorporated
the cavity losses into the integration steps, the CW model
includes the losses in the threshold gain. The threshold
gain is the gain required to balance both the favorable and
unfavorable cavity losses. The threshold gain is also
proportional to the reciprocal of the cavity lifetime as
given by Douglas-Hamilton.

$$Gc = \ln[(1-k)(1 - a)]/2 L = 1/\tau_{cav} c \qquad (47)$$

where Gc is the threshold gain; $k = 1 - R$, the output
coupling; R is the reflectivity of the output mirror; a is
the unfavorable losses in the cavity per round trip; and L
is the optical resonator length (7:56).

The gain during lasing, however, is calculated by
Equation 10. Solving the state equation for the photon flux
(Equation 42) for the gain reveals that the gain, G, is
equal to the threshold gain, Gc. This is a logical result
for a CW laser, because as long as the gain is above
threshold gain, the cavity flux will continue to increase.
Increasing photon flux will drive the gain down. Once the
cavity flux has increased to the point where the gain equals

the threshold gain, the flux will stop increasing, and has reached steady-state.

Small-Signal Gain. Small-signal gain was not calculated in the pulsed model, however, it is an important parameter in the CW model. According to Witteman, the small-signal gain is the gain of the active medium when the photon flux is zero (24:62). Small-signal gain, Go, is the maximum possible gain for the given pumping conditions. It is calculated by the following equations:

$$Go = n_{ao} \, \sigma_U - n_{bo} \, \sigma_L \, gu/gl \qquad (48)$$

$$n_{ao} = n_{ae} + (w_a + w_c)/ \, \gamma_a \qquad (49)$$

$$n_{bo} = n_{be} + (\gamma_a \, nae + w_a + w_c + 4 \, w_b)/4 \, \gamma_b \qquad (50)$$

The equation for n_{ao}, the population of CO_2 (001) for zero flux, is derived from Equations 39 and 41 by setting the flux equal to zero and solving for n_a. Similarly, n_{bo} is found from Equations 39 and 40 under zero flux. The equations show that the small-signal gain is proportional to the ratio of the pump terms to the relaxation terms.

Saturation Flux. Like the small-signal gain, the saturation flux was not calculated in the pulsed model, but is an important parameter of the CW laser. The saturation flux, according to Fowler, is the flux required to reduce the gain to one half the value of the small-signal gain

90

(10:3480). Douglas-Hamilton describes the saturation flux as the flux required to cause the laser deactivation of the upper laser level to be equal to the collisional deactivation (7:68). Using Douglas-Hamilton's definition, the laser deactivation is equal to the collisional deactivation of CO_2 (001) when

$$I \ c \ \sigma_U \ n_a = \gamma_a \ n_a \qquad (51)$$

Solving for I yields

$$Is = \gamma_a \ / \ c \ \sigma_U \qquad (52)$$

where Is is the saturation flux in photons/m^3. Witteman also derived an equation, $Is = h \ \nu \ / \ \tau \ \sigma \ (W/m^2)$, for the saturation flux for steady-state conditions, where τ is the time constant for the collisional loss of the inversion (24:62). τ can be set to $1/\gamma_a$ when γ_a is much less than γ_b, making γ_a the controlling rate. If Equations 52 and Witteman's are converted to the same units, and $\tau = 1/\gamma_a$, then the two equations are identical.

If, however, τ is a function of both γ_a and γ_b, then the equation from Verdeyen must be used.

$$Is = h \ \nu \ / \ \sigma \ (\tau_1 + \tau_2 - \tau_1 \ \tau_2/\tau_{21}) \qquad (53)$$

91

where

τ_1 = time constant for the relaxation of the lower laser level to the ground state

τ_2 = time constant for the relaxation of the upper laser level to the ground state

τ_{21} = time constant for the relaxation of the upper laser level to the lower laser level (22:167)

For this model, however, $\tau_1 = 1/\gamma_b$, $\tau_2 = 1/\gamma_a$, and $\tau_{21} = 1/\gamma_a$, so Verdeyen's equation reduces to Equation 52 and the simpler equation is accurate under all conditions.

Although Douglas-Hamilton's definition of saturation flux was used to derive Equation 52, the resulting model does not conflict with Fowler's definition of saturation flux; when the gain equals one half the small-signal gain (Fowler's definition), the cavity flux is equal to the saturation flux and the laser deactivation of the upper vibrational level is equal to the collisional deactivation.

Rigrod Equation. The final addition to the CW model calculations is the Rigrod equation. It relates all the important parameters of the CW laser: the gain, the flux, the saturation flux, and the small-signal gain (7:68)(24:62). The Rigrod equation is

$$G = Go / (1 + I/Is) \tag{54}$$

All of the parameters in the Rigrod equation can be determined analytically except the cavity flux, I. Go is found by Equation 48, Is by Equation 52, and G by Equation 10. The steady-state cavity flux, I, can then be determined analytically by solving the Rigrod equation for I. Because there are no additional simplifying assumptions used in calculating Go, G, or Is, the cavity flux found by the Rigrod equation is always equal to the cavity flux found iteratively by Newton's method, within tolerance.

The cavity flux, I, can be related to the output power by a factor found in Douglas-Hamilton.

$$Pout = I \ f \ h \ \nu \ c/L \tag{55}$$

where

Pout = the Power out in Watts per m^3 of active medium

f　　= {k (-.5) ln[(1-a)(1-k)]}/[k(1-a)]　　(7:56)

I　　= photon flux in the cavity (photons/m^3)

Verification and Analysis

After the model was developed, it was verified by comparison with a quasi-CW code constructed from the pulsed code. The quasi-CW code was constructed by using the pulsed

93

code at constant temperature with input parameters designed to produce a quasi-steady-state laser pulse. The pulsed model was run with a 100 microsecond pump to allow the flux and populations to reach a quasi-steady-state (Figure 30) after the initial laser spike and before the pump shut off. If the laser reaches steady-state before the pump shuts down, the flux and populations should be the solution to the CW problem.

After constructing the quasi-CW code, this study
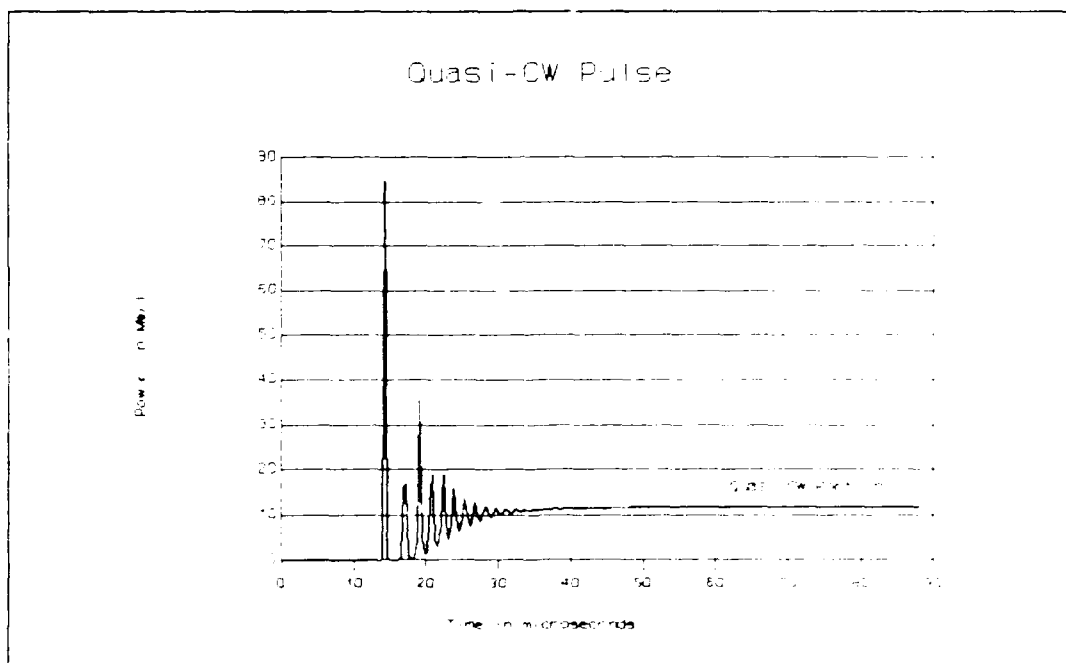
Figure 30. Laser Pulse from the Quasi-CW code. P = 0.1 atm; T = 300°K; Mix = 10% CO_2, 10% N_2, 80% He; Refl = 71.63%, Length = 1.0 m; Pump Pulse = 100 μsec, square; Losses = 3%.

verified the CW output with quasi-CW output. Verification involved 16 total runs, varying all input parameters

94

(pressure, temperature, mix, . .) one at a time. The laser power from the CW code was always slightly larger than the power from the quasi-CW code. Using the CW code's output as the baseline the largest difference in power was 46%, the next largest difference was 16%, and the other 14 runs differed by 10% or less. The populations also correlated to within ± 20%.

There are two possible reasons for the differences. First, the quasi-CW pulse may have not really reached steady-state. Under some conditions, the laser flux was steady and unchanging to three decimal placed for several microseconds. At low pressure or short photon lifetime, however, the laser did not entirely settle down after 5000 time steps (100 msec).

A second reason for the differences may be due to the different line shapes used in each code. The pulsed code used a pressure-broadened Lorentzian line shape, but the CW code used a quasi-Voigt line shape. To test this, the CW code was run once with the pressure-broadened line shape. Although the excited populations changed about 6%, the power did not change significantly.

A second test of verification was the effect of reflectivity. According to Tarasov, there is an optimum output coupling, Nopt, which is a function of reflectivity, for each combination of small-signal gain and cavity losses.

95

$$Nopt = (Go\ a)^{\frac{1}{2}} - a \qquad\qquad (20:79) \qquad (56)$$

Tarasov's definition of the output coupling is
$N = Ln(1/R)/(2\ L)$, where R is the reflectivity of the
output mirror (assuming the other mirror is 100%
reflecting), and L is the length of the optical cavity
(20:74). Solving both equations for the optimum
reflectivity yields

$$Ropt = 1/[exp(Nopt\ 2\ L)] \qquad\qquad (57)$$

Figure 31 shows the calculated output as a function of
reflectivity at two different pump powers and two levels of
losses. The calculated optimum reflectivity is also
displayed on the figure.

Because the CW output was only slightly different than
the quasi-CW output and matched its trends, and the model
correctly predicts the optimum reflectivity, the CW code is
considered verified.
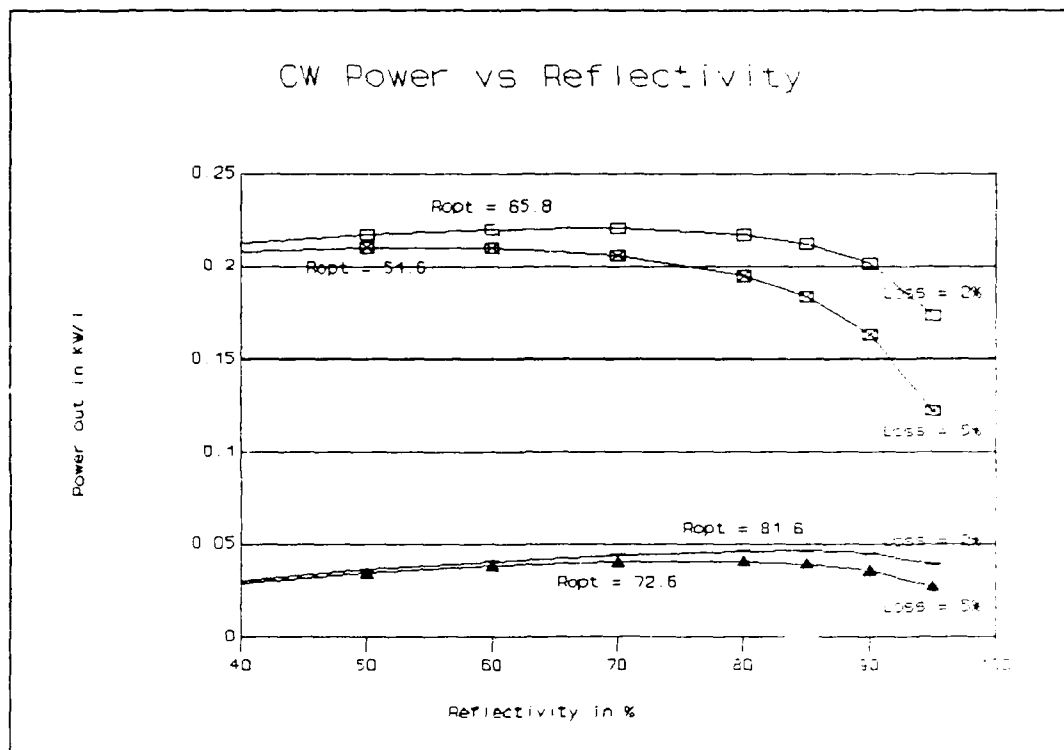
Figure 31. CW Power vs Reflectivity. P = 18.1 torr (0.02382 atm); T = 300°K: Mix = 13.8% CO_2, 13.8% N_2, 72.4% He; Length = 1.5 m.

Validation and Analysis

After verification, the CW code was validated against experimental lasers and other CW models.

Validation Against Experimental CW Lasers. The CW model was validated against five experimental CO_2 CW lasers. The following paragraphs describe the experimental laser, its operating parameters, the model's calculated output, and an analysis of the difference.

Validation Against Witteman. The first validation run compared the model against experimental results reported by Witteman. Witteman reported the output of a small,

sealed CO_2 laser operated at low pressure and pumped very strongly. The pressure was 18.8 torr and the gas mix consisted of 13.3% CO_2, 18.6% N_2, 63.8% He, 3.2% Xe, and 1.1% H_2O. Neither the temperature, the reflectivity, nor the losses were specified. The pump power was 5 kilowatts per liter of active medium (kW/l) which is equal to 202 kW/l-atm, and the laser power out was 0.686 kW/l (24:81).

This study ran the CW code under the same conditions, except an additional 3.2% He was substituted for the Xenon. In addition, the reflectivity was assumed to be 71%, the temperature was assumed to be 300°K (approximately room temperature), and the losses to be 3%. The code calculated the laser output power to be 1.2 kW/l, which is 74% high. The temperature inside such a strongly pumped laser, however, will not be room temperature, so the code was run again at 500°K With the pressure at 31.3 torr, and the output was calculated to be 0.91 kW/l. 500°K was chosen based on Witteman's temperature profile (24:91), and the pressure was chosen to keep the number density constant inside the constant volume, sealed cavity. At 600°K the CW code's output is 0.546 kW/l.

The calculated output agrees very well with the actual output considering the actual temperature, reflectivity, and losses were unknown. Of those three parameters, the temperature has the greatest effect as discussed above. The

gas mixture may have caused some error because the CW model does not include xenon as a possible gas.

Another contribution to the error is the use of the point model for the CW code. The point model assumes uniform pumping, flux, and temperature throughout the cavity, however, the actual flux and temperature are far from uniform (page 23). Both the temperature and flux are very high at the center of the cavity and much lower along the radial wall. Because the CW code assumes uniform pumping and photon flux throughout the entire cavity, it will probably always overestimate the power output of an actual laser (19).

Validation Against Wutzke. The second validation run compared the CW model against a laser described by Wutzke. Wutzke operated a large, high-pressure, fast-flow laser with moderate pumping. The pressure was 280 torr, the mix was 3.6% CO_2, 24.8% N_2, 70.9% He, and 0.7% water vapor. The losses were specified at 3%, but the reflectivity and average temperature were unspecified. The pump power was 40 kW/l (109 kW/l-atm) and the laser output was 3.65 kW/l (25:i,ii).

The CW model code duplicated Wutzke's conditions (except for the flowing medium) and assumed 71% reflectivity. At 300°K The calculated output is 9.77 kW/l, and at 400°K the calculated output is 5.96 kW/l, which is 63% high. Varying

99

the reflectivity between 50% and 90% only changed the calculated output by approximately 20%.

Validation Against Beverly. The third validation run also involved a fast-flow CW CO_2 system. Like Wutzke, Beverly also reported the results of fast-flowing CO_2 CW laser, except Beverly's operated at low pressure and low pump power. Figure 32 compares Beverly's actual output and the model's calculated output as a function of pump power. The input parameters were specified as follows: pressure was 20.2 torr; mix was 4% CO_2, 40% N_2, and 56% He; reflectivity
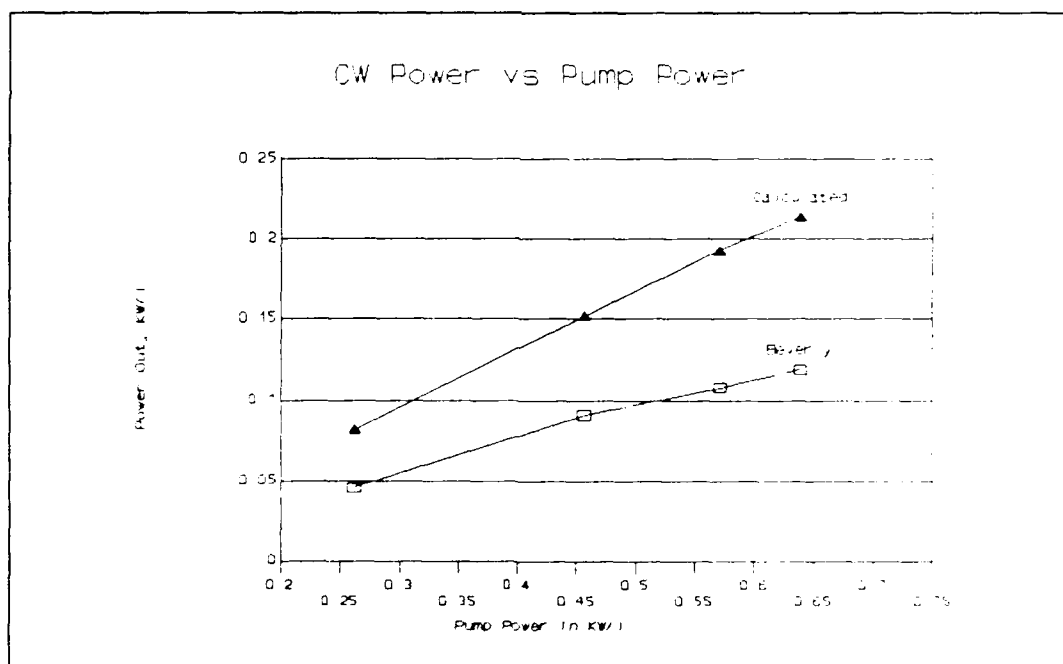
Figure 32. Comparison of Beverly's Experimental Output and Author's Calculated Output vs Pump Power. P = 20.2 torr; T = 293°K; Mix = 4% CO_2, 40% N_2, 56% He; Refl = 48%; Losses = 1%. Experimental Values Extracted from (1:37)

100

was 48%; temperature was 293°K; losses were 1%; the pump power was 0.995 kW/l (37 kW/l-atm); and the resulting laser output power was 0.245 kW/l (1:35,36). In comparison, the calculated output was 0.347, 29% high.

Validation Against Deutsch. Deutsch provides the information for the fourth comparison with a CO_2 CW laser. His small, low pressure, sealed laser was operated with a very low pump power. The pressure was 15.9 torr, and the mix was 10.1% CO_2, 13.8% N_2, 69.2% He, and 6.9% Xe. The pump power was 0.368 kW/l (17.6 kW/l-atm) and the laser output power was 0.066 kW/l. All other parameters were unspecified (6:973).

The CW model duplicated Deutsch's inputs and assumed 71% reflectivity and 1% losses. The calculated power output was 0.0814 kW/l at 300°K and 0.0426 kW/l at 400°K and 21.2 torr (to keep the number density constant).

Summary of First Four Validation Runs. The following table summarizes the validation of the CO_2 CW model against the previous four actual CO_2 CW lasers.

101

Table II. Experimental and Calculated CO_2 CW Laser Output

Author	Output (kW/l)	Model Predictions
Witteman	0.686	1.20 at 300°K 0.91 at 500°K
Wutzke	3.65	9.77 at 300°K 5.96 at 400°K
Beverly	0.245	0.347 at 293°K
Deutsch	0.066	0.0814 at 300°K 0.0426 at 400°K

Validation Against Mitsuhiro. In the fifth

validation run, this study compared the model against

Mitsuhiro's work. Mitsuhiro characterized a flowing, cooled

CW laser by varying the temperature and pressure and

recording the laser output. Figure 33 compares his

experimental observations with his theoretical predictions.

His experimental conditions were as follows: gas mix = 80%

He, 10% CO_2, 10% N_2; reflectivity = 90%; losses = 1%; pump

power = 4.687 kW/l at 100 torr and 220 K. This pump power

was determined using his information that the efficiency was

20% at 220°K for an output of 450 watts (13:679-80).

The pump power for the model was a function of number

density: Pump Power = 4.687 (Press/100 torr)(220/Temp).

The pressure was varied from 20 to 100 torr and the

temperature spanned 200 to 300°K. Figure 34 shows the
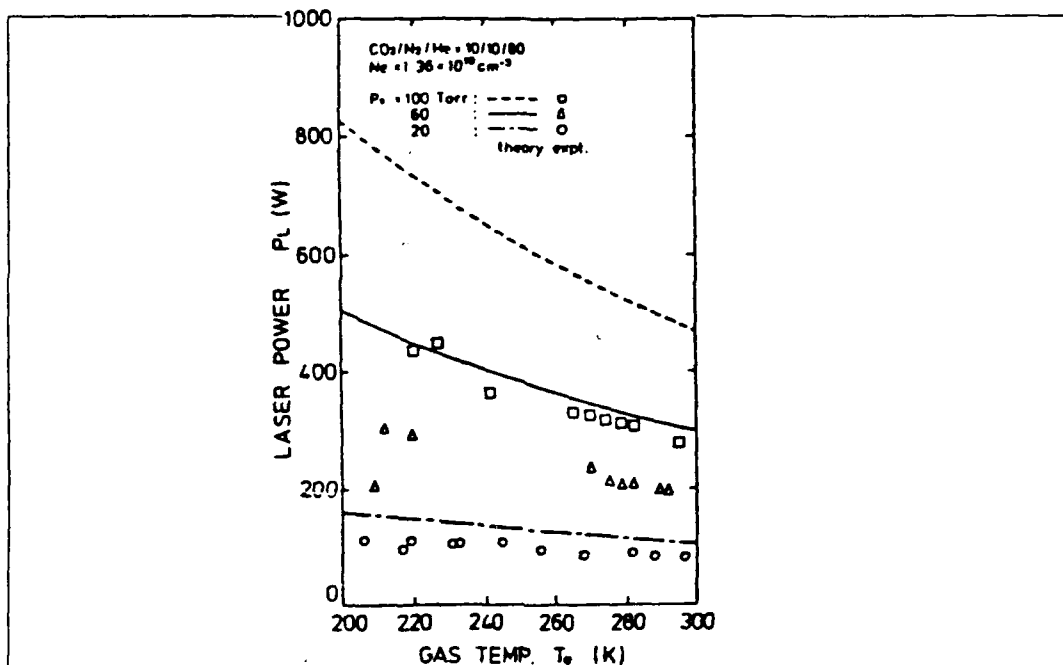
Figure 33. CW Laser Power vs Temperature and Pressure from Mitsuhiro. Lines are Theoretical Calculations, Markers are Experimental Values. Reprinted from (13:680)
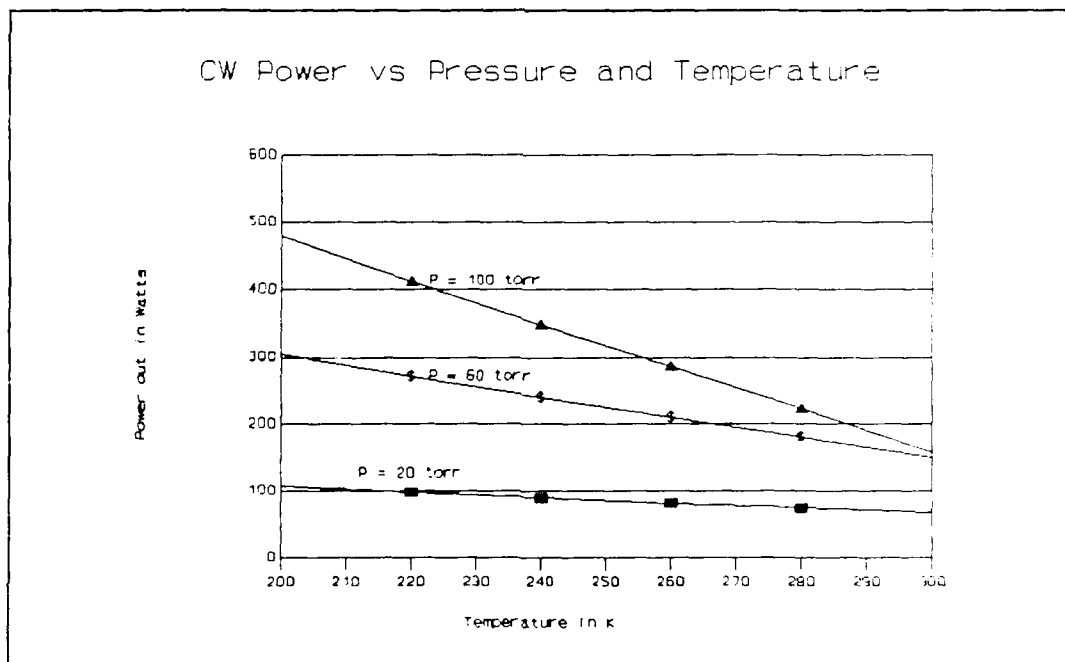
Figure 34. Calculated CW Laser Power vs Temperature and Pressure. Same Conditions as Figure 33.

theoretical predictions from this thesis model under the

same conditions. The agreement with Mitsuhiro's experimental values is very good; the relative position and slope of the calculated curves are correct, and the absolute values are closer than Mitsuhiro's model calculations. In addition, both graphs demonstrates the interaction of temperature and pressure in the CO_2 CW laser.

Validation Against Fowler's CO_2 CW Model. Fowler constructed a fairly complicated four-level model of a CO_2 CW laser which describes the behavior of the small-signal gain, the saturation flux, and the optical power density as a function of pump power, temperature, pressure, and gas mix. He found "very good agreement with experimental data" (10:3485).

Small-Signal Gain vs Temperature and Pump Power. Fowler first described the parametric behavior of the small-signal gain as a function of the temperature and pump power. The pressure was constant at 10 torr, the gas mix was 10% CO_2, 10% N_2, and 80% He, and the average electron energy was 1.5 eV. His pump power was specified in terms of electron number density and average electron energy. No equation for small-signal gain was given (10:3482). Figure 35 shows Fowler's graph of small-signal gain vs pump power and temperature, and Figure 36 shows this model's calculated small-signal gain vs pump power and temperature.
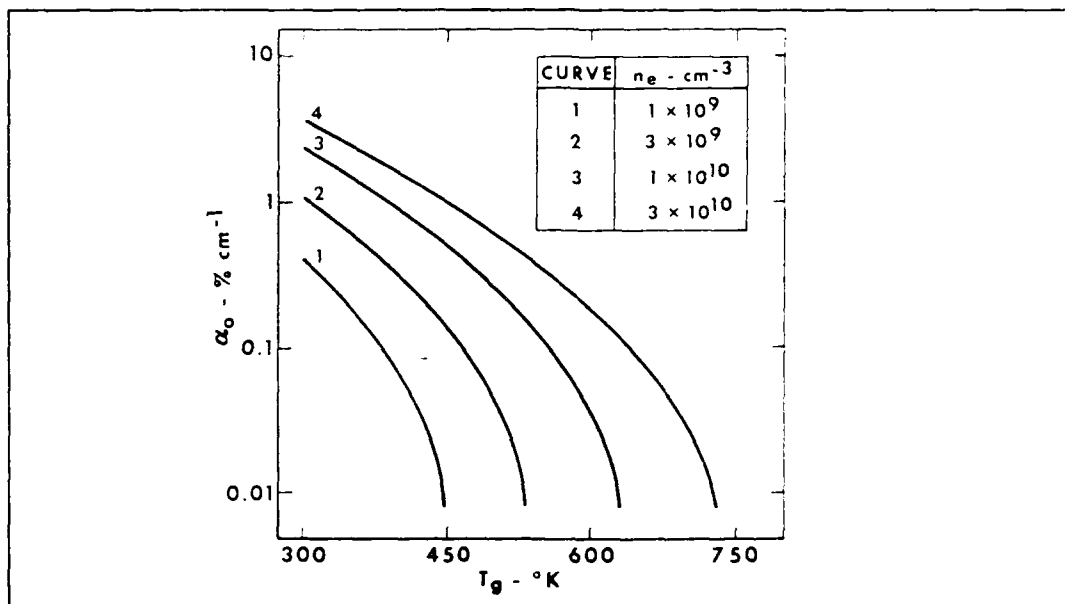
Figure 35. Small-Signal Gain vs Temperature and Electron Number Density from Fowler. Gas Mix = 1 torr CO_2, 1 torr N_2, 8 torr He; Reduced Ave Elec Energy = 1.50 eV.
Reprinted from (10:3482)
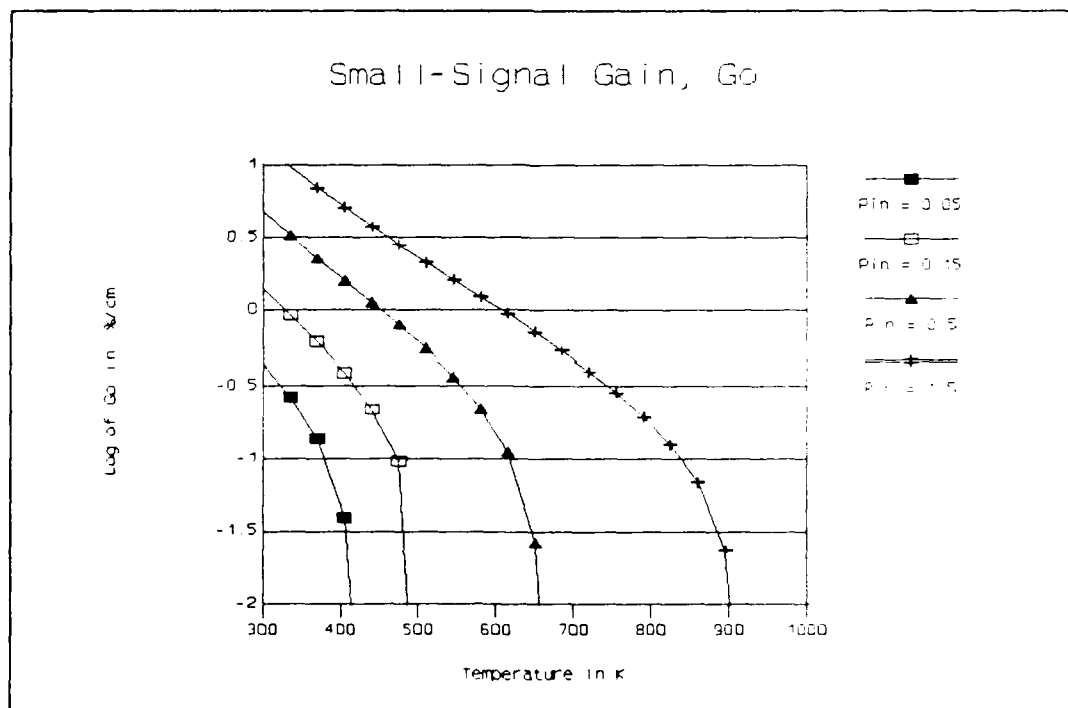
Figure 36. Small-Signal Gain vs Temperature and Pump Power. Same conditions as Figure 35. Pin is the Pump Power in kW/l.

In attempting to match Fowler's curves, this study matched his conditions and varied the pump power to benchmark Fowler's curve number 1 at 300°K. The power required to produce a small-signal gain of 0.4 %/cm was 0.05 kW/l at 300°K. To keep the average electron energy constant, the ratio of voltage to number density, E/N, must be kept constant. This is accomplished by keeping the pump power proportional to the number density. At constant pressure, the pump power for curve number 1 is 0.05 kW/l (300/temp). For curves 2, 3, and 4, the pump power was increased in the same proportion as the corresponding electron density and also varied inversely with temperature.

The results in Figures 35 and 36 show that this CW model agrees very well with Fowler's model. The shape, slope, and intercept of the curves match well except at a high pump power of 1.5 kW/l, where the small-signal gain is a factor of five too high.

This difference may be due to the high populations of the excited states under the heavy pump of 1.5 kW/l. At 300°K and 1.5 kW/l pump power, 59% of all the CO_2 is pumped into the upper vibrational levels of 010, 020, 100, and 001. This completely invalidates the original assumption of sparsely populated excited states and demonstrates a limit of the author's model. Fowler's model accounts for the high

excited state population by including both the excitation and de-excitation of molecules by electrons (10:3481).

Saturation Flux vs Temperature. Fowler's second graph, shown in Figure 37, relates the saturation flux, Is, to temperature at three different values of electron density (pump power) (10:3483). Although Fowler's saturation flux is dependent on pump power, this model's comparison of saturation flux at different temperatures shows no such dependence on pump power and is a factor of 5 lower than Fowler (dashed curve in Figure 37). It does, however, demonstrate the proper trend.
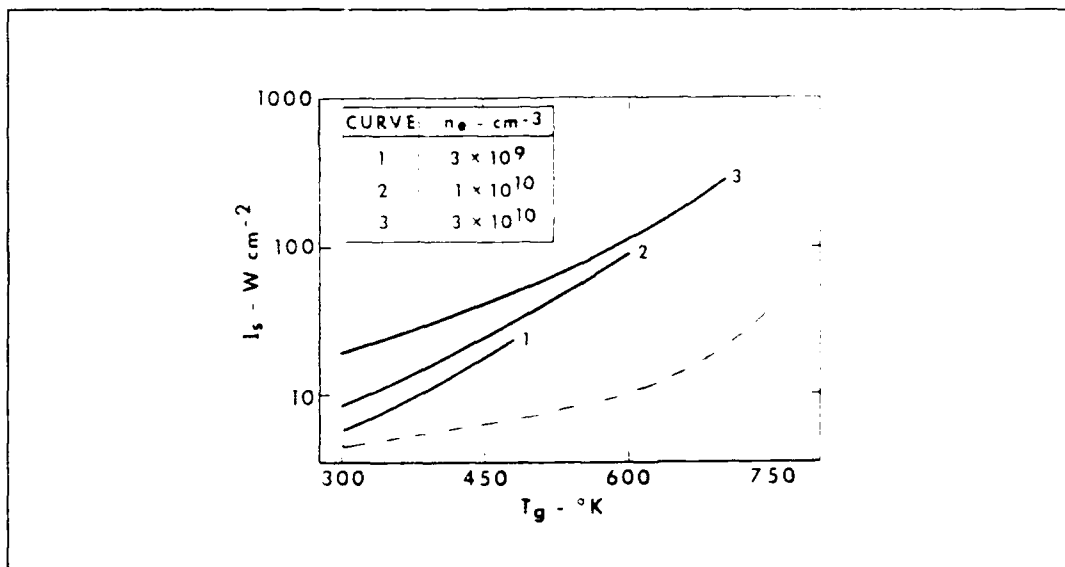
Figure 37. Saturation Flux Calculated by Fowler and Author's Model. Dashed Curve is Author's Model. Gas Mix = 1 torr CO_2, 1 torr N_2, 8 torr He; Reduced Ave Elec Energy = 1.50 eV.   Reprinted from (10:3483)

This model's equation for saturation flux (Equation 52) was derived from Verdeyen's equation which contains no factors related to the pump power (22:167). In addition, neither Witteman's (24:62) nor Douglas-Hamilton's (7:68) equations include a dependence on pump power. Figure 38 compares the saturation flux calculated by Douglas-Hamilton and this model.
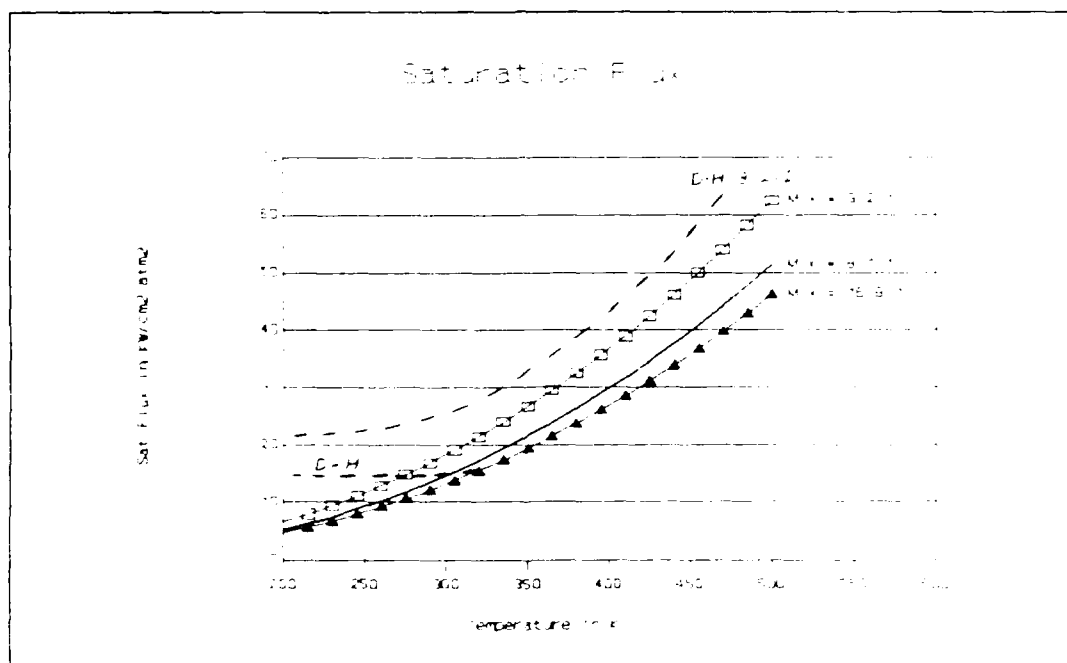
Figure 38. Calculated Saturation Flux from Douglas-Hamilton and Author's Model vs Temperature. Dashed Curves are extracted from Douglas-Hamilton. P = 1 atm; Mix = He:N_2:CO_2. (7:48)

<u>Optical Power Density vs Temperature and Pump</u>

<u>Power</u>. Fowler's third graph, Figure 39, shows the behavior

of the optical power density as a function of the

temperature and pump power (10:3484). Fowler defines the

maximum available optical power density as the product of

the small-signal gain and saturation flux (10:3481) derived

from the Rigrod equation as Is Go = I G + Is G .
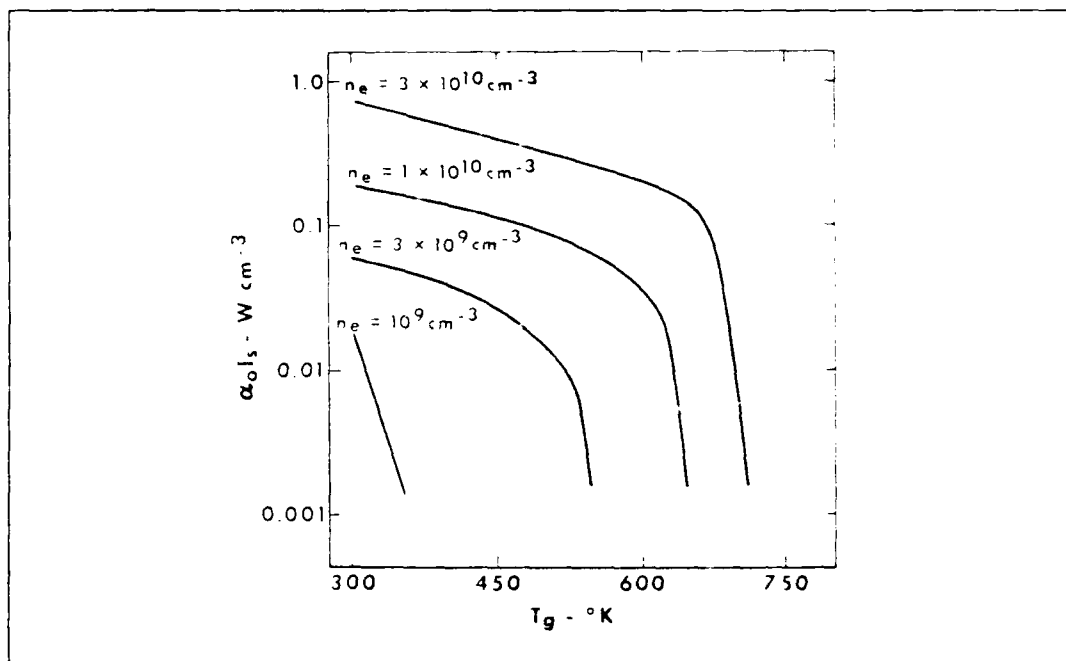
Figure 39. Optical Power Density, Is*Go, vs Temperature
and Electron Number Density from Fowler. Gas Mix = 1 torr
CO_2, 1 torr N_2, 8 torr He; Reduced Ave Elec Energy = 1.50
eV.   Reprinted from (10:3484)

Figure 40 shows this model's calculated optical power

density as a function of temperature and pump power.

Comparing Figures 39 and 40 reveals a good agreement

between Fowler's output and the author's model. The shape
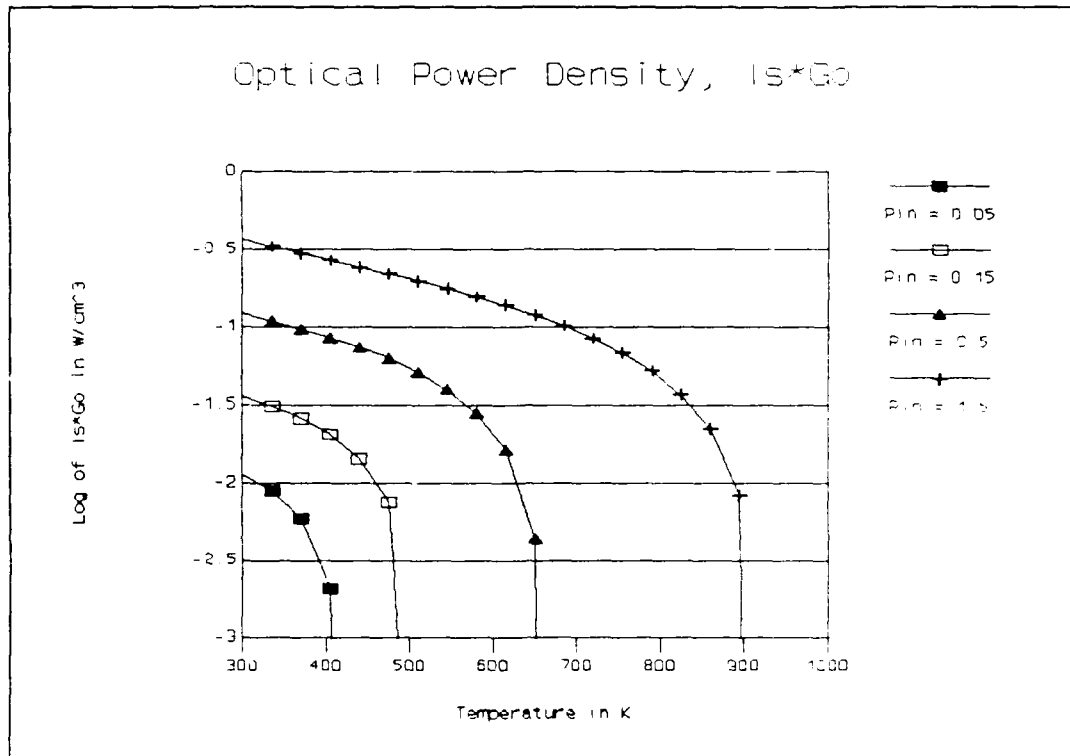
Figure 40. Calculated Optical Power Density, Is*Go, vs Temperature and Pump Power. Same conditions as Figure 39. Pin is the Pump Power in kW/l.

and trends match very well. Once again, however, the effect of high pump power is seen in the curve number 4, which does not drop off until $900°K$.

According to Fowler, this abrupt drop in power density occurs when the small-signal gain is driven to zero by the increasing thermal population of the lower vibrational level at higher temperatures (10:3485). At high temperatures the thermal population of the lower vibrational level, n_b, will exceed the population of the upper vibrational level, n_a, reducing the gain to zero and shutting the laser down.

110

Small-Signal Gain and Saturation Flux vs Pressure.

In his fourth parametric study, Fowler graphed the small-signal gain and saturation flux as a function of pressure at a constant temperature of $450^\circ K$. Figure 41 shows Fowler's curves, Figure 42 shows this model's curves of small-signal gain and saturation flux.
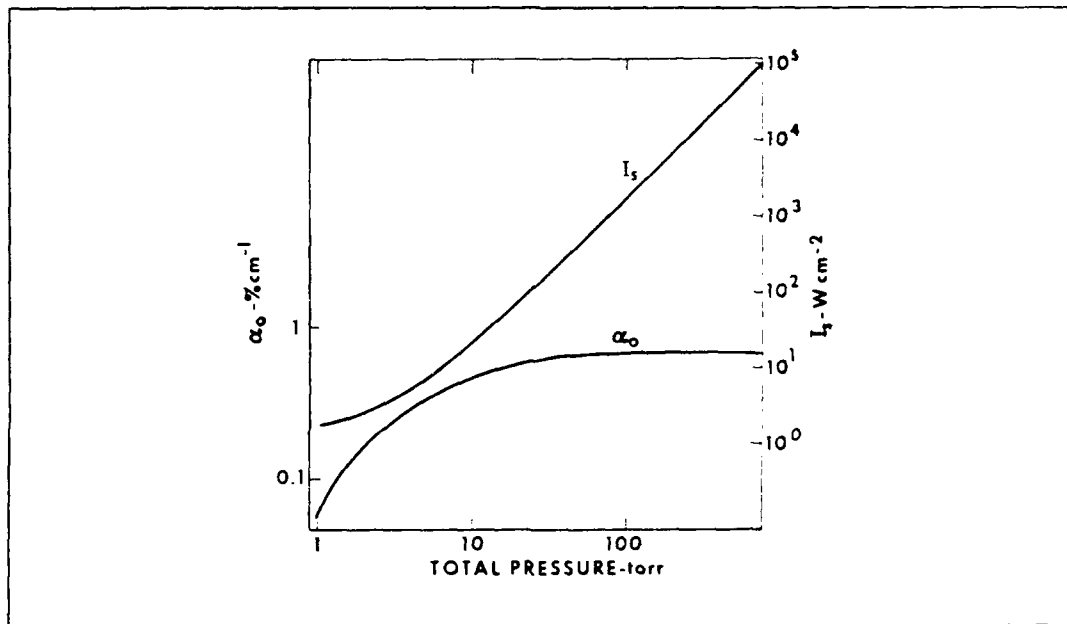
Figure 41. Small-Signal Gain and Saturation Flux vs Total Gas Pressure from Fowler. $T = 450^\circ K$; Gas Mix = 10% CO_2, 10% N_2, 80% He; Reduced Ave Elec Density = 1.50 eV; ne/P = 1×10^9 cm^{-3}-$torr^{-1}$. Reprinted from (10:3484)

The calculated pump power in this case, however, is proportional to the square of the pressure. Fowler keeps the average electron energy, and thus E/N, constant. He also keeps the ratio of electron density to pressure, n_e/P, constant to keep the ratio of 1.5 eV electrons to molecules constant (10:3485). Therefore the pump power varies as the
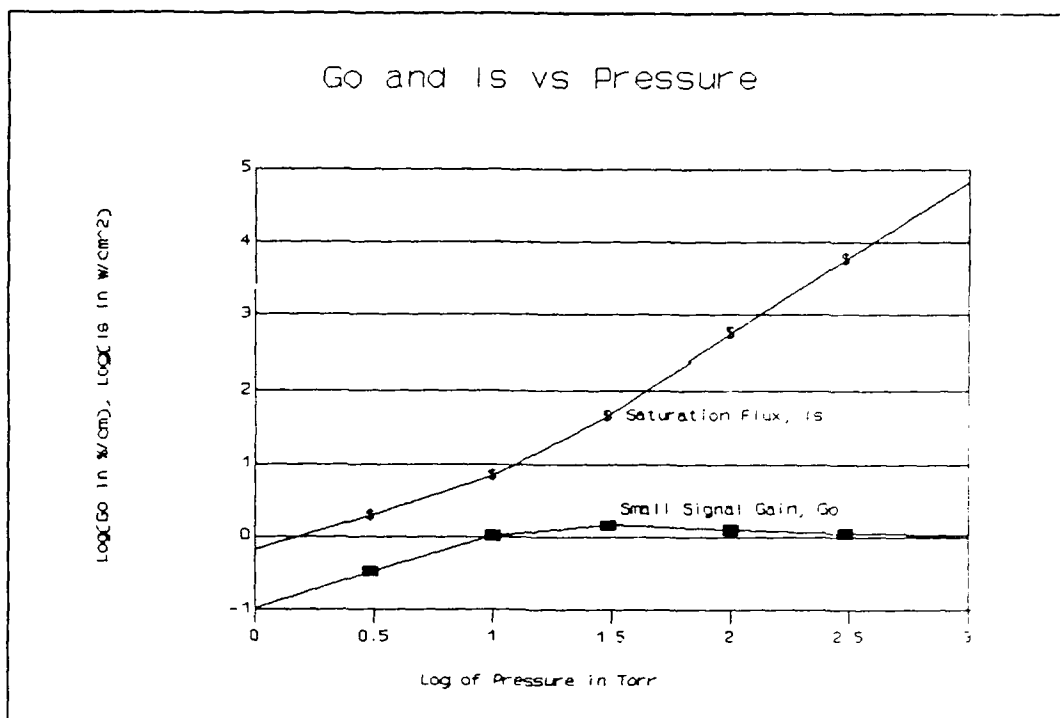
Figure 42. Calculated Small-Signal Gain and Saturation Flux vs Total Gas Pressure. Same conditions as Figure 41.

square of the pressure as follows:

$$\text{Pump power} = 0.5 \ kW/l(300°K/450°K)(P/10 \ torr)^2 \qquad (58)$$

The agreement between this model and Fowler's graph is good (Figures 41 and 42): this model shows the same trends for small-signal gain and saturation flux as the pressure is increased.

The behavior of the small-signal gain over the pressure range is determined by the pressure effect on both the radiative cross section and the population inversion (Equation 48, $Go \approx \sigma (n_{ao} - n_{bo})$). Given the appropriate

112

pump power, the population inversion increases with pressure. At low pressures, however, the radiative cross section is Doppler-broadened and a function of temperature only. At low pressures, therefore, the small-signal gain increases proportionally with pressure.

At higher pressures, however, the radiative cross section is pressure-broadened and inversely proportional to pressure. This cancels the proportional pressure dependence of the excited populations, and the small-signal gain remains constant with pressure.

Small-Signal Gain and Optical Power Density vs Gas Mix. The last relation Fowler studied was the effect of gas mix on the small-signal gain, Go, and optical power density, Is Go, (10:3486). Figure 43 shows Fowler's curves, and Figures 44 and 45 show this model's curves of small-signal gain and optical power density vs gas mix. Small-signal gain calculated by this model is a factor of two higher than Fowler's and the trend at low number densities of CO_2 is incorrect.

Figure 44 shows the author's calculated small-signal gain vs gas mix.

This incorrect trend for the small-signal gain at low number densities of CO_2 is an excellent example the limits of the author's model. One of Gilbert's basic assumptions was that the excited populations are sparsely populated, but

113
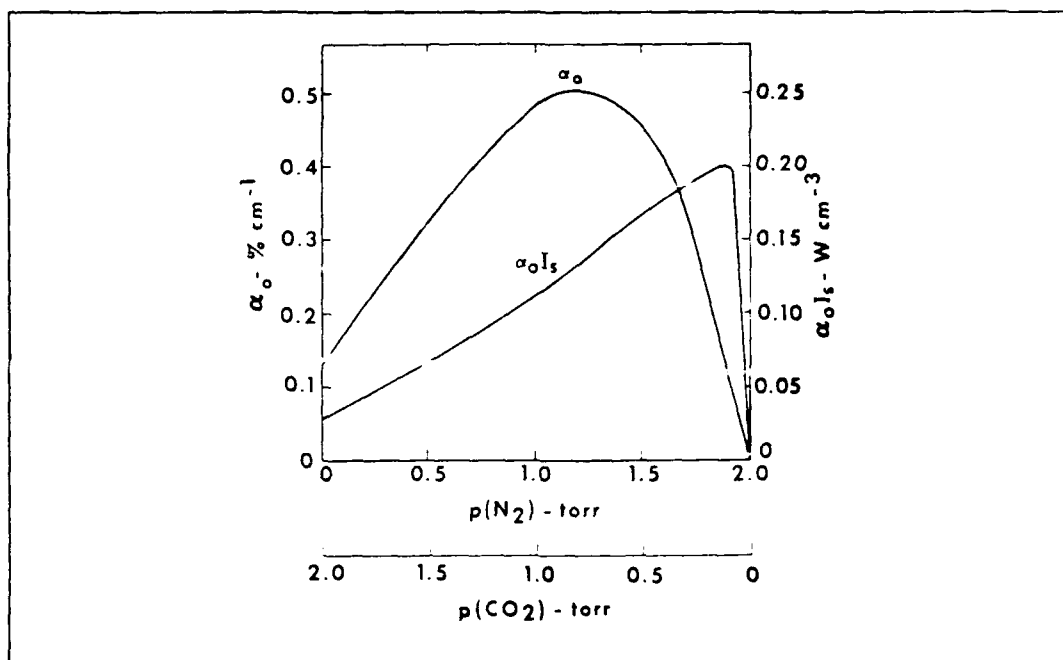
Figure 43. Small-Signal Gain and Optical Power Density vs Gas Mix from Fowler. Total P = 10 torr; T = 450°K; Mix = 8 torr He; Reduced Ave Elec Density = 1.50 eV; ne = 1×10^{10} cm^{-3}. Reprinted from (10:3486)
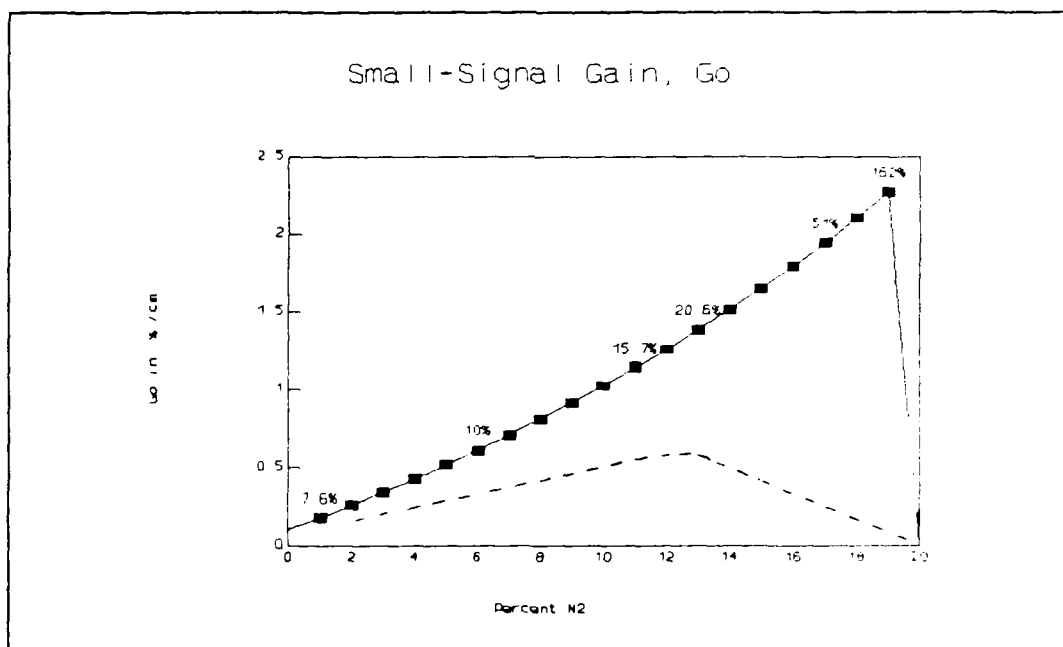
Figure 44. Calculated Small-Signal Gain vs Gas Mix. Same conditions as Figure 43. Numbers on the Curve are the % of CO_2 Pumped into Excited States. Dashed curve is Fowler's Small-Signal Gain from Figure 43.

114

that assumption is violated under the conditions of Figure

43. Figure 44 lists the percent of CO_2 pumped into all the

excited vibrational states this model tracks (010, 020, 100,

and 001). Figure 45 shows calculated optical power density.

The author's model diverges from Fowler's at 7% or less

of CO_2 where Fowler's small-signal gain peaks and begins to

decrease. This divergence occurs when about 20% of the CO_2
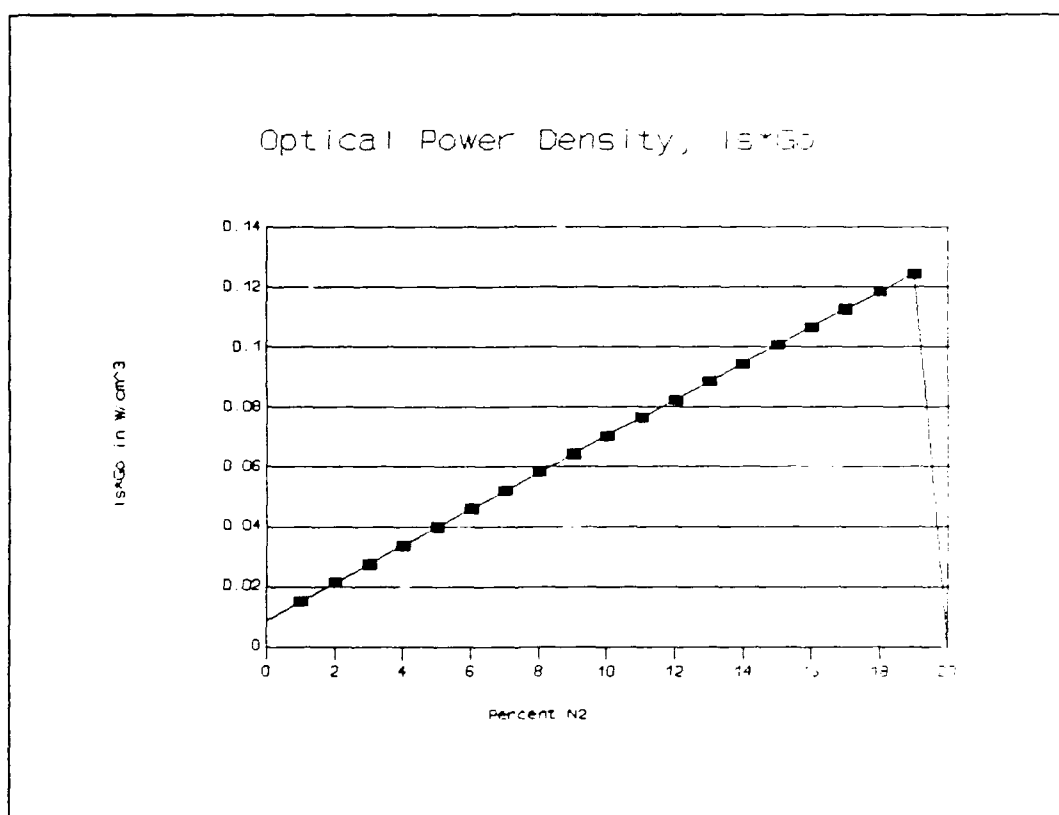
Figure 45. Calculated Optical Power Density vs Gas Mix.
Same Conditions as Figure 43.

has been pumped into all the excited states.

The percentage of CO_2 in the excited states increases

with decreasing CO_2 number density in the author's model

115

because for a given cavity configuration, the gain stays constant at the threshold gain. For the gain to remain constant, the population inversion (n_a - n_b) must remain constant. As the number density of CO_2 becomes smaller, n_a and n_b become a larger percentage of the total CO_2.

This model's maximum optical power density (Is*Go), however, compares very well with Fowler's (Figures 43 and 45). Although the curves match well, the author's model is still violates the assumption of sparsely populated excited states below 7% CO_2 under the conditions of Figure 43.

Fowler says that the optical power density continues to increase after small-signal gain begins to decrease because the increasing number density of N_2, coupled with the very effective pump mechanism provided by N_2, more than makes up for the decreasing gain and number density of CO_2 (10:3486).

Summary of Validation. In summary, the author's model was compared to five very different experimental CO_2 CW lasers with good agreement. When compared against a single laser run, the author's model calculated the laser output 23% to 63% higher (depending on the temperature) than the experimental output. In the parametric study by Mitsuhiro, the model correctly predicted the interactive effects of pressure and temperature at 200 to 300°K, and yielded good agreement with the experimental values (+10% to -40% at 100 torr, ± 5% at 20 torr).

In comparing the author's model with Fowler's, this study found very good prediction of the effects of temperature, pressure, pump power, and mix on small-signal gain, saturation flux, and optical power density. In each case, the author's model correctly predicted the trends, and at low pump power, matched small-signal gain to within 10%. The author's model also correctly predicted the effect of gas mix on small-signal gain and optical power density except at low CO_2 number densities.

Limits to the CW Model

Like the pulsed model, the CW model is limited by its assumptions, practical limits found during validation, and the valid range of its equations.

Limits Imposed by Assumptions. The following paragraphs discuss the limits imposed by the assumptions of point model, the four-level model, fast vibrational and rotational relaxation, and sparsely excited states.

Point Model. Although the assumption of a point model greatly simplifies the calculation of the CW laser output, it leads to an overestimation (about 50%) of the power produced in the experimental laser. This is because the photon flux, temp, and gain vary greatly within the laser cavity, and the model may only accurately predict the conditions in the center of the cavity.

117

In addition, the output mirror reflectivity must be greater than 50% for the point model to be valid.

Four-Level Model and Fast Relaxation. The assumptions of a four-level model and fast vibrational and rotational relaxation do not impose any limits because the CW laser operates at steady-state. Since the CW laser "pulse" is infinitely long and steady, the populations of CO_2 020 and 100 actually are equal, and the relaxation rates are "fast" compared to the "pulse" forming process.

Sparsely Populated Excited States. The assumption of sparsely populated excited states can be invalidated for the CW model at high pump powers and/or low number density of CO_2 and/or N_2. The pumping process can be viewed as a reaction between the electron and the CO_2 molecule.

$$CO_2 + e^* \; \rightleftharpoons \; CO_2^* + e \tag{59}$$
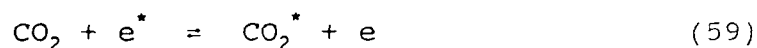
where e^* is an energetic electron, CO_2^* is an excited CO_2 molecule (vibrational level 001), and e is the electron after the interaction. The net pumping rate is equal to the rate of the forward reaction minus the rate of the reverse reaction.

$$\text{Net pump rate} = [CO_2][e^*]\gamma_f - [CO_2^*][e]\gamma_r \tag{60}$$

118

where [] denotes the concentration (number density) of the molecule or electron, and γs are the rate constants. If the number density of the excited state, CO_2^*, is small, then the net rate is approximately equal to $[CO_2][e^*]\gamma_f$ and the pump rate is a function of ground state and electron populations only.

If, however, the number density of the CO_2^* reaches a significant portion (say, 20%) of the total CO_2, then the reverse reaction (super-elastic collisions) becomes appreciable. As the number density of CO_2^* increases, the net pump rate decreases toward zero, and increasing the pump energy further will not increase the excited population appreciably. This is called saturation.

Although Smith described this phenomenon of saturation for the pulsed case (Figure 27, page 81), the concept also applies to the CW model. The author's model, however, does not account for saturation, so it may overestimate the output when the percent of CO_2 pumped into excited states exceeds 20%.

Practical Limits Found During Validation. The first practical limit found during validation was related to the phenomenon of saturation. The assumption of sparsely populated excited states was violated during validation when the ratio of pump power (kW/1) to the product of the partial pressures of CO_2 and N_2 (torr) exceeded approximately 5.0

119

kW/1-torr^2. Above this ratio, more than 20% of the CO_2 was pumped into excited states, and the small-signal gain began to diverge radically from Fowler's model (Figure 44).

The second practical limit found during validation was the pressure range. Unlike the pressure line shape in the pulsed model, the quasi-Voigt line shape is valid over a very large pressure range. The pressure is probably limited to greater than one torr by the number of CO_2 molecules available to lase, and to less than 300 torr by relaxation rates. The highest experimental pressure for a CO_2 CW laser found during the literature search was 280 torr.

Limits Imposed by Valid Range of Equations. The last limit to the CW model is that imposed by the valid range of the equations used. Similar to the pulsed model, the temperature is limited to 200 to 700°K by the valid range of the relaxation rates.

Summary of Limits to Model. In summary, although the model is not limited by the assumptions of the four-level model or of fast relaxation rates, it is limited by the assumptions of the point model and sparsely populated excited states. The CW model will overestimate the laser power output by about 50% based on the simplifications introduced by the point model. In addition, the ratio of pump power to product of the partial pressures of CO_2 and N_2 is limited to less than 5.0 kW/1-torr^2 by the requirement of

120

sparsely populated excited states. If this limit is exceeded, the model will overestimate the power output because it does not account for saturation of the upper vibrational level, CO_2 (001). Finally, the model is limited to a temperature range of $200°K$ to $700°K$ by the valid range of the relaxation rate equations, and the pressure is limited to 1 to 300 torr by practical limits.

V. OPTIMIZING THE CW MODEL USING RSM

Overview

The purpose of building a Response Surface Methodology (RSM) model of the CW laser model is two-fold. First is to use RSM to characterize the laser model and to find the optimum operating point to maximize power output. The second purpose is to lay a foundation for characterizing and optimizing the pulsed CO_2 laser model.

This chapter briefly describes RSM and the development of the CW RSM model, and briefly describes the different experimental designs that were tried and lessons learned from each. The validation and optimization of the resulting RSM models is then covered. The Results and Analysis section compares a third-order RSM model with a second-order model. Finally, this chapter discusses the conclusions and makes recommendations for further study.

Response Surface Methodology (RSM)

"Response surface methodology comprises a group of statistical techniques for empirical model building and model exploitation." (2:1) RSM was developed to empirically model the responses of a system, and can be applied to

122

stochastic or deterministic processes. Since the CW CO_2 laser models are deterministic, the RSM process becomes a curve-fitting exercise.

The object is to find a polynomial equation, based on the Taylor series, that will accurately predict the response of the system over the region of interest. For this study, the system is the CW laser model and the response is the output power. The polynomial equation, called the RSM model, ~nsists of a linear combination of the first order terms, higher order terms, and interaction effects of the predictor variables. The predictor variables are selected input variables (temperature, pressure, gas mix, etc.) that have been transformed and/or coded.

The great benefit of the RSM model is that this polynomial equation can be optimized analytically using calculus or Newton's Method (described on page 85). For instance, the pulsed CO_2 model cannot be analytically optimized, and the CW CO_2 model would be very difficult to optimize analytically, but an RSM model of either code could be optimized over the region to which it was fit. The robustness of the optimum point can also be determined (2:329-330). In addition, an RSM model of the CO_2 pulsed code could run very quickly (as opposed to the actual pulsed code) because it consists of only one polynomial equation. Finally, the interaction terms of the polynomial might give

123

insight into the physical relations between the input variables of the laser.

Developing the CW RSM Model

The CW RSM model is based on the assumption that, at most, a third-order polynomial is adequate to fit the data from the CW laser model.

Four iterations of CW RSM experimental designs were required to find the predictor variables and parameter space that contained the maximum operating point for the CW laser model. Each RSM model of the CW laser model was constructed using the following six steps.

Choose the Experimental Design. The first step in developing the RSM model is to choose the experimental design. The experimental design is the predictor variables, their range, and the number of levels for each variable. The input parameter space was chosen based on the probable operating regime of the CW laser and the operating regimes found in the literature. The first experimental design consisted of five independent variables (temperature, pressure, $\%CO_2$, $\%N_2$, and reflectivity) each at three levels. The only other independent variable, pump power, was constant at 5 kW/l. At high pressure, however, the power output was less than zero, and at low pressure and low temperature, the excited population of CO_2 exceeded 70%.

Since the optimum pump power is dependent on the pressure, the variable of pressure was dropped and an appropriate pump power chosen for 10 torr.

The second and third experimental designs expanded the range of $\%N_2$ and reflectivity to capture the optimum point. The third design also included four levels of reflectivity to improve the fit.

The improvements in the second and third designs were incorporated into the fourth and final experimental design, which is: Temperature = $200^\circ K$ - $425^\circ K$, percent N_2 = 20% - 80%, and reflectivity = 50% - 95%, each varied over four levels. The pressure was chosen to be 10 torr and the pump power fixed at 0.3 kW/l to keep the model within valid limits (excited CO_2 at 20% or less and the optimum reflectivity at 50% or greater). The losses were held constant at 1% because the best loss is the lowest, and 1% losses help bring the optimum reflectivity up to 50% or greater. Since the resonator length and reflectivity together determine the cavity lifetime, the resonator was fixed at 1 meter and the reflectivity was varied. This also allowed the optimum reflectivity predicted by the RSM model to be compared with the optimum reflectivity calculated by the CW model. Finally, the fraction of CO_2 was held constant at 4% with N_2 and helium making up the remaining 96% of the gas mix.

The fraction of CO_2 was held constant after it became clear that the optimum value for CO_2 would be zero because of a shortcoming in the CW laser model. Neither the saturation of the upper vibrational level nor the ground state of CO_2 are accounted for (explanation on page 115). As a result, the CW model calculates higher output power for decreasing $\%CO_2$, even down to .01% CO_2. Therefore, $\%CO_2$ was not used as a predictor variable and was held constant at 4% (the lowest fraction found in the literature).

The CW laser model does not calculate a higher output power at <u>high</u> concentrations of CO_2 because CO_2 very effectively depopulates the upper vibrational level. When the photon flux is low, as in a CW laser, the CO_2 may depopulate much of the upper vibrational level before it can be stimulated by the photons; therefore, low concentrations of CO_2 are desirable.

The fourth experimental design was also run at a pressure of 50 torr and a pump power of 8.0 kW/l to determine the effect of pressure on the location of the optimum point.

<u>Obtain the Data</u>. The second step of developing the RSM model is to obtain the data. For the fourth experimental design, the CW laser model was run 64 times, varying the temperature, $\%N_2$, and reflectivity over four equally spaced

126

levels spanning their ranges, and the resulting output power was recorded.

Fit the Data. The third step of developing the RSM model is to fit the data using a least squares linear regression. The predictor variables of temperature, %N2, and reflectivity were coded into levels (Appendix B) and the regression performed using the Statistix computer package. A second- or third-order equation that is linear in its coefficients is obtained by creating new predictor variables through combinations of the original variables. For example, if $X1$ = temperature (coded), then $X11 = X1^2$, and the polynomial can be written $Y = bo + b1\ X1 + B11\ X11$. The initial polynomial equation (RSM model) from an experimental design includes all the original predictor variables, all second-order terms and interactions, and all third-order terms and interactions. Later, predictor variables can be removed to reduce the complexity of the RSM model if the goodness of fit is not substantially reduced.

Check the Residuals. The fourth step of developing the RSM model is to check the residuals. The residuals are the difference between the actual power calculated by the CW laser model and the fitted value calculated by the CW RSM model. The residuals were checked for both absolute error and evidence of lack of fit. Figure 46 shows the residual plot from the second RSM experimental design, the evidence

127

for lack of fit, and the absolute error. This evidence for lack of fit led to using a four-level experimental design so a third-order polynomial could be fit.
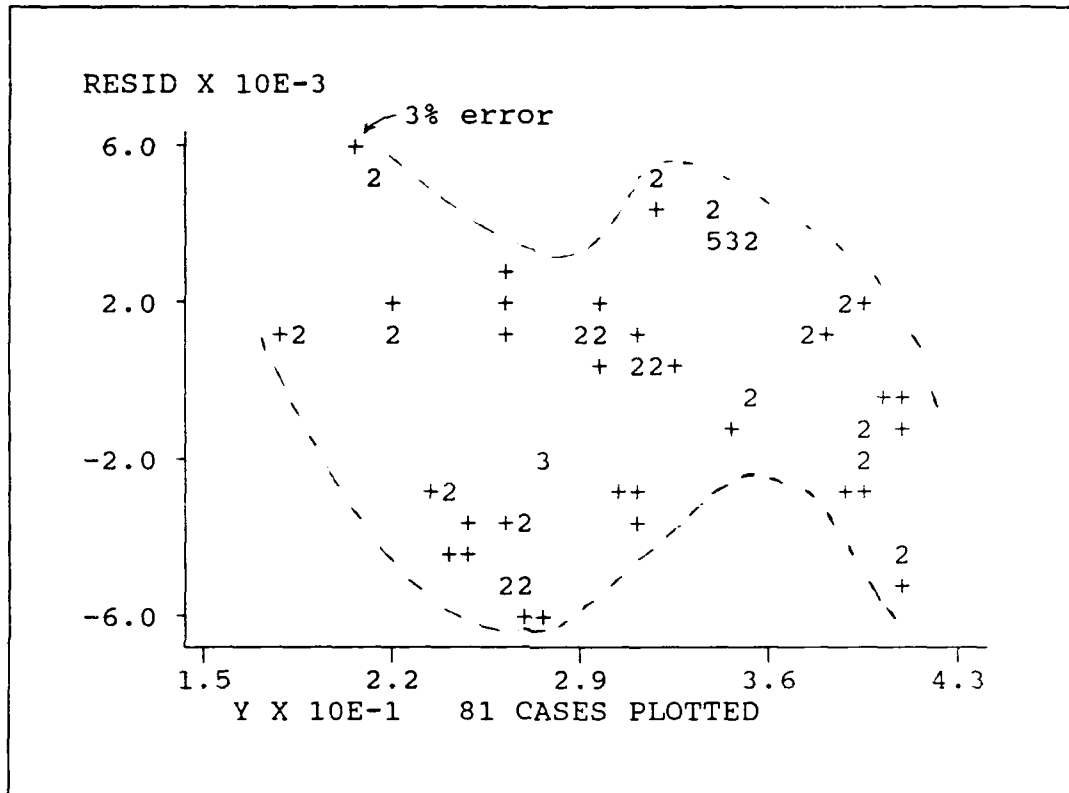
Figure 46.   Residual Plot from the Second CW RSM Experimental Design, Second-Order Model.

Reduce the Model. The fifth step of developing the RSM model is to reduce the complexity of the model, if possible, without substantially decreasing the goodness of fit.

A measure of the goodness of fit of the RSM model is the adjusted R^2

$$\text{adjusted } R^2 = 1 - \frac{(n - 1)}{(n - p)} \frac{SSE}{SSTO} \tag{61}$$

128

where n is the number of observations (runs), p is the number of predictor variables, SSE is the sum of squares of the error, and SSTO is the total sum of squares. Since the CW laser model is deterministic, there is no stochastic error and SSE is all error due to lack of fit. If a predictor variable can be eliminated from the model without increasing the SSE, then the adjusted R^2 increases, indicating a better fit.

By removing predictor variables with small individual sums of squares (ISS), the complexity of the model can be reduced without substantially decreasing the adjusted R^2. The individual sum of squares is a measure of that predictor variable's contribution to the goodness of fit of the RSM model, and small is defined as ISS/SSTO less than 0.0001.

Finally, the last step in developing the RSM model is to repeat steps 3 to 5 until the desired balance is achieved between a small, simple RSM model and a high adjusted R^2 (good fit). In the fourth and final iteration of RSM experimental designs, the author selected three CW RSM models to optimize: a third-order, high-resolution model with two third-order terms and three third-order interactions; a middle-resolution model with one third-order term; and a second-order, low-resolution model.

Validation

Validation tests the CW RSM model against the original CW laser model in the regions between the four levels where the RSM model was run, and compares the residual error with the validation error. The residual error is calculated during the linear regression at the four experimental levels. The validation error, however, is the difference found during the validation runs between the four experimental levels. If the two errors are approximately equal, then the RSM model should be good over the whole input range to which it was fit.

Nine validation runs were performed for the high-resolution and the low-resolution CW RSM models. The largest validation error for the high-resolution CW RSM model was 2%, and the average was 1.2%, compared with the largest residual error of 0.6%. The largest validation error for the low-resolution RSM model was 4%, and the average was 1.6%, compared with 2% for residual error. These errors are acceptable and the models are considered validated.

Optimization

Optimization consists of finding the stationary points of the polynomial for the CW RSM model, determining if that point is a maximum, and then determining if it is within the

input parameter space. Each RSM model was optimized using the following steps.

First, the polynomial was differentiated with respect to each of the predictor variables, and the resulting equations set equal to zero. The resulting set of simultaneous equations was then solved to find the stationary points. For the second-order polynomial, the solution consists of one matrix operation:

$$\mathbf{X}_s = -\tfrac{1}{2} \mathbf{B}^{-1} \mathbf{b} \tag{62}$$

where $\mathbf{X}_s$ is the vector of predictor variables for the stationary point, $\mathbf{B}$ is the matrix of coefficients for the second-order terms, and $\mathbf{b}$ is the vector of coefficients for the first order terms. For the third-order polynomials, however, Newton's method was used because the set of partial differential equations are non-linear.

The next step is to determine if the resulting stationary point is a maximum. For the second-order RSM model, the eigenvalues of the matrix of second-order coefficients ($\mathbf{B}$) were all negative, indicating a global maximum (2:341). For the third-order RSM model, the Jacobian matrix (used in Newton's method) is evaluated at the stationary point. If the matrix is negative-definite, then the stationary point is a maximum. A third-order

131

polynomial, however, has two stationary points, so both must be found and evaluated. For both third-order RSM models, both stationary points were found and evaluated; the maximum points are tabulated on page 134.

The final optimization step is to verify the maximum point and de-code the predictor variables. The CO_2 CW model was evaluated at several points around the stationary points of each RSM model, and the actual maximum was found close to the stationary points of the third-order RSM models. This technique verified the maximum point and revealed that the output power was fairly robust around the maximum. Finally, determining if the stationary point is within the parameter space simply involves decoding the predictor variables and comparing their value with the original range of the input variables. If the maximum had not been within the parameter range, then the parameter range could be selectively expanded, or the edges of the parameter space explored to find the constrained maximum.

Results and Analysis

The fourth and final experimental design provided the RSM models that are analyzed here. The range of the predictor variables and accuracy provided by four levels was sufficient to locate the maximum operating point for the CW laser model. In addition, the residuals (Figure 47) did not

132

show any visual evidence of lack of fit. Finally, the

result of adding the fourth level was an adjusted R^2 of

0.998 and a maximum residual error of 0.6% for the third-

order high-resolution model, which is excellent.
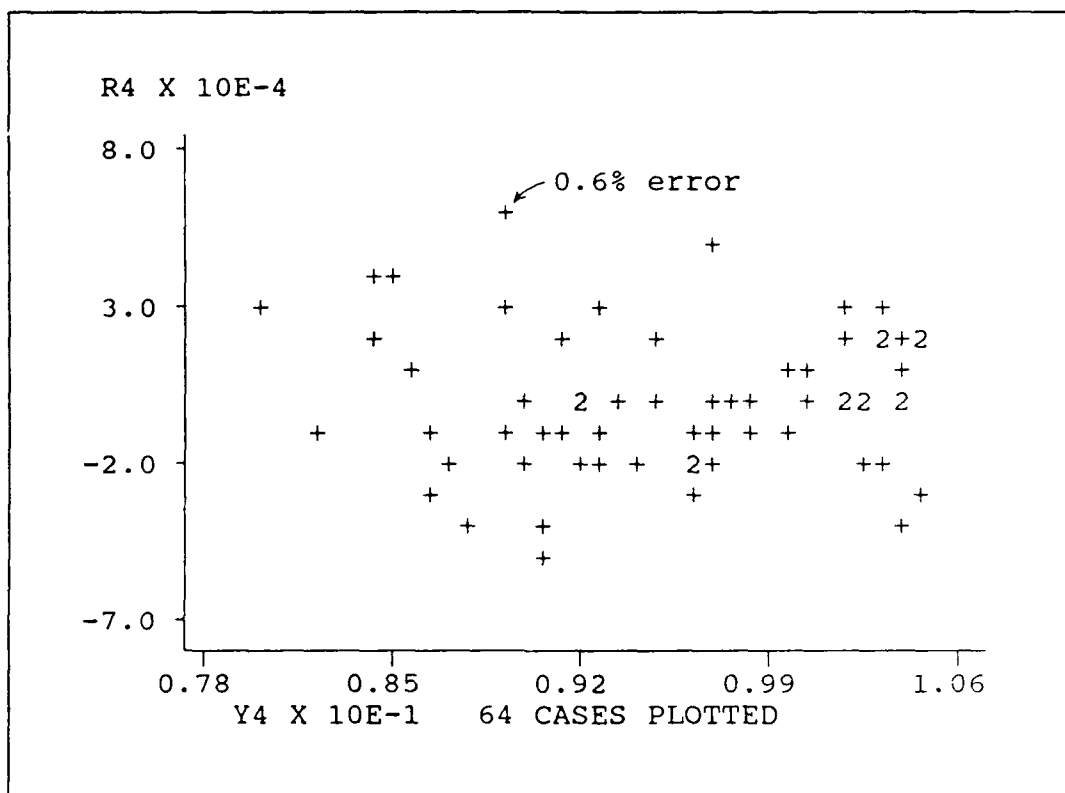
Figure 47.   Residual Plot from the Fourth CW RSM
Experimental Design, Third-Order High-Resolution Model.

The residuals for each CW RSM model showed no visual

evidence for lack of fit which supports the assumption that

a third-order fit is adequate. Even the second-order model

from the fourth experimental design showed no evidence for

lack of fit.

The following table presents the results from each of

the CW RSM models constructed from the fourth experimental

design. Each succeeding model was reduced from the previous by removing the predictor variables with the smallest individual sum of squares.

Table III. Summary of CW RSM Models

| Model | Adj R^2 | Max Resid Error | Stationary | Point | | Fitted Power, kW/l |
			Temp	N_2	R	
Third Ordr High Res	0.998	0.6%	230°K	63%	71%	0.1052
Third Ordr Med Res	0.992	1.5%	213°K	65%	70%	0.1059
Scnd Ordr Low Res	0.964	2%	185°K	65%	62%	0.1072
Actual CW Model	N/A	N/A	220°K	66%	65%	0.1051

This successful fourth experimental design was also run at a total pressure of 50 torr and a pump power of 8.0 kW/l. The stationary points predicted by the 50 torr CW RSM models were the same as the 10 torr models (within 2%), and the actual maximum point was exactly the same: 220°K, 66% N_2, and 65% reflectivity. The maximum point then, may not change much over a small pressure range.

An interesting result found in all three RSM models is a strong interaction between temperature and reflectivity which was not readily apparent in the CW laser model. The temperature and reflectivity do, however, interact through

134

the Rigrod equation (Equation 54). The temperature greatly affects the small-signal gain, Go, and the reflectivity determines, in part, the threshold gain, G. The Rigrod equation then relates those two terms to the cavity flux.

Not only did the RSM models reveal the temperature-reflectivity interaction, but they also correctly predicted the optimum reflectivity. The reflectivity of the maximum point compares very well with the optimum reflectivity calculated by the CO_2 CW code (Equation 57, page 96). The reflectivity at the maximum point for the high-resolution model is 71%, and the optimum reflectivity calculated by the CW code at the maximum point conditions is 65%. The difference in output power at 71% vs 65% reflectivity is 0.1%.

Although the location of the predicted optimum points were close, there is some error. Box and Hunter describe the calculation of a confidence region for the location of the actual maximum point if the error is due to the observations and the error due to lack of fit is ignored (3:192). For this RSM model, however, there is no error in the observations (the output power from the CW laser model); all the error is lack of fit. Therefore, a confidence region cannot be calculated using Box and Hunter's method, but the error in the location of the maximum can be compared between the three RSM models. The two third-order RSM

models come much closer to predicting the true maximum point than the second-order RSM model.

Although the second-order model is not as accurate, the eigenvalues at it's maximum do yield information about the point. The eigenvalues evaluated at the stationary point for the second-order, low-resolution model are $-.00366$, $-.00146$, $-.00096$. The fact that each eigenvalue is negative means that the stationary point is a maximum. Their small absolute value means that the region around the stationary point is fairly flat and insensitive to changes in the predictor variables. Both results were confirmed by the verification of the actual maximum point. The output power varied by less than 1% over a range of $40°K$, 10% reflectivity, and 10% N_2 around the actual maximum point. Because the maximum point is so flat, a small error in fitting the slope there by the RSM model can cause a large error in locating the maximum point. Figure 48 graphically shows the location and robustness of the maximum power for the CW laser model at 10 torr.
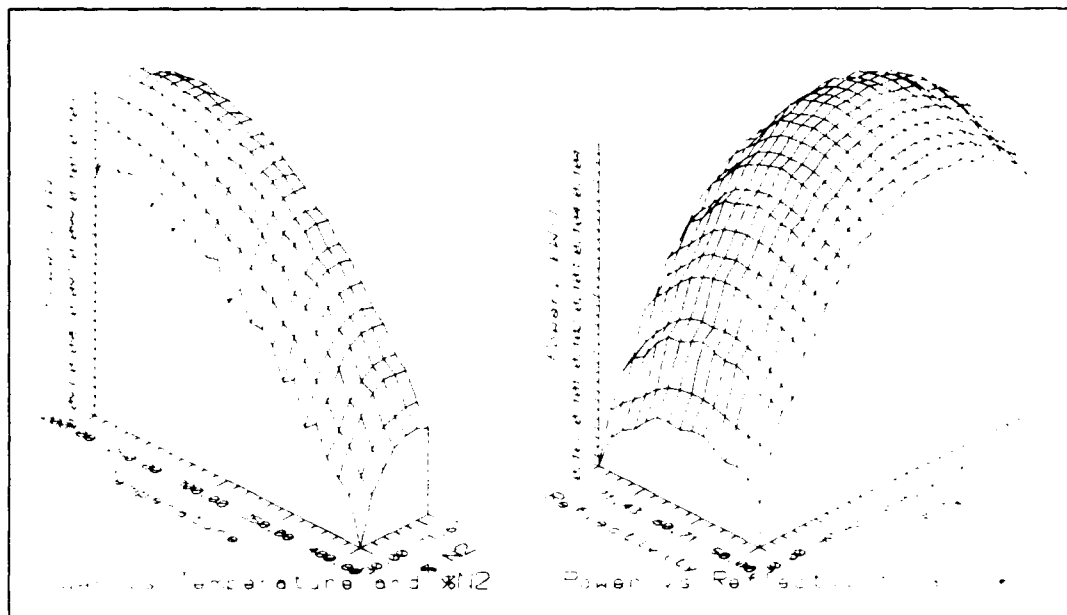
Figure 48. CW Output Power as a Function of % N_2 and Temperature, and % N_2 and Reflectivity. 10 torr and 4% CO_2.

Conclusions

There are two possible figures of merit for judging the RSM models. If the figure of merit is how closely they come to predicting the actual maximum point, then the third-order, medium-resolution model is the best. This figure of merit, however, can only be used after the actual optimum point is found. The other figure of merit, the fit of the RSM model, can be applied before the actual optimum point is calculated. The third-order, high-resolution model had the best fit and lowest residual error, and predicted a stationary point close to the actual, but was the most complicated. The second-order, low-resolution model,

however, had the poorest fit and was farthest from predicting the actual maximum point.

The accuracy of prediction of the stationary point depends on several factors. First, the stationary point must be within the space covered by the predictor variables. The stationary point for the second experimental design is $170^{\circ}K$, 40% N_2, and 51% reflectivity, which is moderately close to the actual maximum, but the fourth experimental design is much closer because it covered the stationary point. Second, expanding the range of the predictor variables increases the chance of catching the stationary point, but reduces the goodness of fit. The second experimental design has an adjusted R^2 of 0.997 and a residual error of 3%, while the third experimental design (which covered a greater range) has an adjusted R^2 of 0.977 and a residual error of 6%. This increase in error can be compensated for by adding a fourth level and fitting a third-order model. The fourth experimental design includes four levels and it's third-order RSM model has an adjusted R^2 of 0.998 with a residual error of 0.6%. Part of this improvement, however, may also be due to dropping one of the predictor variables.

One of the shortcomings to dropping predictor variables from the RSM model is that it limits the useful range of the RSM model. The models constructed from the fourth

experimental design are useful only at 10 torr, 0.3 kW/l pump power, 4% CO_2, etc. Thus, the experimental design must be chosen carefully with the final purpose of the RSM model in mind.

Since the final purpose of the CW RSM model was to explore the usefulness of RSM for characterizing the CW CO_2 laser model and for finding the optimum operating point, that purpose was accomplished. The third-order, high-resolution CW RSM model can predict the output power for the CW model to within 2% and correctly predicted the operating point for maximum power.

Finally, both laser models should be upgraded before proceeding further with RSM. There is an optimum mix for CO_2, but the CW laser model must be upgraded before it can be found. In addition, RSM does appear promising for optimizing the pulsed laser model.

VI.   CONCLUSIONS

Both the pulsed and continuous wave CO_2 laser models were successfully verified, and extensively validated. Both models met the goal of correctly predicting trends in the output based on input parameters. Finally, the CW laser model was optimized using RSM. The following paragraphs review the strengths and limits of each model.

Strengths of the Pulsed CO_2 Model

The author's model was compared against two five-level models over a wide range of pump powers, cavity configurations, and gas mixes. In each case the model correctly predicted the trends in peak power, time to the peak, and the pulse shape. It predicted the absolute value of the peak power and timing of the laser spike to 60% or better. The model also correctly calculated a linear temperature rise during the pump pulse to within 10%. The model was very useful in studying the relationship between temperature and gain, peak power, total pulse energy, and the laser pulse shape.

Limits of the Pulsed CO_2 Model

In summary, the model is limited by the assumptions and by the valid range of the equations used. The point model assumption limited the product of the gain and the length to less than 200% and the output mirror reflectivity to greater than 50%. The assumption of fast relaxation rates limits the laser pulse length to about 10 nanoseconds or greater. The assumption of sparsely populated excited states limits the pump efficiency to 0.2 or less when the mix contains 10% CO_2 and 10% N_2. The assumption that a four-level model is adequate, however, does not appear to place any significant limitations on the model. The last set of limits are imposed by the valid range of the line width and relaxation rate equations, and they limit the pressure to 0.1 to 10 atm, and the temperature to 200 to 700°K.

Strengths of the Continuous Wave CO_2 Model

In summary, the author's model was compared to six very different experimental CO_2 CW lasers with good agreement. When compared against a single laser run, the author's model calculated the laser output 23% to 63% higher (depending on the temperature) than the experimental output. In the parametric study by Mitsuhiro, the model correctly predicted the interactive effects of pressure and temperature at 200

141

to 300°K, and yielded good agreement with the experimental values (+10% to -40% at 100 torr, ± 5% at 20 torr).

In comparing the author's model with Fowler's, this study found very good prediction of the effects of temperature, pressure, and pump power on small-signal gain, saturation flux, and optical power density. In each case, the author's model correctly predicted the trends, and at low pump power, matched small-signal gain to within 10%. The author's model also correctly predicted the effect of gas mix on small-signal gain and optical power density except at low CO_2 number densities.

Limits of the Continuous Wave Model

In summary, although the model is not limited by the assumptions of the four-level model or of fast relaxation rates, it is limited by the assumptions of the point model and sparsely populated excited states. The CW model will over estimate the laser power output by about 50% based on the simplifications introduced by the point model. In addition, the ratio of pump power to the product of the partial pressures of CO_2 and N_2 is limited to less than approximately 5.0 kW/l-torr^2 by the requirement of sparsely populated excited states. If this limit is exceeded, the model will overestimate the power output because it does not account for saturation of the upper vibrational level, CO_2

142

(001). Finally, the model is limited to a temperature range of 200 to 700°K by the valid range of the relaxation rate equations, and the pressure is limited to 1 to 300 torr by practical limits.

Strengths of the RSM Model

Although the RSM model of the CW laser model was limited in its application, it was optimized and provides the basis for further optimization. The third-order, high-resolution CW RSM model can (within limits) predict the output power for the CW model to within 2% and correctly predicted the operating point for maximum power. Although the third-order RSM model is more complex and required Newton's method to find the stationary points, it is more accurate than the second-order RSM model. Finally, characterizing the CW laser model in preparation for optimizing it revealed that RSM could be used to both characterize and optimize the pulsed laser model.

Limits of the RSM Model

The greatest limit to the RSM model is the limiting constraints of the CW laser model. The CW laser model could only be optimized over temperature, percent N_2 in the gas mix, and the reflectivity of the output mirror. The gas mix could not be optimized over percent CO_2 because the CW laser

model does not account for saturation of the upper vibrational level of the CO_2, or it's ground state.

Finally, any RSM model is valid only over the region to which it was fit. In addition, if the maximum point does not lie within the range of the predictor variables, then a new RSM model must be fit, or the boundaries of the experimental design explored to find the constrained optimum point.

VII. RECOMMENDATIONS

Pulsed CO_2 Model

The following recommendations are provided for the guidance of follow on work to the pulsed CO_2 model.

1. Construct a five-level model. This would require one more rate equation in the Runge-Kutta routine for vibrational level 020, and an expression for the collisional exchange rate between vibrational levels 100 and 020.

2. Explicitly account for the thermal population and energy in the 010 vibrational level. Currently the model assumes that the population and energy of the 010 level is equal to the 100 level.

3. Include a graph routine to display output data (power, energy, populations, and gain) in graphical form in addition to the present tabular form.

4. Validate the pulse shape and peak power as a function of temperature (Figures 6 to 9). This behavior was not found in the literature.

5. Incorporate a program to more accurately model the pump pulse. An AFIT thesis completed by David Honey (GEP-

89D) contains a model that solves the Boltzmann equation to model the pump pulse.

6.   Use Response Surface Methodology or another analytical tool to optimize the computed output of the pulsed model. No such effort was found in the literature.

Continuous Wave CO_2 Model

The following recommendations are provided for the guidance of follow on work to the CW CO_2 model.

1.   Explicitly account for the population of CO_2 010 and the ground populations of CO_2 and N_2. This is in preparation for Recommendation Number Two.

2.   Empirically model the pump rates. Currently, the pump rates for the various vibrational levels are constant, regardless of the population of the ground state or the vibrational level population. Page 119 discusses super-elastic collisions, the phenomenon of saturation, and a possible model for the pump process. This might involve specifying the number density of the electrons and E/N for the pump, and including equations for the ground populations of CO_2 and N_2 in the set of state equations solved by Newton's Method.

3. Model the heat transfer out of the CW laser. For convective and conductive heat transfer, the heat transfer rate can be modeled as

$$q = K_T \ A \ \Delta T \qquad (63)$$

where q is the heat transfer rate (J/sec), K_T is the combined heat transfer coefficient (J/sec-m^2-$^{\circ}$K), A is the area available for heat transfer (m^2), and ΔT is the temperature difference between the bulk gas temperature and the cooling jacket. Additionally, for steady-state conditions, q = pump power - output power . The modeler can find a representative heat transfer coefficient, K_T, in the literature, set the cooling jacket temperature and area, and then iteratively solve for the gas temperature and resulting output power.

Once the heat transfer has been modeled, it might be validated against data provided by Deutsch. Deutsch varied the input power and reflectivity to find the optimum combination, and the results appear to be a function of the internal temperature of the laser (6:974).

4. Incorporate a routine to graph the CW laser output as a function of an input parameter. For instance, given a pressure and gas mix, the model could graph the output power as a function of temperature over a given temperature range.

147

5. Use Response Surface Methodology or another analytical tool to optimize the computed output of the CW model. No such effort was found in the literature.

RSM Modeling and Optimization

The following recommendations are provided for the guidance of follow on work to the RSM modeling and optimization.

1. Before proceeding any further with RSM, both the pulsed and CW laser models should be upgraded according to the previous recommendations.

2. RSM should be used to both characterize and optimize the pulsed CO_2 laser model. Characterizing might require a different experimental design than optimizing, but it could produce an RSM model that can be used to quickly calculate the peak power and total energy of the pulsed CO_2 laser.

3. After the CW laser model is upgraded, an optimum fraction of CO_2 and the optimum pump power or pressure may be found.

4. When building the RSM models, use a four- or five-level design to fit third-order polynomials.

Appendix A: _Definition of Terms_

Electron Pumping:

Pin = pump power (W)
I_c = current (amps)
E^c = voltage (volts)
N_o = total molecular number density (number/m^3)
N_e = electron number density in the active medium
      (number/m^3)
[] = concentration (number density) of the molecule or
      electron
γs = rate constants (1/sec)

Rate Equations:

n_a = number density of the upper vibrational level CO_2
        (001) (number/m^3)
$n_{b'}$ = number density of the lower vibrational level CO_2
        (100 + 020 + 010) (number/m^3)
n_b = number density of lower vibrational level CO_2 (100)
        (number/m^3)
n_c = number density of the excited N_2 (v=1) (number/m^3)
n_{ae} = thermal equilibrium number density of CO_2 (001)
        (number/m^3)
nbe   = thermal equilibrium number density of CO_2 (100)
        (number/m^3)
gu/gl = degeneracy ratio of the upper vibrational level to
        the lower level
I   = photon flux in the cavity (photons/m^3)
σ = effective radiative cross section of CO_2 (m^3)
σ_U = effective radiative cross section of the upper laser
        level CO_2 (001, j=19) (m^3)
σ_L = effective radiative cross section of the lower laser
        level CO_2 (100, j=20), (m^3)
γ_a = relaxation rate from CO_2 (001) level to 100 level
        (1/sec)
γ_b = relaxation rate from CO_2 (100) level to ground state
        (1/sec)
γ_c = energy transfer rate between CO_2 (001) level and N_2
        (v=1) (1/sec)
γ_{co2} = energy transfer rate from N_2 (v=1) to CO2 (001)
        (1/sec)
γ_{cn2} = energy transfer rate from CO_2 (001) to N2 (v=1)
        (1/sec)
γ_{co} = relaxation rate of excited N_2 to ground state
        (1/sec)

W_a = pump rate into CO_2 (001) level from ground state (number/m^3-sec)

W_b = pump rate into (100) level from ground state (number/m^3-sec)

W_c = pump rate into excited N_2 (v=1) from ground state (number/m^3-sec)

W_s = spontaneous emission rate into the axis of the mirrors (photons/m^3-sec)

τ_{cav} = photon lifetime in the cavity (sec)

Laser Cavity and Gain Parameters:

N_o = number density of the gas (number/m^3)
P = gas pressure
T = temperature ($^{\circ}$K)
k = $1 - R$
$Nopt$ = optimum output coupling
R = reflectivity of the output mirror
$Ropt$ = output mirror reflectivity that provides the optimum output coupling
a = the unfavorable losses in the cavity per round trip
L = the resonator length (m)
G = gain of the laser (%/m)
Gc = threshold gain (fraction/m)
Go = small-signal gain (%/m)
n_{ao} = number density of CO_2 (001) under zero flux conditions (number/m^3)
n_{bo} = number density of CO_2 (100) under zero flux conditions (number/m^3)
f = relates cavity flux to output flux
Is = saturation flux (photons/m^3)
$Pout$ = the laser power out in Watts per m^3 of active medium
τ_1 = time constant for the relaxation of the lower laser level to the ground state
τ_2 = time constant for the relaxation of the upper laser level to the ground state
τ_{21} = time constant for the relaxation of the upper laser level to the lower laser level

Boltzmann Distributions:

N_i = number of molecules in the ith vibrational level (number/m^3)
E_i = energy difference between the ground and the ith vibrational level (J)

f_{vj} = fraction of molecules in vibrational level v that are in rotational level j

n_{vj} = number of molecules in rotational level j and vibrational level v (number/m^3)

n_v = number of molecules in vibration level v (number/m^3)

C = 2 h B_v /k T, a normalization factor

$F(j)$ = B_v j(j + 1) + D_v $j^2(j+1)^2$ (Hz)

B_v, D_v = rotational constants, different for each vibrational level (Hz)

j = rotational line number

Relaxation Rates:

γ_i = temperature dependent relaxation rate of vibrational level i (1/sec)

$\gamma_{i'}$ = relaxation rate at 300°K (1/sec)

ν_1 = frequency of emission for the 100 level (Hz)

ν_2 = frequency of emission for the 010 level (Hz)

ν_3 = frequency of emission for the 001 level (Hz)

h ν_i = energy of the ith vibrational level (J)

τ_3 = 1/γ_a, time constant for relaxation of the upper vibrational level as a function of temperature (sec)

τ_{3o} = $(P(\Sigma \psi_i K_i))^{-1}$, time constant at To for the particular pressure and gas mix involved (sec)

ψ_i = fraction of gas component i

K_i = rate constant for gas component i (1/torr-sec)

T_o = base line temperature ($^\circ$K)

K_i' = fitted rate constant for gas component i

N_i = number density of gas component i

x = $T^{-1/3}$

A'-D' = fitted constants

Line Shapes:

Sv = quasi-Voigt line shape at line center (sec)

$\Delta\nu_d$ = Doppler-broadened line width, half width at half maximum (Hz)

$\Delta\nu_p$ = pressure-broadened line width, half width at half maximum (Hz)

$\Delta\nu$ = pressure-broadened line width, half-width at half maximum (cm^{-1}) from Brimacombe's equation

a_1 = 0.1149 - 9.2x10^{-4} (-j)   for CO_2 (cm^{-1}/atm)

a_2 = 0.0794 - 4.3x10^{-4} (-j)   for N_2 (cm^{-1}/atm)

a_3 = 0.0598 - 2.8x10^{-4} (-j)   for He (cm^{-1}/atm)

j = rotational number

n = 0.42$\pm$ 0.06, exponential term for temperature

ψCO_2 = fraction of CO_2 in the gas mix
ψN_2 = fraction of N_2 in the gas mix
ψHe = fraction of He in the gas mix
ν = frequency at line center (Hz)
M = molecular weight of the lasing molecule (Kg/kgmol)
f_U = fraction of CO_2 001 molecules in the j=19 rotational level
f_L = fraction of CO_2 100 molecules in the j=20 rotational level
A = Einstein coefficient
ν = laser frequency in Hz

Energy Balance Equations:

Cv	= Constant volume heat capacity of CO_2 (J/kgmol-$^\circ$K)
q	= rate of thermal energy added to the gas (W/m^3)
W	= rate of total energy added to the medium by pump (W/m^3)
R_e	= rate of energy pumped into all vibrational levels (W/m^3)
R_{st}	= rate of energy lost to stimulated radiation (W/m^3)
R_{vt}	= rate of energy converted to heat from vibrational relaxation to the ground state (W/m^3)
R_{vv}	= rate of energy converted to heat from vibrational energy exchanges between molecules (W/m^3)
Wi	= rate molecule (i) is pumped into an excited vibrational state (number/m^3-sec)
f_η	= fraction of pump energy that directly heats the gas
TotPumpE(j)	= cumulative pump energy at step time step j (J/m^3)
Δt	= time step size in units of laser cavity lifetime (sec)
NiEng	= the energy density of the corresponding vibrational level (J/m^3) (not including that added by thermal energy)
Energy(j)	= cumulative photon energy (J/m^3) at the jth time step
Power(j)	= current laser light power (W/m^3)
T_{init}	= initial temperature at time 0 of the laser ($^\circ$K)
TotHeatE(j)	= cumulative thermal energy added to medium up to time j (J/m^3)
Cv_i	= constant volume heat capacity of constituent i (degrees of freedom)

K_T = combined heat transfer coefficient (J/sec-m^2-$^\circ$K)

A = area available for heat transfer (m^2)

ΔT = temperature difference between the bulk gas temperature and the cooling jacket

Newton's Method:

X = (n_a, n_b, n_c, I)
$F(X)$ = (d(n_a)/dt, d(n_b)/dt, d(n_c)/dt, dI/dt)
$J(X)$ = The Jacobian matrix of $F(X)$

RSM Equations:

adjusted R^2 = measure of goodness of fit
n = number of observations (runs)
p = number of predictor variables
SSE = sum of squares of the error
SSTO = total sum of squares.
X_s = vector of predictor variables for the stationary point
B = matrix of coefficients for second-order terms
b = vector of coefficients for first order terms

Constants:

c = speed of light (3x10^8 m/s)
h = Planck's constant (6.62x10^{-34} J-sec)
k = Boltzmann's constant (1.38x10^{-23} J/$^\circ$K)
R = universal gas constant (8314 J/kgmol-$^\circ$K)

Appendix B: RSM ANOVA Tables

The following pages contain the coefficient and ANOVA
tables for the third-order, high-resolution; third-order,
medium-resolution; and the second-order, low-resolution CW
RSM models.   These models were constructed at a pressure of
10 torr.

The coded variables were calculated in the following
manner:

X1 = (Temperature - 312.5) / 75

X2 = (%N$_2$ - 50) / 20

X3 = (Я - 72.5) / 15

Xij = Xi * Xj

Xijk = Xi * Xj * Xk , etc.

where

Temperature = 200°K to 425°K in steps of 75°K

%N$_2$ = 20% to 80% in steps of 20%

Я   = 50% to 95% in steps of 15%

Coefficient and ANOVA Tables

for the Third-Order, High-Resolution CW RSM Model

UNWEIGHTED LEAST SQUARES LINEAR REGRESSION OF PWRA

PREDICTOR VARIABLES	COEFFICIENT	STD ERROR	STUDENT'S T	P
CONSTANT	1.0309E-01	7.5825E-05	1359.52	0.0000
X1	-2.9006E-03	4.5523E-05	-63.72	0.0000
X2	1.5364E-03	1.0730E-04	14.32	0.0000
X3	9.4213E-04	1.0730E-04	8.78	0.0000
X11	-1.2738E-03	3.1794E-05	-40.06	0.0000
X22	-1.4582E-03	3.1794E-05	-45.86	0.0000
X33	-3.3511E-03	3.1794E-05	-105.40	0.0000
X13	1.7262E-03	2.5435E-05	67.87	0.0000
X222	4.0294E-04	4.7396E-05	8.50	0.0000
X333	-1.5378E-03	4.7396E-05	-32.45	0.0000
X112	-1.3483E-04	2.8438E-05	-4.74	0.0000
X113	3.1596E-04	2.8438E-05	11.11	0.0000
X331	-1.7186E-04	2.8438E-05	-6.04	0.0000

STEPWISE ANALYSIS OF VARIANCE OF PWRA

SOURCE	INDIVIDUAL SS	CUM DF	CUMULATIVE SS	CUMULATIVE MS	ADJUSTED R-SQUARED
CONSTANT	5.8347E-01				
X1	7.7645E-04	1	7.7645E-04	7.7645E-04	0.2687
X2	3.8505E-04	2	1.1615E-03	5.8075E-04	0.4003
X3	2.6365E-04	3	1.4252E-03	4.7505E-04	0.4903
X11	1.0384E-04	4	1.5290E-03	3.8225E-04	0.5217
X22	1.3609E-04	5	1.6651E-03	3.3302E-04	0.5668
X33	7.1872E-04	6	2.3838E-03	3.9730E-04	0.8460
X13	2.9799E-04	7	2.6818E-03	3.8311E-04	0.9643
X222	4.6760E-06	8	2.6865E-03	3.3581E-04	0.9656
X333	6.8106E-05	9	2.7546E-03	3.0607E-04	0.9936
X112	1.4543E-06	10	2.7560E-03	2.7560E-04	0.9941
X113	7.9862E-06	11	2.7640E-03	2.5128E-04	0.9975
X331	2.3628E-06	12	2.7664E-03	2.3053E-04	0.9985
RESIDUAL	3.2995E-06	63	2.7697E-03	4.3963E-05	

CASES INCLUDED	64	MISSING CASES	0
DEGREES OF FREEDOM	51		
OVERALL F	3.563E+03	P VALUE	0.0000
ADJUSTED R SQUARED	0.9985		
R SQUARED	0.9988		
RESID. MEAN SQUARE	6.470E-08		

Coefficient and ANOVA Tables

for the Third-Order, Medium-Resolution CW RSM Model

UNWEIGHTED LEAST SQUARES LINEAR REGRESSION OF PWRA

PREDICTOR VARIABLES	COEFFICIENT	STD ERROR	STUDENT'S T	P
CONSTANT	1.0309E-01	1.7877E-04	576.64	0.0000
X1	-3.1154E-03	6.7046E-05	-46.47	0.0000
X2	2.1939E-03	6.7046E-05	32.72	0.0000
X3	1.3371E-03	2.3868E-04	5.60	0.0000
X11	-1.2738E-03	7.4960E-05	-16.99	0.0000
X22	-1.4582E-03	7.4960E-05	-19.45	0.0000
X33	-3.3511E-03	7.4960E-05	-44.71	0.0000
X13	1.7262E-03	5.9968E-05	28.79	0.0000
X333	-1.5378E-03	1.1174E-04	-13.76	0.0000

STEPWISE ANALYSIS OF VARIANCE OF PWRA

SOURCE	INDIVIDUAL SS	CUM DF	CUMULATIVE SS	CUMULATIVE MS	ADJUSTED R-SQUARED
CONSTANT	5.8347E-01				
X1	7.7645E-04	1	7.7645E-04	7.7645E-04	0.2687
X2	3.8505E-04	2	1.1615E-03	5.8075E-04	0.4003
X3	2.6365E-04	3	1.4252E-03	4.7505E-04	0.4903
X11	1.0384E-04	4	1.5290E-03	3.8225E-04	0.5217
X22	1.3609E-04	5	1.6651E-03	3.3302E-04	0.5668
X33	7.1872E-04	6	2.3838E-03	3.9730E-04	0.8460
X13	2.9799E-04	7	2.6818E-03	3.8311E-04	0.9643
X333	6.8106E-05	8	2.7499E-03	3.4374E-04	0.9918
RESIDUAL	1.9779E-05	63	2.7697E-03	4.3963E-05	

CASES INCLUDED	64	MISSING CASES	0
DEGREES OF FREEDOM	55		
OVERALL F	955.9	P VALUE	0.0000
ADJUSTED R SQUARED	0.9918		
R SQUARED	0.9929		
RESID. MEAN SQUARE	3.596E-07		

Coefficient and ANOVA Tables

for the Second-Order, Low-Resolution CW RSM Model

UNWEIGHTED LEAST SQUARES LINEAR REGRESSION OF PWRA

PREDICTOR VARIABLES	COEFFICIENT	STD ERROR	STUDENT'S T	P
CONSTANT	1.0309E-01	3.7345E-04	276.03	0.0000
X1	-3.1154E-03	1.4006E-04	-22.24	0.0000
X2	2.1939E-03	1.4006E-04	15.66	0.0000
X3	-1.8154E-03	1.4006E-04	-12.96	0.0000
X11	-1.2738E-03	1.5659E-04	-8.13	0.0000
X22	-1.4582E-03	1.5659E-04	-9.31	0.0000
X33	-3.3511E-03	1.5659E-04	-21.40	0.0000
X13	1.7262E-03	1.2527E-04	13.78	0.0000

STEPWISE ANALYSIS OF VARIANCE OF PWRA

SOURCE	INDIVIDUAL SS	CUM DF	CUMULATIVE SS	CUMULATIVE MS	ADJUSTED R-SQUARED
CONSTANT	5.8347E-01				
X1	7.7645E-04	1	7.7645E-04	7.7645E-04	0.2687
X2	3.8505E-04	2	1.1615E-03	5.8075E-04	0.4003
X3	2.6365E-04	3	1.4252E-03	4.7505E-04	0.4903
X11	1.0384E-04	4	1.5290E-03	3.8225E-04	0.5217
X22	1.3609E-04	5	1.6651E-03	3.3302E-04	0.5668
X33	7.1872E-04	6	2.3838E-03	3.9730E-04	0.8460
X13	2.9799E-04	7	2.6818E-03	3.8311E-04	0.9643
RESIDUAL	8.7885E-05	63	2.7697E-03	4.3963E-05	

CASES INCLUDED	64	MISSING CASES	0	
DEGREES OF FREEDOM	56			
OVERALL F	244.1	P VALUE	0.0000	
ADJUSTED R SQUARED	0.9643			
R SQUARED	0.9683			
RESID. MEAN SQUARE	1.569E-06			

Bibliography

1. Beverly, R. E. III. " Kinetic Modelling of a Fast-Axial-Flow CO_2 Laser," _Optical and Quantum Electronics,_ _14_: 25-40 (January 1982).

2. Box, George E.P. and Norman R. Draper. _Empirical Model-Building and Response Surfaces_. New York: John Wiley and Sons, 1987.

3. Box, George E.P. and J.S. Hunter. "A Confidence Region for the Solution of a Set of Simultaneous Equations with an Application to Experimental Design," _Biometrika_ _41:_ 190-199 (1954).

4. Brimacombe, Robert K. and John Reid. "Accurate Measurements of Pressure-Broadened Linewidths in a Transversely Excited CO_2 Discharge," _IEEE Journal of Quantum Electronics, QE-19_: 1668-1673 (November 1983).

5. Burden, Richard L. and J.D. Faires. _Numerical Analysis_ (Third Edition). Boston: PWS-Kent Publishing Co., 1985.

6. Deutsch, Thomas F. _et al_. "Life and Parameter Studies on Sealed CO_2 Lasers," _IEEE Journal of Quantum Electronics, QE4_: 972-976 (November 1968).

7. Douglas-Hamilton, D. H. and R.S. Lowder. _Carbon Dioxide Electric Discharge Laser Kinetics Handbook_, 2 July 1973 to 30 June 1974. Contract F29601-73-C-0116. Everett, MA; AVCO Everett Research Laboratories, Inc., April 1975 (AD-A008650).

8. Drobyazko, S. V. and L.G. Zhuraskii. "Emission Characteristics of a Pulse-Periodic CO_2 Laser Utilizing an Air-CO_2 Mixture," _Soviet Journal of Quantum Electronics, 9_: 26-30 (January 1979).

9. Fedorov, S. V. and M.S. Yur'ev. "Numerical Analysis of Thermal Self-Interaction in the Active Medium of Electron-Beam-Controlled CO_2 Lasers," _Soviet Journal of Quantum Electronics, 13_: 629-632 (May 1983).

10. Fowler, Michael C. "Influence of Plasma Kinetic Processes on Electrically Excited CO_2 Laser Performance," _Journal of Applied Physics, 43_: 3480-3487 (August 1972).

11. Gilbert, J. et al. "Dynamics of the CO_2 Atmospheric Pressure Laser with Transverse Pulse Excitation," Canadian Journal of Physics, 50: 2523-2535 (June 1972).

12. Gross, Larry A. and Peter R. Griffiths. "Pressure and Temperature Dependence of the Self-Broadened Linewidths of the Carbon Dioxide Laser Bands," Applied Optics, 26: 2250-2255 (June 1987).

13. Iyoda, Mitsuhiro et al. "Theoretical Analysis of a Transverse Discharge CW CO_2 Laser Operated Below Room Temperature," Proceedings of the International Conference on Lasers '85. 677-680. Virginia: STS Press, 1986.

14. Manes, R.K. and H.J. Seguin. "Analysis of the CO_2 TEA Laser," Journal of Applied Physics, 43: 5073-5078 (December 1972).

15. Milonni, P.W. "Density and Temperature Variations in Pulsed Discharge Lasers," Journal of Applied Physics, 54: 3595-3597 (June 1983).

16. Parazzoli, Claudio G. and Kuei-Ru Chien. "Numerical Analysis of a CW RF Pumped CO_2 Waveguide Laser," IEEE Journal of Quantum Electronics, QE-22: 479-499 (March 1986).

17. Press, W.H. et al. Numerical Recipes. New York: Cambridge University Press, 1986.

18. Smith, A.L.S. and J. Mellis. "Operating Efficiencies in Pulsed Carbon Dioxide Lasers," Applied Physical Letters 41: 1037-1039 (December 1982).

19. Stone, Major David H. Personal interview. AFIT, Wright-Patterson AFB OH, 21 September 1989.

20. Tarasov, L.V. Laser Physics. Moscow: Mir Publishers, 1983.

21. Taylor, R.L. and S. Bitterman. "Survey of Vibrational Relaxation Data for Processes Important in the CO_2 - N_2 Laser System," Reviews of Modern Physics 41: 26-47 (January 1969).

22. Verdeyen, Joseph T. Laser Electronics. Englewood Cliffs, New Jersey: Prentice-Hall, Inc., 1981.

23. Vincenti, W.G. and C.H. Jr. Kruger. Introduction to Physical Gas Dynamics. New York: Robert E. Krieger Publishing Co., 1977.

24. Witteman, W. J. The CO_2 Laser. Berlin Heidelberg: Springer-Verlag, 1987.

25. Wutzke, S. A. et al. CW Pin Discharge Laser, 15 March 1973 to 30 September 1974. Contract N00014-73-C-0318. Pittsburgh,PA; Westinghouse Electric Corporation Research Laboratories, November 1974 (AD-A014 649).

Vita

Captain Thomas B. Melancon was born on 18 April 1955 in El Paso, Texas. He graduated from high school in Spokane, Washington in 1973 and attended Washington State University in Pullman, Washington. He graduated summa cum laude with a Bachelor of Science in Chemical Engineering. Upon graduation in 1979, he received a reserve commission in the USAF through the ROTC program. He entered pilot training at Lubbock, Texas, graduated in 1980, and reported to Loring AFB, Maine to serve as a KC-135 pilot for three years in the 42d Aerial Refueling Squadron. After a PCS move to Fairchild AFB, Washington, where he served as a KC-135 pilot and a Command Post controller, he entered the School of Engineering, Air Force Institute of Technology, in June, 1988.

Permanent address: 3800 Manchester

El Paso, TX 79930

REPORT DOCUMENTATION PAGE

Form Approved
OMB No. 0704-0188

1a. REPORT SECURITY CLASSIFICATION	1b. RESTRICTIVE MARKINGS
UNCLASSIFIED	

2a. SECURITY CLASSIFICATION AUTHORITY	3. DISTRIBUTION/AVAILABILITY OF REPORT
	Approved for public release
2b. DECLASSIFICATION/DOWNGRADING SCHEDULE	Distribution unlimited

4. PERFORMING ORGANIZATION REPORT NUMBER(S)	5. MONITORING ORGANIZATION REPORT NUMBER(S)
AFIT/GSO/ENP/ENS/89D-5	

6a. NAME OF PERFORMING ORGANIZATION	6b. OFFICE SYMBOL (If applicable)	7a. NAME OF MONITORING ORGANIZATION
School of Engineering	AFIT/ENP/ENS	

6c. ADDRESS (City, State, and ZIP Code)	7b. ADDRESS (City, State, and ZIP Code)
Air Force Institute of Technology Wright-Patterson AFB, OH 45433-6583	

8a. NAME OF FUNDING/SPONSORING ORGANIZATION	8b. OFFICE SYMBOL (If applicable)	9. PROCUREMENT INSTRUMENT IDENTIFICATION NUMBER
WRDC	AARI	

8c. ADDRESS (City, State, and ZIP Code)	10. SOURCE OF FUNDING NUMBERS			
	PROGRAM ELEMENT NO.	PROJECT NO.	TASK NO	WORK UNIT ACCESSION NO.
Wright-Patterson AFB, OH 45433				

11. TITLE (Include Security Classification)

A Model of Temperature Effects in Pulsed and CW CO_2 Lasers and Optimization Using Response Resurface Methodology

12. PERSONAL AUTHOR(S)
Thomas B. Melancon, B.S., Captain, USAF

13a. TYPE OF REPORT	13b. TIME COVERED	14. DATE OF REPORT (Year, Month, Day)	15. PAGE COUNT
M.S. Thesis	FROM _____ TO _____	1989 December	161

16. SUPPLEMENTARY NOTATION

17. COSATI CODES			18. SUBJECT TERMS (Continue on reverse if necessary and identify by block number)
FIELD	GROUP	SUB-GROUP	Carbon Dioxide; Laser; Model; Optimization;
09	03		Response Surface Methodology

19 ABSTRACT (Continue on reverse if necessary and identify by block number)

Thesis Advisor: Dr. David H. Stone
Assistant Professor
Department of Engineering Phys⋅

20. DISTRIBUTION/AVAILABILITY OF ABSTRACT	21 ABSTRACT SECURITY CLASSIFICATION	
☒ UNCLASSIFIED/UNLIMITED ☐ SAME AS RPT ☐ DTIC USERS	UNCLASSIFIED	
22a. NAME OF RESPONSIBLE INDIVIDUAL	22b TELEPHONE (Include Area Code)	22c OFFICE SYMBOL
David H. Stone, Assistant Professor	(513) 255- 4498	ENP

DD Form 1473, JUN 86   Previous editions are obsolete.   SECURITY CLASSIFICATION OF THIS PAGE